Experimental and Numerical Investigations of Bone Drilling for the Indication of Bone Quality during Orthopaedic Surgery

By

Waqas Akbar Lughmani

A doctoral thesis submitted in partial fulfilment of the requirements for the award of doctor of philosophy of Loughborough University

Wolfson School of Mechanical and Manufacturing Engineering

March 2016

Certificate of Originality

This is to declare my responsibility of the work submitted in this thesis. All the original work is my own except as stated in the acknowledgment. Neither the thesis nor the original work included has been submitted to this or any other institution for a degree.

Signed.....

Date.....

Dedicated to my Parents, Wife and Daughters

Thank you for all your patience, understanding and support.

ABSTRACT

Bone drilling is an essential part of many orthopaedic surgical procedures, including those for internal fixation and for attaching prosthetics. Drilling into bone is a fundamental skill that can be both very simple, such as drilling through long bones, or very difficult, such as drilling through the vertebral pedicles where incorrectly drilled holes can result in nerve damage, vascular damage or fractured pedicles. Also large forces experienced during bone drilling may promote crack formation and can result in drill overrun, causing considerable damage to surrounding tissues. Therefore, it is important to understand the effect of bone material quality on the bone drilling forces to select favourable drilling conditions, and improve orthopaedic procedures. Currently, manual hand drilling tools are used which do not involve any means to estimate bone quality. Therefore, the outcome of the procedure depends completely on the surgeon's manual skills and experience, and thus the information about the bone quality is subjective, obtained through manual feedback experienced by the surgeon. The aim of this research was to study the efficacy of using bone drilling data in estimating bone quality during the orthopaedic surgery. However, as bone drilling data does not give a direct measurement of bone quality, a programme of experiments, a finite element analysis and an analytical analysis were conducted to achieve the goal of this study. This research demonstrates that bone drilling force data if recorded in-vivo, during the repair of bone fractures, can provide information about the quality of the bone.

Drilling results at different anatomic positions on the same cortex showed that the thrust force varies across different positions for the same drilling conditions. This indicates the ability of drilling force to detect structural variability within the cortex. Also, drilling into wet and dry bone gave different results for the same drilling conditions at the same anatomic position; this proves the effectiveness

of using drilling data as a predictor of bone quality. Furthermore, a good correlation ($r^2 > 0.95$) was found between drilling force and normalised screw pullout force in bovine and pig cortical bone, which also shows the potential of using drilling force as quality indicator. Drilling and screw pullout tests conducted on synthetic bone material covering a density range simulating osteoporotic and cancellous bone were also conducted and they gave similar results.

A 3D finite-element model has been developed in order to analyse drilling forces using the explicit approach under various drilling conditions. Similarly, a mechanistic model has also been developed. For both the FE and the mechanistic models, Split Hopkinson pressure bar tests for cortical bone were conducted to extract the material properties at high strain and high strain rate conditions, taking into account that drilling is a high strain and strain rate process. The results show that cortical bone at high strain rate behaves as rate dependent quasi brittle material. The developed models provided high-quality results, and most importantly, they adequately reflected the experimental data.

The main outcome of this thesis is a comprehensive experimental and numerical analysis of drilling forces at different conditions, which prove the efficacy of using drilling force as an indicator of bone quality.

Keywords: *Orthopaedic surgery, Drilling, Cortical bone, Bone quality, Screw pullout, Finite element analysis, Mechanistic model, Bone mineral density.*

ACKNOWLEDGEMENTS

I would like to express my gratitude to Dr Kaddour Bouazza-Marouf for the supervision of this research, for his support and constructive criticisms. I would also like to thank Dr Ian Ashcroft for his useful inputs at various stages of this research. I would also like to thank Dr Atul Jain for his valuable inputs during this research.

I would like to acknowledge Wolfson School of Mechanical and Manufacturing Engineering at Loughborough University for providing financial assistance throughout the project, without which this research wouldn't have been possible. I would like to thank the technical staff in the Wolfson School, particularly Steve Hammond, David King and all the technical staff in the mechanical and electronics workshop for their patience and help in the setups of the electromechanical test rig.

I wish to acknowledge my fellow researchers Dr Farrukh Farrukh, Dr Vaibhav Phadnis, Dr Adel Abdel-Wahab and Dr Usman Ghani for their wonderful companionship and support.

Finally I would like to express my sincerest thanks to Ammi, Maria, Ayesha, Aamna, Baji Gul, Bahi Jani, Shah Gul, Apia, Didi, Yousaf Bahi and Yasir for their love, patience and support, which makes success more enjoyable and disappointments more bearable.

CONTENTS

LIST OF FIGURES

LIST OF TABLES

NOMENCLATURE

Symbols	Meanings & Units
A	Material constant in Johnson Cook material model, MPa
B	Material constant in Johnson Cook material model, MPa
BMC	Bone mineral content
BMD	Bone mineral density
BUA	Broadband ultrasound attenuation
C	Material constant, dimensionless
D	Damage parameter (dimensionless)
D_o	Maximum diameter of the external thread, mm
DXA	Dual X-Ray Absorptiometry
D_d	Drill bit diameter, mm
E_{11}	Longitudinal stiffness (GPa)
E_{22}	Transverse stiffness (GPa)
E_b	elastic modulus of the pressure bars (GPa)
F_{ind}	Indentation force (N)
F_d	Drilling thrust force (N)
F_{NSP}	Normalised screw pullout force (N/mm)
LC_{Drill}	Load cell used to measure drilling force
LC_{Pullou}	Load cell used to measure screw pullout force
QCT	Quantitative Computer Tomography
QUS	Quantitative ultrasound
SHPB	Split Hopkinson pressure bar
SM_{Feed}	Feed stepper motor
TSF	Thread shape factor (dimensionless)
SOS	Speed of sound
L_{th}	Length of thread engagement (mm)

r	radial distance (mm)
t	uncut chip thickness (mm)
V_c	Cutting velocity (mm/s)
u	Yield displacement (cm)
τ	Shear stress of thread material (N/mm^2)
$z_{\alpha/2}$	standard normal distribution
dF	Elemental force (N)
σ_{y0}	Compressive ultimate strength
σ_t	True Stress
k	Specific cutting energy (J/mm^2)
$\acute{f}_{drill}$	Feed rate of drill bit (mm/rev)
ω	rotational speed (rev/min)
σ_d	drilling strength (N/mm^2)
φ	half point angle
n	strain hardening exponent
$n1$	number of drilled holes
m	temperature sensitivity index
T_0	reference temperature (Kelvin)
$\bar{\varepsilon}^p$	equivalent plastic strain
$\dot{\bar{\varepsilon}}$	reference strain rate
ε_t	True strain
ε_e	Engineering strain
ϕ_f	feed angle (radian)
δ	normal rake angle (radian)
η	stress triaxiality
Rij	Hill's potential constants
ψ	helix angle

i	Inclination angle (radian)
σ_y	Yield stress (N/mm^2)
α_d	dynamic rake angle (degree)
$\alpha_{n,ch}$	Normal rake angle (radian)
λ	friction angle (radian)
γ	shear angle (radian)
θ	Angle of resulting forces (degree)
f_r	Feed rate (mm/min)
ϕ	Diameter (mm)

CHAPTER 1

INTRODUCTION

This chapter highlights the major research issues of the drilling in orthopaedic surgery and estimation of the bone quality, and identifies the problems in the current techniques. A detailed description of the research aims and objectives are given. Thesis layout and research methodology are also presented in this chapter.

1.1 Background

Fractures due to bone quality are common; it causes more than 8.9 million fractures annually worldwide and over one-third of all of these fractures occur in Europe [1-5]. By 2050, the worldwide number of hip fractures is estimated to rise from 1.66 to 6.26 million [3], and their incidence is projected to increase up to 240% in women and 310% in men [4]. Bone fractures are, therefore, large and growing public health concerns. A fracture occurs when the external force applied to a bone exceeds its strength. For a given loading condition, the ability of a bone to resist fracture depends on the amount of bone, the spatial distribution of the bone mass and the intrinsic properties of the materials that comprise the bone [6].

In modern orthopaedic practice, the traditional traction and plaster-casting of fractured bones have mostly been replaced by principles of open reduction and internal fixation. This is also known as osteosynthesis, which involves reducing

the fracture to restore bone fragments to their anatomical locations before using nails or plates, and screws to achieve fracture stabilisation as shown in Figure 1-1. These techniques of internal fixation have been shown to achieve excellent results in fracture stabilisation and healing, restoring full functional capability of the fractured bone, and allow for early mobilisation [7].

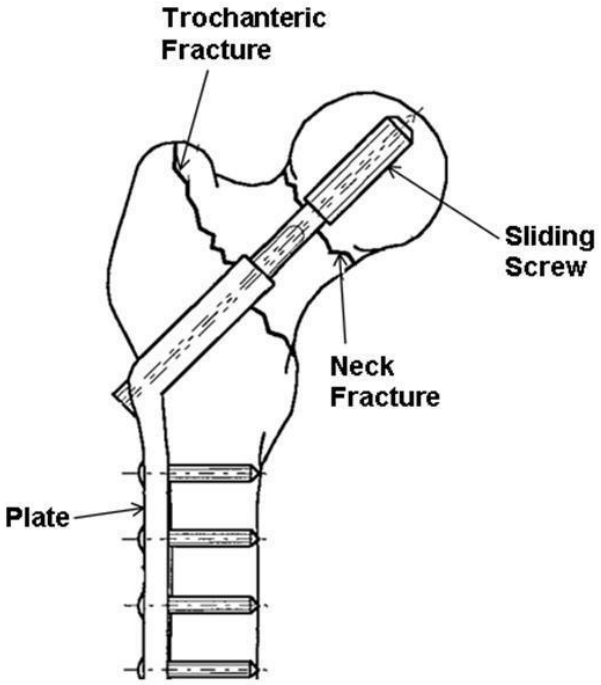

Figure 1-1 Fracture Fixation of Femur using Dynamic Hip Screw (both Trochanteric and Neck Fractures are shown)

In orthopaedic surgery, drilling and tapping are extensively carried out before the insertion of screws into bone. The desired outcome of bone drilling process is accurately positioned holes without mechanical and thermal damage to surrounding tissues. Estimation and control of bone drilling process is critical to prevent drill breakthrough, excessive heat generation, or mechanical damage to the bone. At present, in orthopaedic surgery, bone drilling is performed using

hand drills and the feed rate of the drill-bit is manually controlled by the surgeon. The drilling performance depends, to a great extent, on the surgeon's manual skill and ‘drilling by feeling’ [8]. Drilling into bone is a fundamental skill that can be both very simple, such as drilling through long bones, or very difficult, such as drilling through the vertebral pedicles where incorrectly drilled holes can result in nerve damage, vascular damage or fractured pedicles [9, 10]. Large forces experienced during bone drilling may result in drill overrun, causing considerable damage to surrounding tissues [11, 12].

Research associated with drilling in orthopaedic surgery can be classified into (i) drilling performance (ii) mechanical quality of bone, and (iii) automation of the drilling process as shown in Figure 1-2. These strands are interrelated. The improvement of bone drilling performance depends upon the optimization of the measurable parameters, such as thrust force, torque, feed rate, rotational speed and temperature, which in turn depend on the strength of bone also along with other factors (such as, size, location and bone type). Furthermore, the enhancement of safety to avoid drill bit breakthrough and the quality of the hole made also depend upon the quality of the bone. As shown in Figure 1-2, bone quality of the patient is useful information for the surgeon during orthopaedic surgery, especially if the bone is affected by low density or diseases such as osteoporosis or cancer.

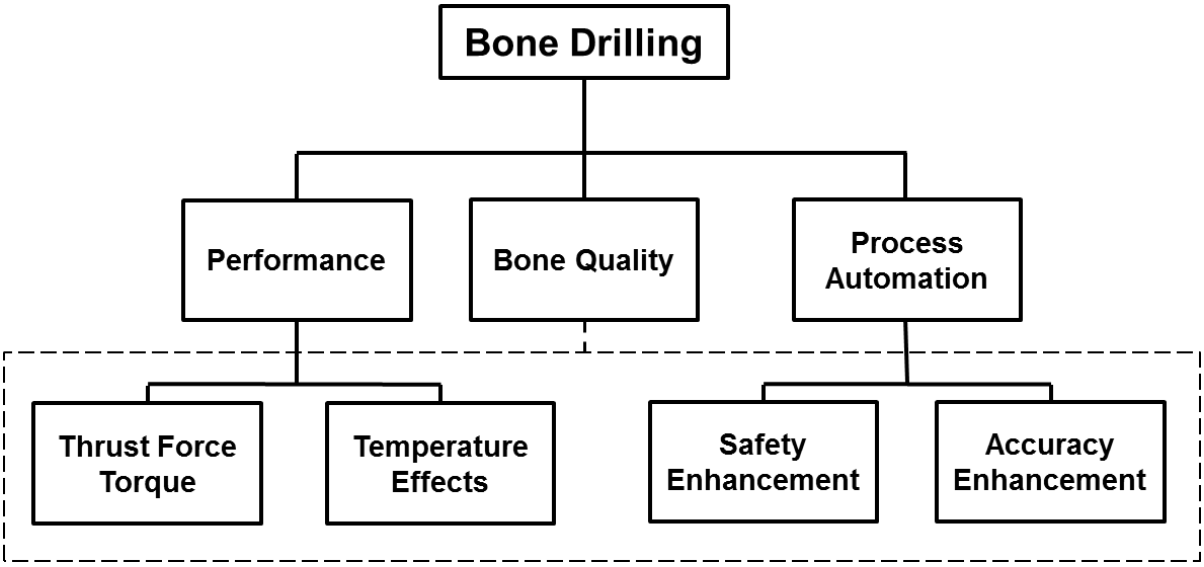

Figure 1-2 Research Areas in Bone Drilling

In clinical practice, the basic investigation allowing bone quality to be estimated is through the measurement of bone mineral density (BMD) [13, 14]. On the basis of the values of BMD and bone mineral content (BMC) parameters obtained experimentally (in medical practice mainly T-score, Z-score), an indirect evaluation of the bone strength is also possible. However, bone health does not only depend upon bone quantity or bone mass but also depends on bone quality [15-19], as shown in Figure 1-3. The factors which contribute to bone quality include (i) bone architecture and morphology; (ii) degree of mineralization; (iii) accumulated fatigue damage; and (iv) properties of the intrinsic organic matrix [20]. Bone quantity includes BMD and size [6]. While BMD is a predictor of fracture risk [2], it lacks sensitivity and specificity. Most women with osteoporosis do not sustain a fracture and over 50% of women who sustain a fracture do not have osteoporosis [21]. Moreover, changes in BMD following therapy explain only 4–30% of the fracture risk reduction [22, 23]. Furthermore, these commercially available BMD measurement techniques have

inherent errors which could lead to a wrong prediction of the bone health [24]. Therefore, estimating bone health using imaging techniques could lead to a less accurate prediction of a patient's bone quality, especially in the case of osteoporotic patients [25]. In addition, bone mineral density measurement techniques are expensive and expose the human body to harmful radiation, and also in emergency or trauma cases where fractures follow an accident there is less time or resources to implement conventional techniques to detect osteoporosis or to get an estimation of the patient's bone health.

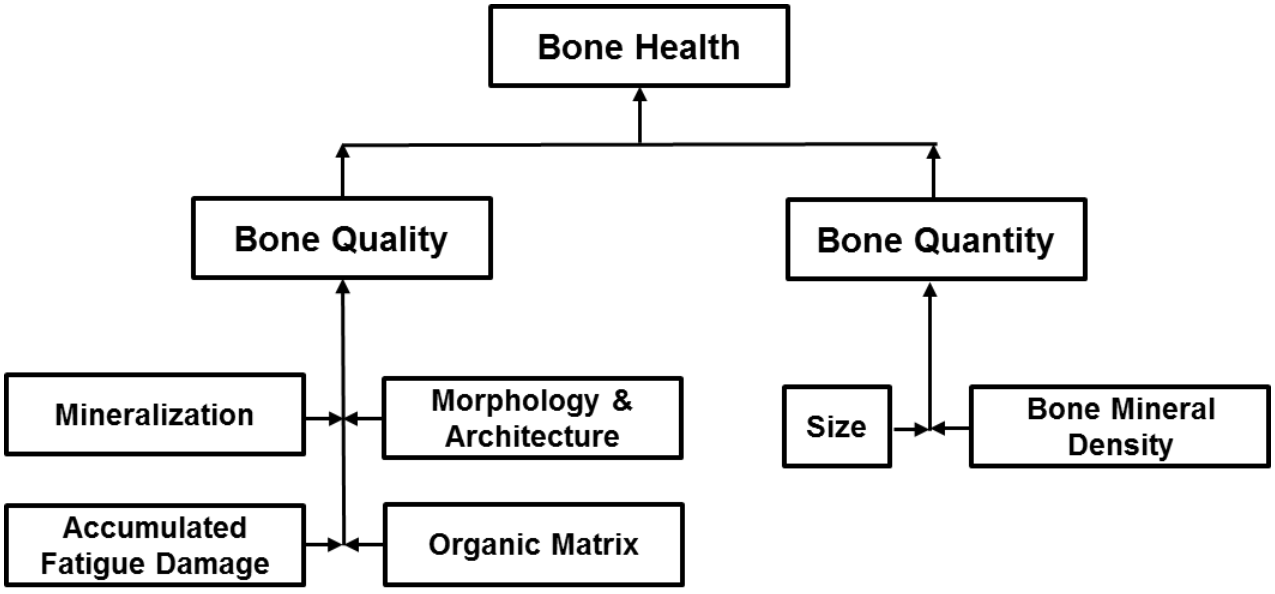

Figure 1-3 Definition of Bone Health

The efficiency of bone screw in internal fixation is related to its axial tension. This tension produces a clamping force between bone plate and bone surface, which is proportional to screw tightening torque. Presently surgeons perceive optimal torque by feel of screw tightening torque. This torque based on feel is significantly closer to thread stripping failure limit and generally past the yield point of bone [26]. Therefore, the holding power of screws also depends on

bone quality. Knowledge of quality and thickness of the bone can provide some measure of the fixation's success rate. This is especially crucial for internal fixation of femoral neck fractures since the success of such fixation depends largely on the mechanical behaviour and architecture of bone [27].

These observations have motivated development of new more accurate, easy, cheap and effective in-vivo bone quality prediction technique. Most of these problems can be addressed by a handheld mechatronic drill for orthopaedic surgery.

1.2 Indication of Bone Quality using Drilling Force Data

Bone drilling data could be used for bone quality prediction and automation of the bone drilling process. Dynamostratigraphy [28] showed clear change of drilling forces across the femoral head for different drilling trajectories at constant advancing rate. Therefore, it is proposed to investigate quantitative in-vivo information of bone quality using bone drilling force data. The main objective of this research is to investigate the use of bone drilling force data in indicating bone quality. In order to study bone quality based on drilling mechanics, a preliminary correlation with established methods of bone quality determination has to be validated. One method is to correlate drilling data to bone densitometry, which has its limitations as discussed above. Another method of determining bone quality is related to basic engineering principles of evaluating mechanical properties, distribution of material and applied loads. The accuracy of the results is limited by the size of the bone specimen.

Previous studies were carried out to correlate densitometry measurements and the structure of the bone with drilling force data [29, 30]. Therefore, a method of

determining a relation between drilling data and constitutive material model of bone is required. The femur is chosen for bone quality investigation since it can be singled out as an important skeletal site where the bone structure is more uniform. Results of this investigation will contribute towards the development of a drilling tool for mechatronic/robotic assisted orthopaedic surgery. This drilling tool can be used routinely during orthopaedic surgical procedures to automatically obtain bone quality along the drilled hole.

1.2.1 Using Finite Element (FE) Model to Validate the Use of Drilling Data to indicate Bone Quality

Bone drilling force data does not give a direct measurement of the bone quality, as it does not give directly any information on the mechanical properties of the bone. Therefore, a preliminary correlation of the drilling data with an established material model of bone has to be established to evaluate the effectiveness of using drilling force data in bone quality prediction. Different direct methods of bone quality measurement are presented in chapter 2 to facilitate the selection of a constitutive material model for this research. As drilling is a high strain and strain rate process, a rate dependent constitutive material model with damage is proposed to simulate the drilling process. Validation of the finite element model can establish a relationship between bone quality and drilling force data.

1.2.2 Using Analytical Drilling Model to indicate Bone Quality

A suitable model for predicting the thrust force felt while drilling bone does not exist. The key factors affecting the thrust force are the drilling feed rate, drill bit geometry and bone quality. All the mechanistic models in the literature obtained specific cutting energy from a number of calibration tests, and are only valid for a certain range of cutting conditions and drill-bit geometries. Any theoretical model,

which take advantage of the bone material properties and drill-bit geometry and requires no calibration experiments, are not available because the machining mechanics of bone material is not fully understood and bone material properties, such as damage initiation and propagation, are not available. Therefore, an analytical drilling model is proposed incorporating all key factors. Validation of the analytical model can establish a relationship between bone quality and drilling force data, and also provide a basis for development of the mechatronic drill.

1.2.3 Development of the Mechatronic Drill

Based on the outcome of this research, a handheld mechatronic drill can be designed as proposed by Bouazza-Marouf [31]. The proposed mechatronic drill was not designed or developed as a part of this research which has been carried out to investigate, both analytically and experimentaly, the relationship between drilling force profiles and bone quality. The mechatronic drill will have the following features,

1. Indication of bone quality by analysing drilling force data.
2. A range of bone drilling speeds should be available, which could be set or adjusted based on the measured bone quality.
3. Safety enhancement feature of drill bit breakthrough prevention.
4. Measurement of screw fixation strength to optimise screw tightening.

Based on the aforementioned background in the above sections, the research aim and objectives of this study are defined below.

1.3 Research Aim and Objectives

The aim of this study is to show the efficacy of using drilling force data for an indication of bone quality during orthopaedic surgery.

From the aim, a number of objectives for research have been established. These are given as:

1. To critically review the use of various direct and indirect bone quality assessment techniques, and identify the limitations and errors involved in such techniques.
2. To study and review current progress of the bone drilling process. Also, to identify the range and effect of various drilling parameters. This helps in developing the analytical model of bone drilling.
3. Characterisation of cortical bone at high strain rate to determine the mechanical properties for use in numerical models for drilling.
4. Acquiring drilling force data for different cortex positions from pig and bovine bone. This is to verify that the drilling data can capture quality variation within different anatomical sites.
5. Investigate the effects of drilling conditions on drilling force data for bovine cortex. This is to validate the finite element model of bone drilling.
6. Investigate the effects of densities on drilling force data for synthetic bone.
7. To demonstrate a correlation between the drilling force and screw pullout force by using the data acquired during drilling and screw pullout testing of synthetic bone material and animal bone.
8. Development of a finite element model to simulate drilling in bone. This is to verify the use of drilling data for indication of bone quality.
9. Formulating an analytical (mechanistic) model of the bone drilling process to establish a relationship between drilling force and bone quality.

1.4 Research Methodology

A schematic of the overall research methodology is given in Figure 1-4. The research is comprised of experimental, finite element modelling, and analytical modelling parts. Experimentation was divided into three parts as drilling, screw pullout and high strain rate testing using SHPB. In the drilling part, the thrust force was acquired at different anatomical positions for dry and wet cortical bone from two different animals, and at various drilling conditions. The results from these experiments were used to investigate the efficacy of drilling force data to indicate the quality of bone. These results were also used to validate the finite element model and the analytical model for drilling in cortical bone. Drilling experiments of polyurethane (PU) foam of different densities were also carried out to investigate the efficacy of the drilling force data to predict the quality of bone. Screw pullout tests on cortical bone and PU foam were carried out in the second part of experimental work. The results from these experiments were used to define correlation between normalised pullout force and drilling thrust force. The third part of experimentations was to characterise the behaviour of cortical bone at high strain rates. Split Hopkinson pressure bar (SHPB) apparatus was used to acquire mechanical properties at high strains. These properties were used in FE and analytical analyses of drilling in cortical bone.

In order to predict the drilling thrust force at different drilling conditions, finite element models were developed. An element removal scheme was used based on ductile damage initiation criterion to replicate the hole making process. The modelling results were validated by comparison with experimental data. To correlate the bone drilling force data with quality, an analytical drilling model was developed

incorporating, drill bit geometry, drilling conditions and strength of bone. The modelling results were validated by comparison with experimental data.

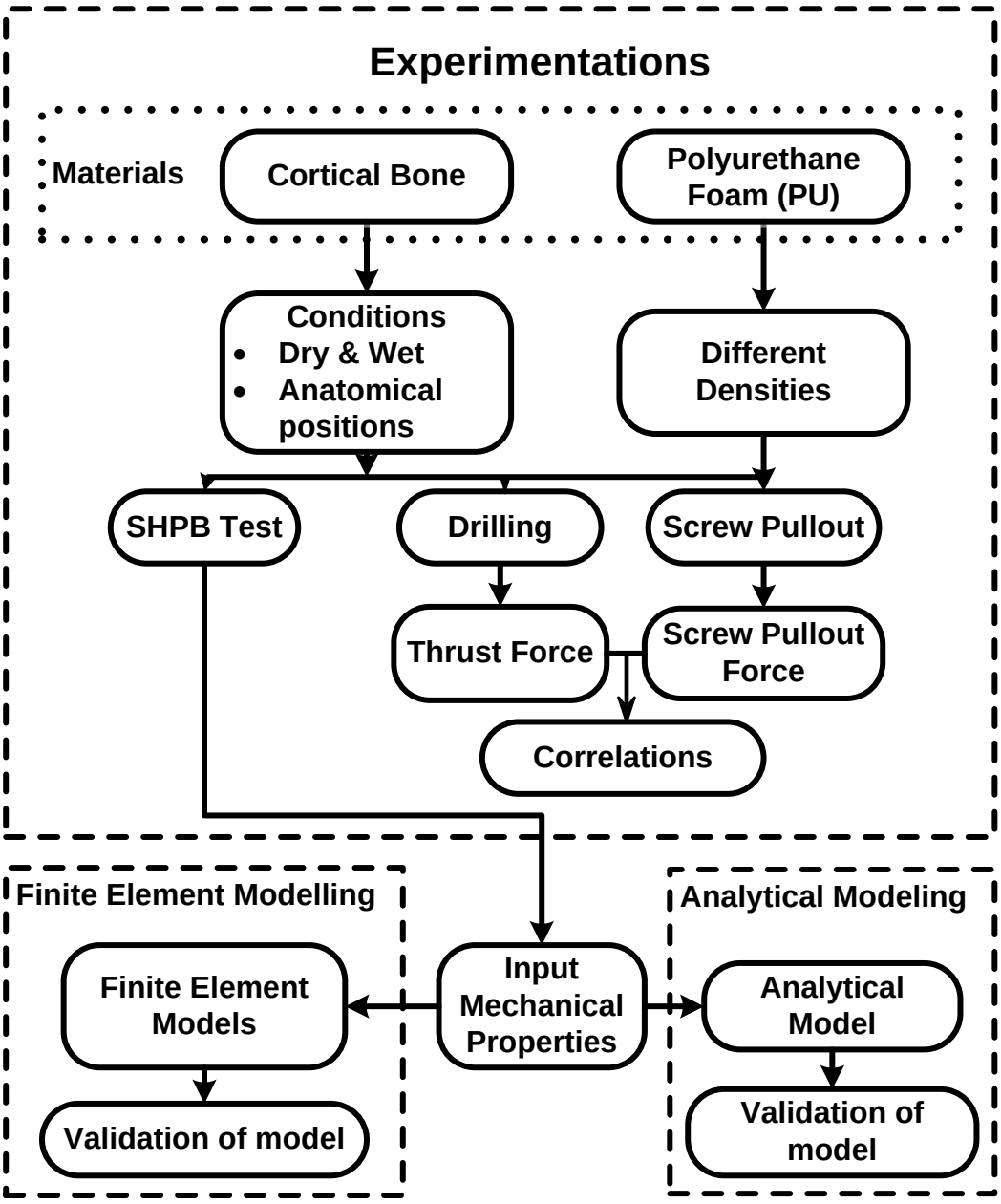

Figure 1-4 Research Methodology

1.5 Thesis Overview

Chapter 1 presents the aims and objectives of this research. This includes background, aims and objectives of this research. This chapter proposes to use bone drilling data to indicate bone quality.

A review of the pertinent literature is presented in Chapter 2. This chapter is divided into two parts. In the first part, various bone quality measurement techniques, which include direct and indirect methods, are discussed. In the second part, the literature on drilling of bone which includes bone drilling performance, analytical models and finite element models of drilling are reviewed.

Details of the materials, experimental plan and experimental methods used in this research are provided in Chapter 3. Results from the experimental programme are provided in Chapter 4.

Chapter 5 provides details of the finite element modelling methods used in the project. The geometry, boundary conditions, meshing methodology, element choice and mesh convergence details are provided. The finite element analysis results and validation are also provided in this chapter.

Chapter 6 provides details of the analytical model derivation, forces from cutting and chisel edges, and comparison between experimental and theoretical results.

Chapter 7 summarises the major conclusions of this work and outlines potential areas of future work.

CHAPTER 2

Literature Review

2.1 Introduction

Structural integrity of the whole bone is determined by bone quality and bone quantity as defined in chapter 1. Due to the multiplicity of contributors to bone quality any mechanical property of the bone, which gives the measurement of its internal stresses produced due to loading (similar to metals), will give a measurement of bone quality [20, 32-37]. In addition, any factor that contributes to the fracture risk of the bone, such as size and bone mineral density will also contribute towards the bone quality. This shows that there is no single definition that is adequate to describe bone strength, and it has increased the clinical and scientific interest in complementary measures of bone quality that could improve fracture risk prediction [38].

The main objective of this research is to investigate the use of bone drilling data, which can be recorded intra-operatively, to evaluate bone quality. Therefore, a review of the techniques available to assess bone mechanical properties, geometry and microarchitecture, and composition across multiple hierarchical levels (as depicted in Figure 2-1) is presented in the first part (Sections 2.2 to 2.4) of this chapter.

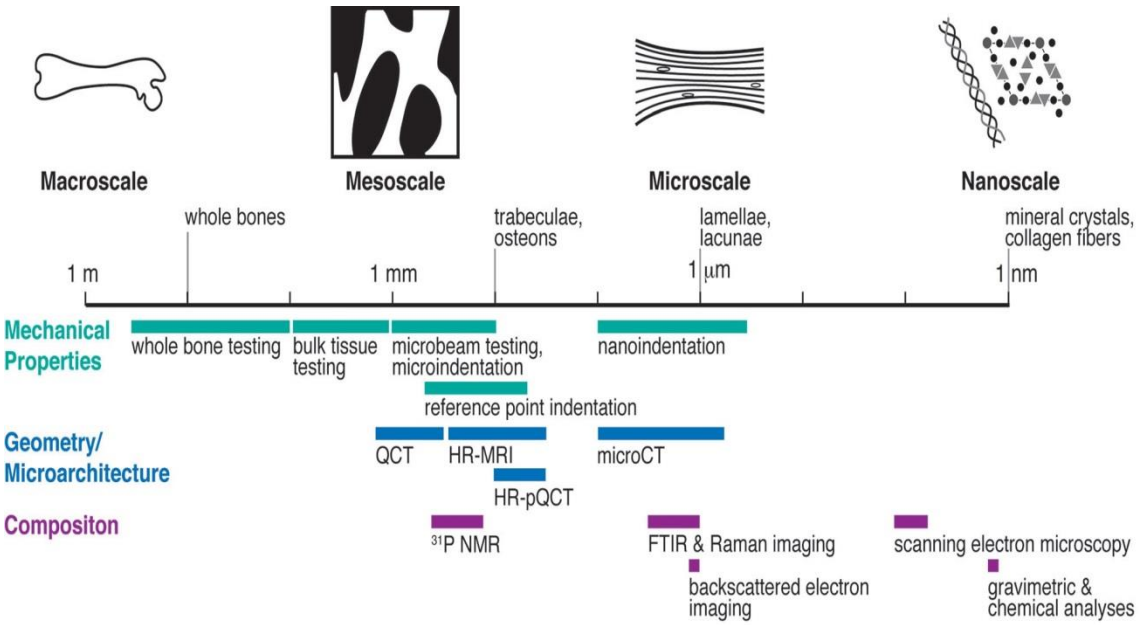

Figure 2-1 Hierarchical structure of bone depicted schematically on a logarithmic scale. Adapted with permission from Donnelly [39]**.**

The following key questions are addressed in the first part: (1) what are the techniques currently available for assessment of the mechanical, geometric, and material components of bone quality? (2) What are the main outcomes of each method? (3) What are the relative advantages and limitations of these methods?

The second part (Sections 2.5 to 2.9) of this chapter focuses on the review of the main contributions in bone drilling with special attention to the drilling performances, analytical and numerical modelling of the bone drilling, and the automation of the bone drilling process. The aim is to give a complete vision of the approaches commonly presented in the literature in order to help in the development of accurate models for bone drilling.

2.2 Bone Quality Assessment Techniques

Techniques available to assess bone quality are broadly divided into two groups. The direct methods, which are performed in-vitro, measure bone mechanical

properties through tensile, compressive, bending, torsion and hardness tests as well as simulating real life bone fracture conditions or screw pullout tests [34, 35, 37]. The indirect non-invasive methods, such as bone densitometry, the Singh Index and ultrasound have been used to estimate bone strength [13, 14, 20, 32]. The indirect methods do not give a direct measurement of bone mechanical properties; therefore various correlational studies between direct and indirect methods have been carried out in order to evaluate the efficacy of the indirect methods in predicting bone quality.

2.3 Direct Methods of Bone Quality Evaluation

Mechanical testing allows direct assessment of a range of mechanical properties across multiple length scales as shown in Figure 2-1, allowing characterization of multiple structural and material properties. At the macroscopic level, whole-bone testing allows assessment of bone structural properties such as structural stiffness and strength. At smaller length scales, material testing techniques enable measurement of the intrinsic properties of the tissue such as elastic modulus and ultimate stress.

Direct test methods involve a specimen of bone sample taken out from the parent bone. Hence, the method of preservation, preparation and mechanical fixation while testing the bone specimen must be considered for reliable test results.

Mechanical properties of the bone specimen can be greatly influenced by the method of bone preservation before conducting any mechanical tests. Water accounts for approximately 6% of the total weight of bone. Thus, any change in the water content has a significant effect on the bone mechanical property. Any treatment of bone like, drying, freezing, storage in saline or alcohol solution, etc. would also change the nature or relative composition of the bone and can influence

its mechanical properties. This is evident from the outcome of an investigation were it was found that after drying the tensile and compressive strength characteristics, the modulus of elasticity and the hardness of bone tested increased as compared to bone tested without drying [34].

A bone should be frozen and kept as moist and hydrated as possible for long term storage, because there is no significant change in the mechanical properties of the bone when frozen and stored at -20^{o}C [40]. To minimise the freeze drying of bone samples, the surrounding musculature should be left intact. A plastic wrap or a bag should be used to cover the musculature to minimise freeze drying and freeze burns. If musculature and surrounding tissues were removed before freezing, the bone sample should be wrapped in gauze, soaked in normal saline and placed in a sealed airtight plastic bag. It should be stored at –20^{o}C and must be placed in a freezer within one hour of harvesting.

2.3.1 Whole Bone Mechanical Testing

At the macroscale, the structural behaviour of bone is determined by the whole-bone mechanical testing. In these tests, a whole bone is typically loaded to failure in compression, bending, or torsion [36, 41]. Structure stiffness, failure load, and the energy absorbed to failure are possible outcomes of these tests. The structural stiffness represents the bone's resistance to elastic deformation. The failure load shows the strength of the bone. The energy absorbed to failure is a measure of structural toughness and represents the energy the bone can absorb before it breaks. The inherent limitation of whole bone testing to failure is that the specimen is broken during testing.

2.3.2 Bulk Tissue Specimen Testing

A bone specimen, or a sample, needs to be prepared for testing. The preparation of the bone specimen involves cutting and machining of the bone. In these tests, regularly shaped specimens (typically cylinders or cubes with diameters or edge lengths of 5–10 mm) are machined from cortical or cancellous bone tissue and tested to failure in tension, compression, bending, or torsion [42, 43].This type of testing has been used to characterize the effects of variables, including porosity [44], anatomic site [43], tissue mineral content [45, 46], and apparent density [47].The effective elastic modulus and ultimate stress are the outcomes of these tests. The effective material properties obtained from these tests are independent of the macroscopic bone geometry but include the effects of porosity and geometric anisotropy arising from osteon or trabecular orientation.

2.3.3 Screw Pullout Testing

Mechanical strength of the bone-screw fixation is an important factor to obtain a rigid fixation and is determined by screw pullout tests. Screw pullout testing refers to the measurement of the force required to pull out a screw inserted in a bone specimen. The analysis of the test gives a direct measurement of bone shear strength and also determines the optimum screw size, insertion technique, angle of penetration and optimum screw hole preparation method. A schematic diagram of a screw pullout test setup (using ASTM F543-02 guidelines) [48] is shown in Figure 2-2. It consists of a test block (bone specimen under testing, referred to as T Block) clamp and base. The test base is fixed to the base of the load frame. Prior to the pullout, a screw is inserted into a predrilled hole in the test block. A suitable load fixture is used to apply tensile pullout load on the screw head. The tensile force which is transferred through the head of the screw should be aligned with the

screw's longitudinal axis. The tensile load should be applied to the test specimen at a fixed rate until the bone threads fail and the screw releases from the test block. The maximum load recorded is known as screw pullout force (F_{SPF}), and is used to calculate the shear stress of the bone specimen using the equation given below [49].

$$F_{SPF} = \tau \times \pi \times D_0 \times L_{th} \times TSF \qquad 2\text{-}1$$

where, F_{SPF} = screw pullout force (N),

τ = shear stress of thread material (N/mm^2),

D_o = maximum diameter of the external thread (mm),

L_{th} = length of thread engagement (mm) and

TSF = thread shape factor (dimensionless)

The main advantage of the screw pullout test is that it can be performed on any shape or size of bone specimen without any prior specimen preparation. However, using surgical screws for the bone screw pullout testing can be very expensive as cost of the surgical screws, drill bits and taps is significantly high. Another shortcoming of the screw pullout testing is that it does not take into account the shearing or cycling loading of screws and the direction of pullout force should be maintained in line with the screw axis to have consistent results.

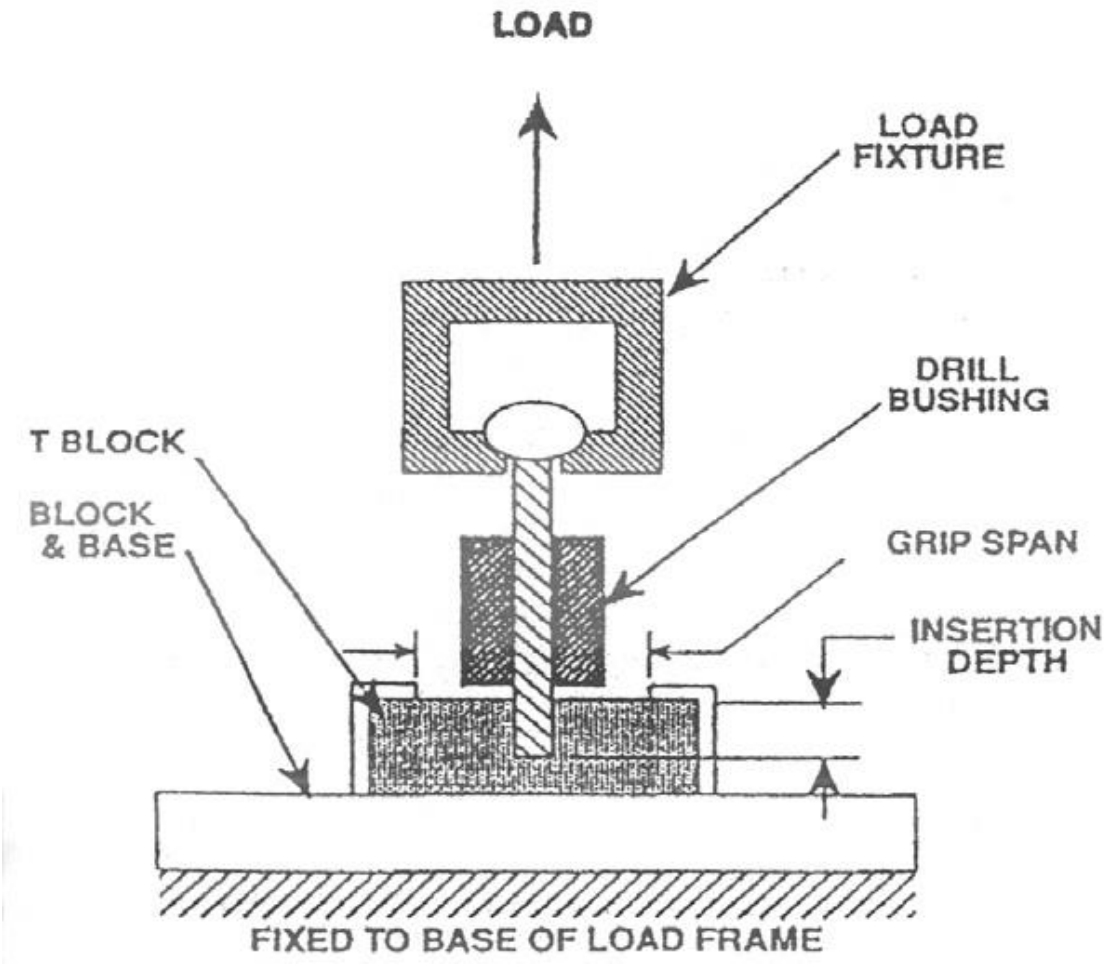

Figure 2-2 Schematic Diagram of Screw Pullout Test Setup [48]

2.3.4 Microbeam Testing

In these tests, bending or tensile loads are applied to microbeams (approximately 200 × 200 × 2000 μm) machined from trabecular and cortical bone [49-51]. The elastic modulus and ultimate stress are determined by these tests. The elastic modulus characterizes the material's intrinsic resistance to elastic deformation. The yield stress characterizes the material's intrinsic resistance to plastic deformation. The material properties obtained from these tests are independent of the macroscopic bone geometry and trabecular microarchitecture yet

still include the effects of discontinuities such as lamellar boundaries and microscale porosity due to lacunae and resorption sites [52].

2.3.5 Micro and Nanoindentation

In an indentation test, a rigid indenter is pressed with a known force into a flat specimen, and the area of the resulting impression is estimated optically [53, 54].The hardness is defined as the force divided by the area of the imprint and characterizes the material's resistance to plastic deformation. Microindentation allows characterization of the mechanical properties of individual trabeculae or osteons [55]. The advantages of this technique include the relative ease of testing and the ability to make measurements in multiple locations within the tissue. A drawback of this technique is that its sole outcome is the tissue hardness.

At the microscale, nanoindentation is capable of probing the mechanical properties of volumes of tissue as small as individual lamellae. In this technique, an indentation test is performed with a depth-sensing indenter tip, often combined with a scanning probe microscope for spatially resolved measurements. The force-displacement data are analysed to obtain the indentation modulus and hardness [56]. Nanoindentation with relatively shallow indentation depths of approximately 100 nm yields spatial resolutions of approximately 1 μm in bone tissue [57]. The advantages of this technique include the capability to measure the material properties of microstructural features such as lamellae [57-59] and to detect localized changes in bone material properties induced by disease or drug treatment [76]. The disadvantages include the need for relatively specialized instrumentation and very smooth specimens if the highest level of spatial resolution is required [60].

2.4 Indirect Methods of Bone Quality Evaluation

The indirect methods do not give a direct measurement of the bone mechanical properties; therefore various correlational studies between direct and indirect methods have been carried out in order to evaluate the efficacy of the indirect methods in predicting bone strength. A review of these studies is presented in the following sections and is subdivided into two sections, (i) imagining techniques, and (ii) ultrasound methods. Imagining techniques, which are based on X-ray absorption, measures the amount of bone mineral (calcium hydroxyapatite) per unit volume of bone tissue and are also used for the measurement of the osteoporosis [15, 61]. Most common imaging techniques are single photon absorptiometry (SPA), dual photon absorptiometry (DPA), dual energy X-ray absorptiometry (DXA or DEXA) and quantitative computer tomography (QCT). Another technique called peripheral quantitative computer tomography (pQCT), which is based on the QCT technique, is also used for bone density measurement of peripheral bones such as the radius. The most common scanning method is DXA. Ultrasound methods are faster, easily available, require less skill and are cheaper; however they are generally used as an initial screening test on patients as they are less accurate than densitometry methods. If results from an ultrasound test indicate that the bone density is low, other indirect techniques are recommended for the confirmation of the results. Broadband ultrasound attenuation (BUA) and the speed of sound (SOS) are the two main types of ultrasound techniques which are used commercially. The Singh Index (SI), which is based on the analysis of proximal femur trabecular patterns using X-ray images, is also used as an additional scanning method. The Singh Index is generally used for a quick analysis of the bone when other indirect methods are not available. The main component of a general densitometry system for bone mineral density measurement

is an X-ray source which produces the radiations. The attenuation in the intensity of the radiation after passing through the body is recorded and is used as a measurement of the bone density.

2.4.1 Single Photon Absorptiometry (SPA)

This method is specially used to diagnose osteoporosis and to measure bone mineralisation in infants as it uses low energy radiations. It uses a narrow beam of mono-energy radiations, emitted from a low energy radio-nuclide source, commonly ^{125}I or ^{241}Am, to measure bone density. Lower energy sources are optimal to measure bone density of smaller bones (such as radius, ulna, metacarpals, etc.) where tissue cover is minimal. Usually a NaI (Tl) scintillation detector is used to monitor the radiation beam. The source and detector are coupled on a yoke and move together over the body part that is being examined, thereby creating an image. Measurements are restricted to the appendicular skeleton, usually the forearm, since the bone must be encased in a constant thickness of soft tissue or its equivalent. Single line or rectilinear scanning is performed over the bone. The difference in the attenuation count rate between the bone and the soft tissue region allows calculation of the bone mineral content in the scan path. This method cannot separate cancellous and cortical bone components. The accuracy and precision error of this method is around ±2-4% [62] and 1-2% [62, 63], respectively.

2.4.2 Dual Photon Absorptiometry (DPA)

Dual photo absorptiometry uses a dual-energy radio-nuclide as radiation source. The most commonly used radio-nuclide is ^{153}Gd. Photons of different energy are attenuated differently by bone and soft tissues. Bone density can be calculated by measuring the percentage of each transmitted beam absorbed by bone and soft

tissue and then applying simple simultaneous equations. DPA eliminates the need for a constant soft tissue thickness across the scan path and it can be used effectively in the spine and femur regions. The accuracy and precision error of DPA is around 1-4% [62] and 1-2% [63], respectively.

2.4.3 Dual X-Ray Absorptiometry (DXA)

The DXA technique uses an X-ray tube as a source to emit radiations rather than using a radioisotope energy source as used in DPA. DXA measures the attenuation (or loss of energy) of X-rays of two different energies when passed through the body, and computes the bone mineral content (BMC, in g) and the bone mineral content per projected area (BMD, in g/cm^2) for a given region of interest. Measurements of BMD by DXA have a prominent role in the WHO guidelines for diagnosis of osteoporosis [64]. A low BMD is a well-established risk factor for fracture [65]. The advantages of DXA include low radiation exposure, excellent precision, low cost, ease of use and short measurement times. However, DXA also has inherent limitations that influence its clinical utility. Measurements are two-dimensional (2D), and DXA cannot therefore distinguish the separate contributions from cortical and cancellous bone, or assess three-dimensional (3D) geometry and microarchitecture. Furthermore, measurements are subject to artefacts caused by degenerative changes, such as the presence of osteophytes and aortic calcification. Although DXA is currently the gold standard for clinical assessment of fracture risk, there is a need to develop new techniques that might overcome some of these limitations.

2.4.4 Quantitative Computer Tomography (QCT)

Macroscopic assessment of three-dimensional (3D) bone geometry can be performed in vivo using quantitative CT (QCT) [66]. In QCT, an X-ray source produces X-rays that are attenuated by an object of interest, and a detector on the opposite side detects the signal. The source and detector rotate about the object, and tomographic algorithms are used to construct a 3D image of X-ray attenuation. QCT outcomes include the 3D macroscopic bone geometry, in which the cortical and trabecular bone are distinct, and apparent volumetric BMD (vBMD, mass mineral/total volume of bone and marrow). The ability to image vertebral sites is strength of this method, although its in-plane resolution (approximately 0.5 mm) is insufficient to resolve trabecular architecture [66]. An important drawback of QCT is its delivery of ionizing radiation to patients.

2.4.5 High-resolution Peripheral QCT

The advent of high-resolution peripheral QCT (HR-pQCT) scanners with isotropic resolution of approximately 80 μm has enabled in vivo imaging of 3D trabecular morphology at peripheral sites such as the distal radius [67, 68]. The primary advantage of this technique is that trabecular bone can be resolved, and morphologic parameters such as bone volume fraction (BV/TV), trabecular thickness (Tb.Th), trabecular separation (Tb.Sp), and trabecular number (Tb.N) can be calculated. Inclusion of calibration phantoms also allows calculation of apparent vBMD. Because the spatial resolution approaches the size of trabeculae, partial volume effects affect the morphologic parameters; nevertheless, the HR-pQCT trabecular measures are correlated with those assessed by micro-CT, the current gold standard for quantification of trabecular morphology [69]. These measurements

are largely restricted to peripheral sites but have the benefit of reduced radiation doses relative to those from whole-body QCT scans.

2.4.6 High-resolution MRI

High-resolution MRI (HR-MRI) allows nonionizing 3D imaging of the trabecular network at peripheral sites. During scanning, a strong magnetic field and a series of radiofrequency (RF) pulses are applied to the specimen to generate 3D images of the hydrogen in the water within skeletal tissues. Bone tissue generates no signal in standard MR images as a result of the low water content of the tissue and the chemical environment of the protons within the bone matrix. When the marrow is imaged, the trabeculae appear as the dark space within the bright marrow [70]. Resolutions as small as approximately 50 × 50 × 200 μm have been achieved ex vivo [71], and resolutions of 156 ×156 ×300 μm are typical in vivo [68]. Consequently, MRI-based trabecular morphologic parameters are also affected by partial volume effects [72]. The MRI-based trabecular measurements, which can detect age and disease induced changes in trabecular morphology, are correlated with their counterparts measured by micro-CT [73]. A critical advantage of this technique is its ability to generate 3D images of bone geometry and microarchitecture without ionizing radiation; disadvantages include the long scan times required for high resolution images of trabecular bone.

2.4.7 The Singh Index (SI)

The Singh Index (SI) is another method which has been used to estimate the degree of osteoporosis using ordinary X-ray radiographs [74].In the Singh Index, the degree of osteoporosis is graded by the radiographic evaluation of the trabecular pattern of the proximal femur from one to six, with grade one being severe

osteoporosis and grade six being normal. The main advantages of using the Singh Index are that it is inexpensive, fast, less harmful and easy to use. However, the Singh Index is subjective in nature and, therefore, should only be used as a rough estimation of bone quality, provided that readings are taken by experienced clinicians. Also, the Singh Index has only been developed for the proximal femur, thus it cannot be used to predict bone quality at other bone skeletal sites.

2.4.8 Micro-CT

At the microscale, micro-CT provides ex vivo characterization of trabecular microarchitecture with isotropic resolutions as small as 1 to 6 μm. The development of desktop in vivo micro-CT scanners has enabled characterization of the macroscopic geometry and microarchitecture of the bones of living animals. Such scanners have enabled longitudinal studies examining skeletal development, adaptation, and response to treatment within the same animals at an isotropic resolution up to approximately 10 μm, although high resolutions require relatively long scan times and large radiation doses [75, 76]. Limitations of these studies include their restriction to small rodents and the need to moderate the ionizing radiation received by the study animals.

2.4.9 Bone Quantitative Ultrasound

In bone quantitative ultrasound (QUS) testing, two ultrasound transducers, one transmitting and one receiving, are placed opposite to one another in a water bath. Bone specimen, usually from peripheral skeleton sites like calcaneus, is placed between the transducers. Ultrasound wave is transmitted, and the attenuation or the change in speed of the wave caused because of the bone specimen is measured. Compared to osteoporotic bone, normal bone demonstrates higher attenuation of the

ultrasound waves and is associated with a greater velocity of the wave passing through bone. Broadband ultrasound attenuation (BUA) and speed of sound (SOS) are the two main types of ultrasound techniques used commercially. There are several advantages in utilizing the QUS method for assessing bone health in children and adolescents. First, QUS can be performed with a portable scanner and it is technically simpler and more economical compared with DXA and pQCT. Second, there is no radiation exposure associated with QUS measurements. Third, some investigators have found that QUS measurements have good correlation with BMD [77, 78], although others suggest that since QUS measures more than just density there should not be a correlation between QUS and DXA [79, 80]. Pluskiewica and co-workers found that DXA and phalangeal QUS measurements do not identify the same patients with reduced bone mineral status and speculated that this was because these two techniques are measuring different bone properties [80]. QUS can also be used to measure geometric properties of the bones. Although QUS may be used as an overall indicator of bone health, a disadvantage is that it is not possible to determine where actual bone deficits are occurring if decreased SOS or BUA are observed since QUS is dependent not only on the density, but also on the stiffness and the macro and microstructure of bone [81].

2.5 Drilling of Bone

In orthopaedics surgery, drilling and tapping are extensively carried out before the insertion of screws into bone. The desired outcome of bone drilling process is accurately positioned holes without mechanical and thermal damage to surrounding tissues. Drilling into bone is a fundamental skill that can be both very simple, such as drilling through long bones, or very difficult, such as drilling through the vertebral pedicles where incorrectly drilled holes can result in nerve damage, vascular

damage or fractured pedicles [10, 82]. Large forces experienced during bone drilling may result in drill overrun, causing considerable damage to surrounding tissues [12, 83] and promote crack formation [84]. Similarly, drilling force is the major contributor of heat generation during bone drilling [85, 86], which can cause thermal necrosis [87, 88]. Studies [89-91] showed that uncontrolled drilling forces and torques caused also surgical complications due to drill-bit breakage. These surgical complications include further surgical procedure and specialised instruments to remove broken drill bits. Therefore, it is important to anticipate drill bit breakthrough and the change in force necessary when drilling bone, which is anisotropic and living. Diseases such as osteoporosis and cancer affect the quality and density of the bone and therefore the thrust force needed. Therefore, it is important to understand the effects of bone drilling conditions, drill-bit geometry and material behaviour on the bone drilling forces to select favourable drilling conditions, and assist in robotic surgery procedures [11, 29, 83, 92].

Most works available in the literature provide an experimental approach. Different aspects influencing drilling forces, temperature and surface quality were analysed. Drill bit parameters including geometry, and cutting parameters such as feed rate, cutting speed and the use of coolant were evaluated. Jacob and Berry (1976) [93]studied drill bits of seven different shapes and geometries to investigate the effect of drilling speed on drilling force and drilling torque for a constant feed rate. The study was carried out on a mature bovine tibia mid-shaft under constant lubrication. They found that drill bits with a point angle of 110^{o} and a helix angle of 24^{o} produced the lowest cutting force and cutting torque. They also recommended that a surgical drill bit should have a rake angle ranging from 25^{o} to 30^{o}. In another study by Wiggins and Malkin (1976) [94], drilling performance was evaluated by

measuring feed rate, drilling torque and specific energy at a constant drilling force. The experiments were carried out on a human cadaveric male femur using three different types of drill bits. They found that less energy is required to drill at higher feed rates. They also observed that the drilling performance under constant drilling force was found to be independent of the rotational speed, implying that the performance depended primarily on the drill bit geometry. Hobkirk and Rusiniak (1977) [95] conducted experiments which represented actual clinical conditions. In the study, the drilling force exerted by surgeons during manual drilling (feed rate not constant) of bone was investigated. Twenty dentists experienced in surgical preparation used six different drill bits at high and low speeds to prepare standardized holes and slots in the angle of bovine mandible. Each operator drilled a hole (10mm deep) and cut a slot (6mm deep and 6mm long) with each drill bit or bur at two cutting speeds. Three categories of operator were found. The A operator, varied the drilling force rapidly while preparing the bone; the B operator maintained a relatively constant drilling force for a somewhat longer period and the C operator exerted relatively higher drilling forces for short periods. Saha and Albright (1982) [96] optimised the design of drill bit for the effective removal of bone chips and to minimize the drilling force and temperature. The performance of the optimised drill bit was compared with other surgical drill bits for drilling into bovine bones, and it was found that the new design decreased the drilling force by 45% and peak temperature rise by 41%. Eriksson and Albrektsson (1983) [88] showed that bone tissue heated to 50^0C for 1 min or 47^0C for 5 min would not remain as functioning bone. Bachus *et al*. (2000) [85] evaluated the effect of the drilling force on the cortical temperature and its duration and concluded that the application of a larger force to the drill can

effectively reduce both the maximum cortical temperature and its duration above 50^0C.

Robinson *et al* (1992) [97]investigated the effect of drill bit guide length and drilling method on accuracy of the diameter of drilled holes. They measured the drill diameter with a micrometer (accuracy of 0.005mm), and drilled 225 holes in fresh porcine mandibles. The holes were drilled using long guides, short guides and without any guides, with a drill press, a pneumatic drilling machine and a manual drilling machine. A drill bit of 2 mm diameter was used in the study and it was changed after drilling 15 holes. The drill press was found to be the most accurate method of drilling followed by the pneumatic drill and then the manual drill. In the case of using drill bit guides, drilling without using any drill bit guide was found to be the most accurate method followed by using the short length drill bit guide and then the long length drill guide. The extensive number of variables involved complicates the statement of concluding remarks and corroborates the interest in developing predictive tools for bone drilling, which are poorly developed to date.

Not only the temperature remains a challenge during drilling, but the prediction of cutting forces is also important, since uncontrolled large forces can cause drill-bit breakage, excessive drill breakthrough, excessive heat generation, and mechanical damage to the bone. Experiments have been conducted to investigate the effects of the drilling conditions and drill-bit geometry on the drilling forces and temperature. Tuijthof et al. (2013) [98] investigated the thrust force for cortical and trabecular bone drilling using eight tools and verified that the drill geometry and bone material have effects on the thrust force. Increasing the feed rate can increase the thrust force and torque as demonstrated [93, 99-101] and that

decreasing the point angle can reduce the thrust force as verified [101, 102]. However, the experimental results for the effect of the spindle speed on the drilling forces from different researchers are inconsistent and even contradictory. The experimental results of Alam *et al.* (2011) [103], Basiaga *et al*. (2011) [102] and Jacob *et al*.(1976) [93] showed that increasing the spindle speed would reduce the thrust force and torque. Yet, Lee *et al*. (2012) [100] found the opposite, that the thrust force and torque increased as the spindle speed increased. Udiljak *et al.* (2007) [101] concluded that the spindle speed had little effect on the thrust force. MacAvelia *et al*.(2012) [104] showed that increasing the spindle speed reduced the thrust force and torque for human femur but had little effect for artificial femur. Augustin *et al*. (2012) [8] and Pandey and Panda (2013) [105] reviewed the effect of drill geometry and drilling conditions on the temperature rise. Cooling by irrigation has been verified by Augustin *et al.* (2008) [86], Sener *et al.*(2009) [106] , and Zhang *et al*. (2013) [107] to be an effective way to reduce the temperature rise when drilling bone. Sener *et al*. (2009) [106] concluded that external irrigation at room temperature could provide a sufficient cooling effect, and lower temperature saline was even more effective. Inconsistent results for the effects of drilling speed and feed rate on the temperature have been obtained by different researchers. Results of Augustin *et al*. (2008) [86], Karaca *et al*. (2011) [108], Lee *et al*. (2012) [109], and Udiljak *et al*. (2007) [101] showed that increasing the drilling speed would increase the temperature rise, whereas increasing the feed rate would decrease the temperature rise. However, Sharawy *et al*. (2002) [110] showed that the mean rise in temperature decreased as the drilling speed was increased from 1225 to 2500 rpm. Alam *et al* (2009) [99] showed that the temperature rise was higher at a feed rate of 50 mm/min than at a feed rate of 20 mm/min.

Prediction of cutting forces is required for the development of realistic training tools for surgery. The advent of haptic simulation systems for orthopaedic surgery procedures has provided surgeons with an excellent tool for training and for preoperative planning purposes. Drilling is one of the operations requiring extensive training because of the difficulties arising from vibration and the risk of drill bit breakage [111]. Proper simulation of the process requires accurate prediction of visual issues and also reproducing the sense of touch [112].However, force prediction has been poorly analysed in the literature. The bone drilling models reviewed below are grouped in subsections. Mechanistic and analytical models are presented first; these models have involved a simplification of the problem. The finite element (FE) models for drilling and orthogonal cutting are reviewed subsequently.

2.6 Mechanistic and Analytical Models

In analytical studies, the drilling models developed for metals have been applied to bone drilling to estimate the bone drilling forces. In order to apply machining theory of metals to bone, an assumption was made that bone behaves like metal when it is machined [94].

In 1976, two separate researchers published the initial work on bone drilling. Jacob *et al* (1976) [93] investigated drilling force and drilling torque versus drill bit rotational speed on samples from the mid-diaphysis of bovine tibia. Using equations presented by Cook (1966) [113] for a single edge cutting of metals, Jacob *et al* presented a theoretical analysis of the drilling force and compared it with experimental data. The theoretical analysis was based on equation 2-2 given below,

$$F_d = k \times \left(\frac{D_d}{2}\right) \times \left(\frac{\acute{f}_{drill}}{2}\right) \qquad 2\text{-}2$$

where, F_d = Drilling thrust force (N),

k = Total energy required to cut per unit volume (joules/mm^3),

D_d = Drill bit diameter (mm),

$\acute{f}_{drill}$= Feed rate of drill bit (mm/rev),

They suggested, k = 1.5 × strain × shear stress.

The shear stress value was obtained from the earlier work in orthogonal cutting by Jacob *et al* [93]. They were unable to obtain a good correlation between the theoretical and experimental drilling force data. The main reason for the poor correlation was because they ignored the effect of chisel edge which is the main contributor to the drilling force [114-116].

Wiggins and Malkin (1976) [94] extended their work done on orthogonal machining of bone to drilling. Using different drill bit geometries, they measured feed rate, drilling force and drilling torque, while drilling through compact bones of the human femur. The experimental data was plotted and regression analysis was performed for the variables involved in drilling.

Karalis and Galanos (1982) [84] applied the theory of rock mechanics and formulation of Somerton (1982) [117] in bone drilling, which resulted in equation 2-3,

$$\frac{f_d}{\omega . C . D_d} = \left(\frac{F_d}{D_d^2 \sigma_d}\right)^2 \qquad 2\text{-}3$$

where f_d (mm/min) is the feed rate, ω (rev/min) is the rotational speed of the drill bit, C is a material constant and σ_d (N/mm^2) is defined as the drilling strength . An experimental study of the bone drilling was conducted to investigate the interrelationship between drilling rates, drilling strength (defined as the ratio of

energy input to volume of bone broken), triaxial strength and hardness of the bone. Human cadaver cancellous bone of the femur head and cortical bone of the tibia shaft were used to carry out the drilling experiments. The coefficients of determination found were very low (r^2 = 0.23), so the validity of the formulation is not entirely convincing.

Chagneau and Levasseur (1992) [28] proposed a technique called dynamostratigraphy for the mechanical testing of bone. In this technique, the drilling force and the drilling torque is continuously measured along the drill depth at constant rotational speed and feed rate, as shown in Figure 2-2. This technique is useful in finding the change of structure, property and the density variation of the bone along the drilling path. They applied dynamostratigraphy to study the morphology of bone structure and mechanical resistance of head of human cadaver femur bone using a 4mm diameter three-lipped drill bit. The mechanical resistance of bone depends on the density, state of hydration, structure, material property and mineral content of the bone. To compare the mechanical resistance of bone, the hardness testing of the right side femoral head was conducted and the left side was used for dynamostratigraphy. The drill bit rotational speed and the feed rate were fixed at 350rpm and 10 mm/min, respectively. The results from dynamostratigraphy showed clear changes in the drilling resistance of the cancellous bone across the femoral head at different drilling trajectories. When compared to results from drilling tests, higher forces were obtained by punching. Correlation between punching, drilling force and a theoretical model to estimate the drilling force was not presented.

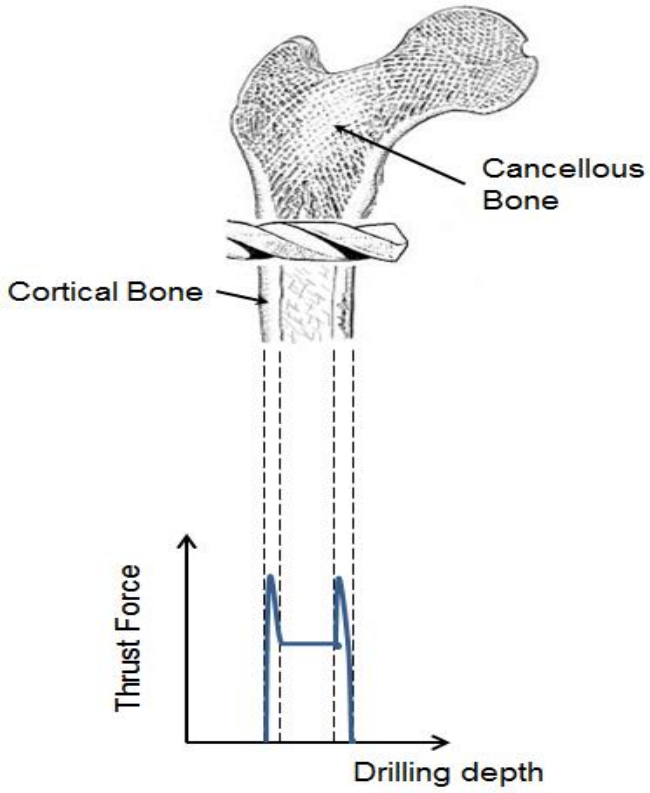

Figure 2-3 Testing of Bone Using Dynamostratigraphy

Allotta *et al* (1996) [118] proposed an analytical model for calculating the drilling force and is given in equation 2-4,

$$F_d = k\acute{f}_{drill}\frac{D_d}{2}\sin\varphi \qquad 2\text{-}4$$

where, φ is the half point angle of the drill bit, and the other terms are as defined in equation 2-2.

They suggested that the value of k is five times the value of ultimate tensile strength of bone, which is not supported in the literature. In addition, the above equation also neglects drilling force component due to the chisel edge.

XU *et al.* (2011) [119] developed a force model by dividing the cutting lips and chisel edge into a number of elemental sections and applying empirical formula for each element. However, they unrealistically assumed that the thrust force was uniformly distributed along the chisel edge and cutting lips and that the chisel edge contributed 50% of the thrust force. These empirical models mainly include the effects of the feed rate and drill-bit diameter on the drilling forces. The effects of the spindle speed and drill-bit geometry are neglected. Moreover, numerous calibration experiments are required to obtain the coefficients for these empirical equations.

Lee *et al*. (2012) [100] developed a mechanistic force model for prediction of thrust force and torque during bone drilling. The model includes analytical calculations of drill-bit parameters, cutting conditions, and cutting geometry, while taking the material and friction properties into account through empirical specific energies. Only a small number of tests were needed to calibrate the specific energies for a broad range of drilling conditions and drill-bit geometries. However, an analysis of the force transformation on the cutting lips using this model contains some errors and the indentation zone adopted from Mauch and Lauderbaugh (1990) [120] is inaccurate.

Sui *et al.* (2014) [121] improved the model developed by Lee *et al.* (2012) [100] to predict the thrust force and torque when drilling bovine bone. The cutting action at the drill point was divided into three distinct regions: primary cutting edge, secondary cutting edge, and indentation zone. Thus, different models were formulated to consider the cutting mechanics of each region. The model was calibrated for bovine cortical bone and validated for a wide range of spindle speeds and feed rates. The predicted results agreed well with the experimental results. The

limitations of the model include the calibration of experiments to determine the coefficients for specific cutting energies, and the assumption of a plastic extrusion mechanism for the bone in the indentation zone.

2.7 Correlation between Drilling force and Bone mineral density

Ong (2000) [29] investigated the relationship between the drilling force and bone mineral density in porcine femurs. Their purpose was to determine the efficacy of using drilling force measurements to estimate the strength of bone. Bone mineral density was obtained by dual X-ray absorptiometry (DXA), which provided an average bone mineral density value over the thickness of the object, in a specified two- dimensional grid. Drilling was done parallel to the DXA scanning direction in the greater trochanter and the femoral head regions, and perpendicular to the DXA scan along the cervical axis (Figure 2-3). They found a good correlation (r^2 = 0.85) in the greater trochanter region but only an average correlation (r^2 = 0.51) in the femoral head region in the holes that were aligned with the DXA scanning direction. However, when the drill holes were perpendicular to the scanning direction, the correlations found were not as good. This could be due to the fact that they used a two dimensional measurement, essentially collecting a bone mineral density for the entire cross section of the bone. However, the drilling trajectory only goes through a small portion of that cross section and thus the bone mineral density (obtained through DXA) does not reflect the bone mineral content at the drilling site. Using a three-dimensional bone mineral density measurement such as those from quantitative computed tomography (QCT), would enable better matching between the drilling force and the bone mineral density of the drilled bone. They further stated that the analysis of bone drilling forces had the potential to provide useful information about the strength of bone.

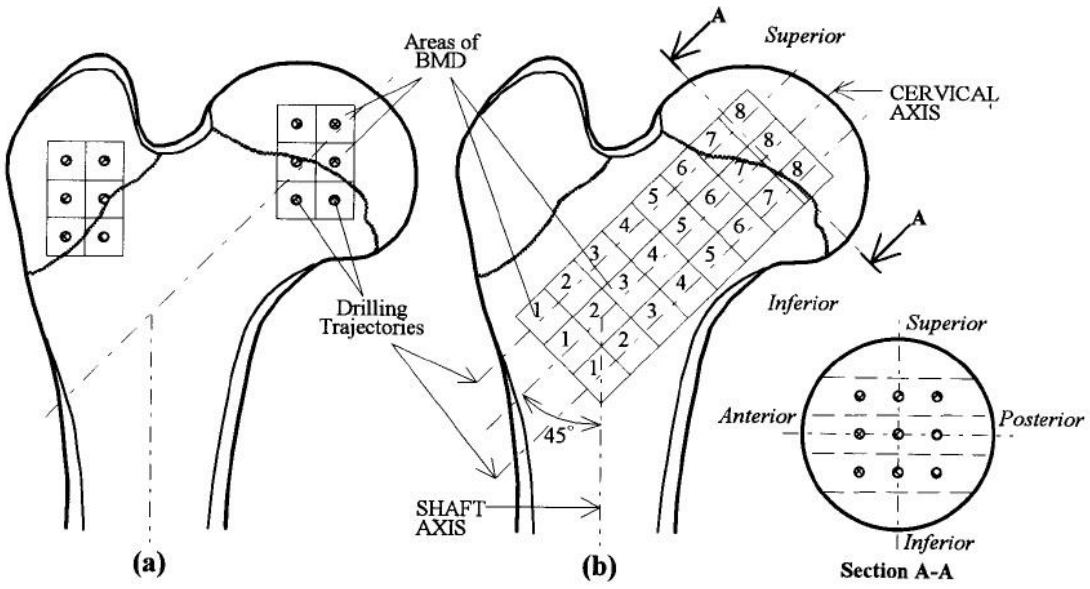

Figure 2-4 Drilling Trajectories and Corresponding DXA Measurements: (a) in the Greater Trochanter and Femoral Head and (b) Parallel to the Cervical Axis [29]

2.8 Finite Element Modelling of Bone Machining

Finite element (FE) modelling has been used extensively over the last 2-3 decades in biomechanics to model the structure of bones [122]. However, FE modelling has only been used a few times to examine issues in bone machining. In general FE drilling models are based on orthogonal cutting principles that have been well established. As the accuracy of simulations depends greatly on the proper choice of the thermo-mechanical properties, an essential part of the numerical model is the constitutive behaviour of the bone tissue, which is considered in different ways in the literature.

An isotropic approach in bone cutting modelling was presented in Alam et al. (2009) [99]. They carried out an experimental and numerical study focused on orthogonal cutting of bone. A two dimensional modelling of the process assuming

elastic-viscoplastic behaviour of the bone for cutting forces and temperature prediction was presented. The mechanical response is represented by the Johnson–Cook law (without thermal softening). The Johnson-Cook hardening law is frequently applied to analyse the dynamic behaviour of metal alloys. This hardening law is generally pre-implemented in FE codes, including ABAQUS/Explicit. The Johnson-Cook model is defined by equation 2-4. In the second part of the equation, the term $(\bar{\varepsilon}^p)^n$ defines the strain hardening , the term $\left(\frac{\dot{\bar{\varepsilon}}^p}{\dot{\varepsilon}}\right)$ defines the strain rate sensitivity, and the last bracket is related to thermal softening.

$$\bar{\sigma}\,(\bar{\varepsilon}^p, \dot{\bar{\varepsilon}}^p, T) = [A + B(\bar{\varepsilon}^p)^n]\left[1 + Cln\left(\frac{\dot{\bar{\varepsilon}}^p}{\dot{\varepsilon}}\right)\right]\left[1 - \left(\frac{T - T_0}{T_m - T_0}\right)^m\right] \qquad 2\text{-}5$$

The terms A ,B and C are material constants, n is the strain hardening exponent, m is the temperature sensitivity, T_0 is the reference temperature, T_m is the melting temperature, $\bar{\varepsilon}^p$ is the equivalent plastic strain, $\dot{\bar{\varepsilon}}$ is the reference strain rate and $\bar{\sigma}$ is the yield strength of the material. The natural logarithm is denoted as ‘’ln’’. Through experimental characterization of bone, Keaveny *et al.* (2004) [123] obtained its strain rate sensitivity at high strain rates. Alam et al. (2009) [99] proposed to neglect the influence of temperature on the yield stress due to small temperature changes leading to negligible thermal softening.

Childs and Arola (2011) [124] assessed the applicability of a metal machining finite element model to predict chip formation and forces in bone cutting. The uncoupled continuum model is based on two different concepts: an elasto-viscoplastic material model and a fracture criterion.

In a recent work by Santiuste *et al. (2014)* [125], orthogonal cutting of cortical bone was analysed using finite elements. The bone was modelled as an anisotropic material using a similar approach to that used for long fiber reinforced composites. In this case the osteons played the role of fibers reinforcing the interstitial matrix. The model commonly used in the literature for the simulation of composite cutting was validated through comparison with experimental results provided in Alam et al. (2010) [126]. In Santiuste *et al*. (2014) [125], the anisotropic cortical bone was modelled assuming an elastic behaviour up to failure. Failure was predicted with the Hou model [127]. The material parameters for Hou's model were obtained from the work of Keaveny *et al*. (2004) [123]. As a result from analyses considering model anisotropy, it was concluded that the influence of osteon orientation on the cutting force is significant. The orientations across and transverse to the cutting speed direction lead to the maximum level of forces, so confirming the behaviour observed experimentally in the literature. The anisotropic approach gave realistic chip morphology similar to that observed as shown in Figure 2-4.

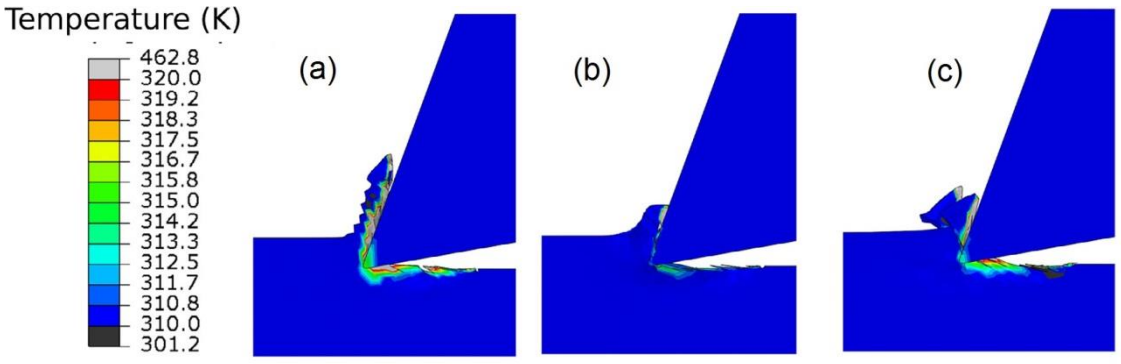

Figure 2-5 Temperature contours and chip morphology obtained for different (a) Longitudinal (b) Transverse (c) Across [125]

Hage et al. (2013) [128] analysed orthogonal cutting of cortical bone from a micro-structural perspective. The micro-structure of the bone was identified from an optical image taken from bovine femur cortical bone slice. The bone images at the microstructure level were enhanced and the micro-constituents of the bone were segregated as separate images. The flow stresses of the osteon and lamellae matrix regions were assumed to behave according to the Johnson-Cook material model. This model is quite simple and further improvement of the microscale modelling of bone cutting is required.

Sezek et al. (2012) [129] developed a FE model using the MSC system in order to predict temperature change during cortical bone drilling (bovine tibia). Remeshing was used in order to prevent the mesh impairment due to chip formation during drilling. The bone was assumed to behave as an elastic isotropic material. The authors concluded that not only cutting parameters influence the maximum temperature, but also bone density has a significant effect (the applied drilling force increased as bone density increased; temperature increased 10% with a 12% increase in bone density). This fact should be accounted for when defining feed-rate and drill bit rotation speed in order to minimise necrosis.

Tu et al. (2013) [130] developed a temperature-displacement coupled FE model to simulate the thermo-mechanical behaviour of the contact region between the drill bit and bone analogue. The dynamic simulations were performed using the commercial ABAQUS/Explicit code. The model included both cortical and cancellous zones. The mechanical behaviour of the bone analogue (cortical and cancellous) was assumed to be elastic-plastic. A dynamic failure criterion was applied to control the element removal during the drilling operation. Element deletion and mass scaling

were employed to enable convergence of the FEM solution in the drilling modelling avoiding distortion and an excessive computational cost. The thermal contact behaviour between the drill bit and bone was modelled using surface-to-surface contact discretization. The friction behaviour between the drill bit and bone was assumed to be governed by Coulomb's friction law, with a coefficient of friction equal to 0.3. The peak bone temperature and the size of the thermally affected zone were found to increase with enhancing drilling speed. The FE model was verified by experiments and was used to predict the peak value of the bone temperature during drilling with speeds of 600, 800 and 1200 rpm. Good accuracy in temperature predictions was achieved, with differences less than 3°C between the peak temperature calculated with FE model and measured from the experiments. The range of velocity is not wide in this work and it would be interesting to check the behaviour of the temperature and the size of the thermally affected zone for higher values of the velocity. Probably these parameters would tend to stabilize when the spindle velocity is high enough.

Complete modelling of drilling is difficult. Even in the well-known field of metal, it is hard to find complete models of drilling including chip removal simulation. The advantage of this type of models is the possibility of predicting cutting forces, temperature and mechanical damage. In the case of bone cutting, all works dealing with chip removal in bone drilling assume an isotropic behaviour of bone with a simple constitutive equation.

2.9 Automation of the Drilling Process

Currently, the efficacy of the drilling procedure depends on the experience and intuition of the surgeon. Therefore, any means of assisting the surgeon during

the operation can decrease the potential for error or mishap. With automation of the drilling process, data such as drilling force, drilling torque, drill bit displacement and rotational speed, etc. can be automatically collected during the drilling process and can be further used for analysis. This analysis of data could be used in implementing a control algorithm for safety enhancement and/or predicting bone quality. In general, control methods for detecting bone layer transitions while drilling are based on the penetration force and cutting torque measured by sensors attached to the drilling tool.

In 1995, Brett et al. [131] were the first authors to provide a solution for an automatic drilling methodology. They proposed a control strategy for the precise drilling of flexible bone tissues during ear surgery. To detect the moment of the drill bit's complete breakthrough, the system identified a persistent increase of the cutting torque simultaneous with a persistent decrease of the penetration force. In subsequent studies [58], aspects of the tool design were examined.

At the same time, Allotta et al. [118] devised a technique for detecting breakthroughs with a mechatronic tool designed for orthopaedic surgery. They also proposed a theoretical model for obtaining the penetration force and cutting torque parameters and detecting a breakthrough by imposing an upper limit threshold to the first derivative of the penetration force.

An alternative detection methodology based on wavelets was presented by Colla and Allota [132]. They investigated the application of a wavelet based controller to a mechatronic drill for orthopaedic surgery. The penetration velocity of the drill bit was generated on the basis of a wavelet analysis of the thrust force signal.

Ong and Bouazza-Marouf [11] devised a robust detection method for drill bit breakthrough when drilling into long bones. This method, based on a modified

Kalman filter, was able to convert the profiles of differences in drilling force between successive samples and/or the drill bit rotational speed into easily recognizable and more consistent profiles, allowing a robust and repeatable detection of drill bit break-through.

Lee and Shih [133] developed a robotic bone drilling system for applications in orthopaedic surgery. The proposed robotic bone drilling system consisted of an inner-loop fuzzy controller for robot position control, and an outer-loop PD controller for feed unit force control. Breakthrough detection was a function of thrust force threshold information and trend in drill torque and feed rate.

Recently, Taylor et al. [134] presented a surgical robotic device that is able to discriminate tissue interfaces and other controlling parameters in the space in front of the drill tip. A smart tool detects the area just in front of the tool tip and is able to control the interaction with respect to the flexing tissue in order to avoid penetration or to control the extent of protrusion with respect to the position of the tissue. In order to interpret the drilling conditions and the conditions leading up to breakthrough at a tissue interface, a sensing scheme that discriminates between the varieties of conditions posed in the drilling environment is used.

Yet another approach found in the literature is based on fuzzy logic and neural networks. A hand-held drilling tool devoted to orthopaedic surgery was presented in [135].The drilling tool used a fuzzy logic controller to control the penetration velocity and identify the time of break-through.

2.10 Concluding Remarks

This chapter summarized the techniques available to assess bone quality, their outcomes, and their advantages and disadvantages. The methods available for

assessment of bone quality include techniques for characterization of bone mechanical properties, geometry/microarchitecture, and composition. The advantages and disadvantages of each technique also relate to the design of the study and the outcomes of interest; in particular, many clinical studies used noninvasive techniques, yet the current noninvasive methods available to clinicians typically provide incomplete information about bone quality. In contrast, most of the mechanical characterization methods require a biopsy but provide a wealth of mechanical information otherwise unavailable noninvasively. Destructive mechanical testing is necessary for direct assessment of bone strength and remains essential to characterization of bone structural performance.

A brief description of the studies conducted to improve the drilling performance, by optimising the drill bit design, feed rate and drilling speed, have been presented. Previous studies have assumed that the cutting mechanism in bone behaves in a similar fashion as that of metals, and as thus the drilling force equations developed for metals were adopted to calculate the drilling force in bone. All the drilling force prediction models used for bone require a value for the specific energy which would need to be determined experimentally.

FE modelling of bone machining is also reviewed in this chapter. Since the anisotropic nature of the bone has been evidenced, it seems that the development of 3D models of real drilling operations in surgery including anisotropic constitutive modelling is one of the challenges in this field.

The automation of the drilling process has also been discussed. It is evident from the literature that the control methods for detecting bone layer transitions while drilling are based on the penetration force and cutting torque measured by sensors

attached to the drilling tool. The control methods and systems proposed in the literature differ in the way they try to detect the variations in torque and force signals. Most of them use detection algorithms by predefining threshold values for these variations, and when these threshold values are reached, the system assumes that the drill bit has arrived at a bone layer transition.

This chapter has highlighted the shortcomings of existing bone quality measurement techniques and lack of information about bone quality to the surgeon during orthopaedic surgery. There is, therefore, a need for a method which determines site specific bone quality information during orthopaedic surgery which involves bone drilling. As bone drilling is an essential part of orthopaedic surgery, a relationship between drilling data and material's strength has the potential of providing a good site specific indication of bone quality. Hence, the main objective of this research is to investigate the use of bone drilling data, which can be recorded intra-operatively, to evaluate bone quality.

CHAPTER 3

EXPRIMENTAL METHODS

This chapter describes the methods and procedures used during the experimental programme carried out in this research, which has two major parts. The first part consists of drilling and screw pullout experiments to determine the effects of materials, and their mechanical properties, and drilling conditions on the drilling and screw pullout forces. The experimental results of drilling were also used to validate the numerical models. The second part characterises the mechanical properties of bovine cortical bone at high strain rate. These properties were used in the numerical models of drilling.

3.1 Material Used

Polyurethane (PU) foam and cortical bone, from bovine and pig femur bones, were used in this research. The bones were obtained from a local butcher. The soft tissue and bone marrow were removed and the bones were thoroughly cleaned with cold water. The epiphysis was then cut off with a hacksaw. The diaphysis of the femur bones, which is predominantly cortical bone, was used in the tests. The bone sections were then excised into rectangular shaped samples according to three anatomic positions (Anterior, Posterior, and Medial) as shown in Figure 3-1. The bovine bone samples were 75-90mm in length with an average thickness of the cortical wall of 7–9mm, and the pig bone samples were 30-40mm in length with an average thickness of 3-

5mm. However, the shape of the bone samples was not suitable for gripping in the holding device of the test rig for the drilling and screw pullout operations. So to eliminate this problem, the bone samples were further cut into three parts along their longitudinal axis, and the resulting sections (the specimens) were clamped to the surface of a metal block, with the bone's top surface facing the drill bit. A total of twelve test specimens were prepared from the bone pieces. Every bovine specimen was divided into seven equal sections and every pig specimen divided into five equal sections, with each accommodating approx. four drilled holes. The main stages of the specimen preparation are shown in Figure 3-2. All femur bones appeared to be normal. After being prepared, the test specimens were put in a 0.9% physiological saline solution for 24 hr; it is well-known from literature that dry bone specimens exhibit higher mechanical properties than wet ones [34]. This procedure is used to reproduce the living conditions as far as possible.

Polyurethane (PU) foam from General Plastics was used as a synthetic bone material in this investigation. The mechanical properties of PU foams are in accordance with the required properties of cancellous bone given in Table 3-1. The advantage of using foam is that it can have a complete range of osteoporotic bone densities. The foam material used for research has a cellular structure, and strength and stiffness values similar to that of cancellous bone. The human cancellous bone density ranges from 0.09 g/cm^3 to 1.26 g/cm^3[35, 136]. The foam samples purchased for this research cover the medium density of the cancellous bone given in Table 3-2. The mechanical response of PU is totally different from cortical bone.

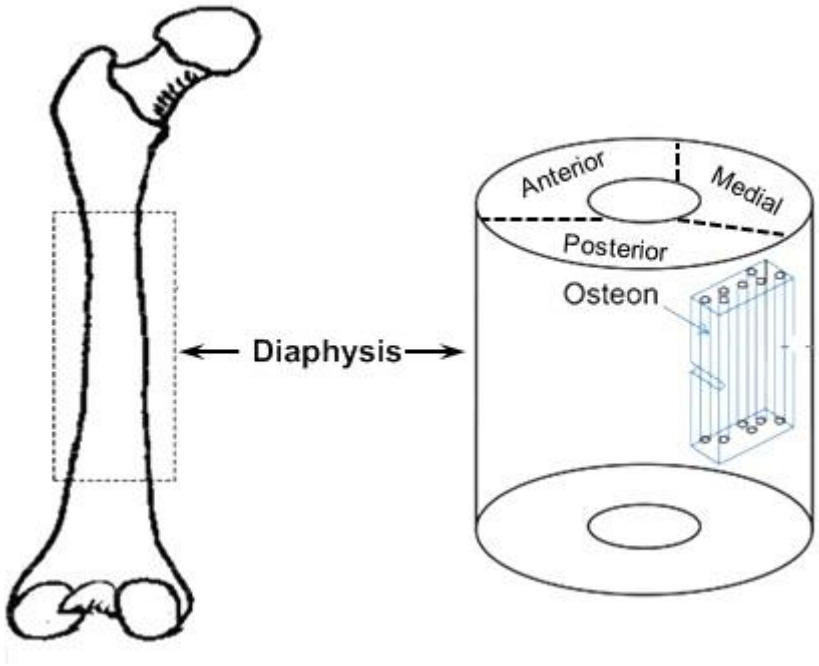

Figure 3-1 Femur Anatomic Positions

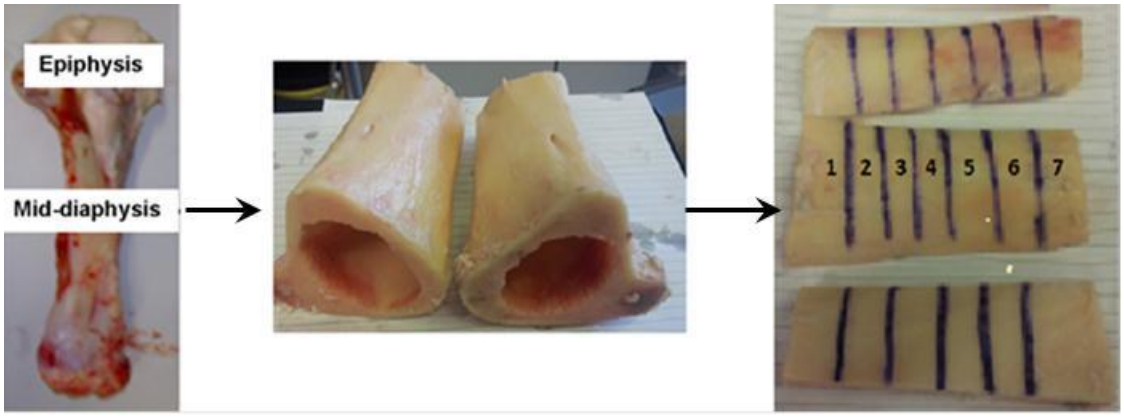

Figure 3-2 Preparations of Bone Specimen for Drilling

Table 3-1 Foam properties as per ASTM 1839-97 for use as Alternate Material to Bone

Grade	Density Range (g/cm^3)	Compressive Strength (MPa)	Compressive Modulus (MPa)	Shear Strength (MPa)	Shear Modulus (MPa)
10	0.1442 – 0.1762	2.095 – 2.895	56.3-76.7	1.660-2.170	20.82-27.68
12	0.1762-0.2082	2.895 – 3.790	76.7-99.2	2.17 – 2.725	27.68-35.10
15	0.2243-0.2583	4.280 – 5.315	111.2-136.65	3.000-3.620	39.00-47.13
20	0.3044-0.3364	7.000 – 8.245	178.1-207.8	4.580-5.276	60.16-69.40
40	0.6247-0.6568	22.41 – 24.300	539.6-582.8	12.34-13.24	167.17-179.47

Table 3-2 Foam used in this research

Foam Model	Density (g/cm^3)	Thickness (mm)
6715	0.2403	19.00
6718	0.2884	19.10
6720	0.3204	18.80
6725	0.4005	19.10

3.2 Test Rig

To accomplish the aims of this research, bone drilling and screw pullout tests were conducted on a custom designed electromechanical test rig with single setting of specimen as per the ASTM F543-02 standard. The main components of the test rig shown in Figure 3-3 are:

- Fixed Outer Frame: this provides support and rigidity to the test rig,
- Moveable Inner Frame: this moves freely in the vertical direction using a guide mechanism,

- Feed Mechanism: this is mounted on the fixed outer frame and provides drill bit displacement and feed rate, as well as screw pullout rate,
- Drilling and Screw Insertion Motors: this performs the desired operation of drilling and screw insertion,
- Specimen Mounting Arrangement: this is mounted on the fixed outer frame and is free to rotate,
- Counterbalancing Weight: The weight of inner frame is counterbalanced using dead weights to stop it from moving under its own weight in the vertical direction.. This is achieved using a combination of pulley and wire rope,
- Sensors: load cells are used to record drilling and screw pullout forces and a cantilever beam is used for torque measurement,
- Tool Holder: this holds the drill bit, the screw driver bit and the attachment for screw pullout, and
- Computer and Electronics Interface: this allows the control of the test rig and data acquisition using a computer.

Figures (3-4, 3-5 a & b) show further details of the rig. During the drilling and screw pullout operations a constant feed rate is provided using the ball screw feed mechanism. An encoder (EnLead) is mounted on the lead screw shaft to record drill bit displacement and feed rate, as well as screw pullout rate. A stepper motor (SMFeed) provides the rotary motion to the ball screw.

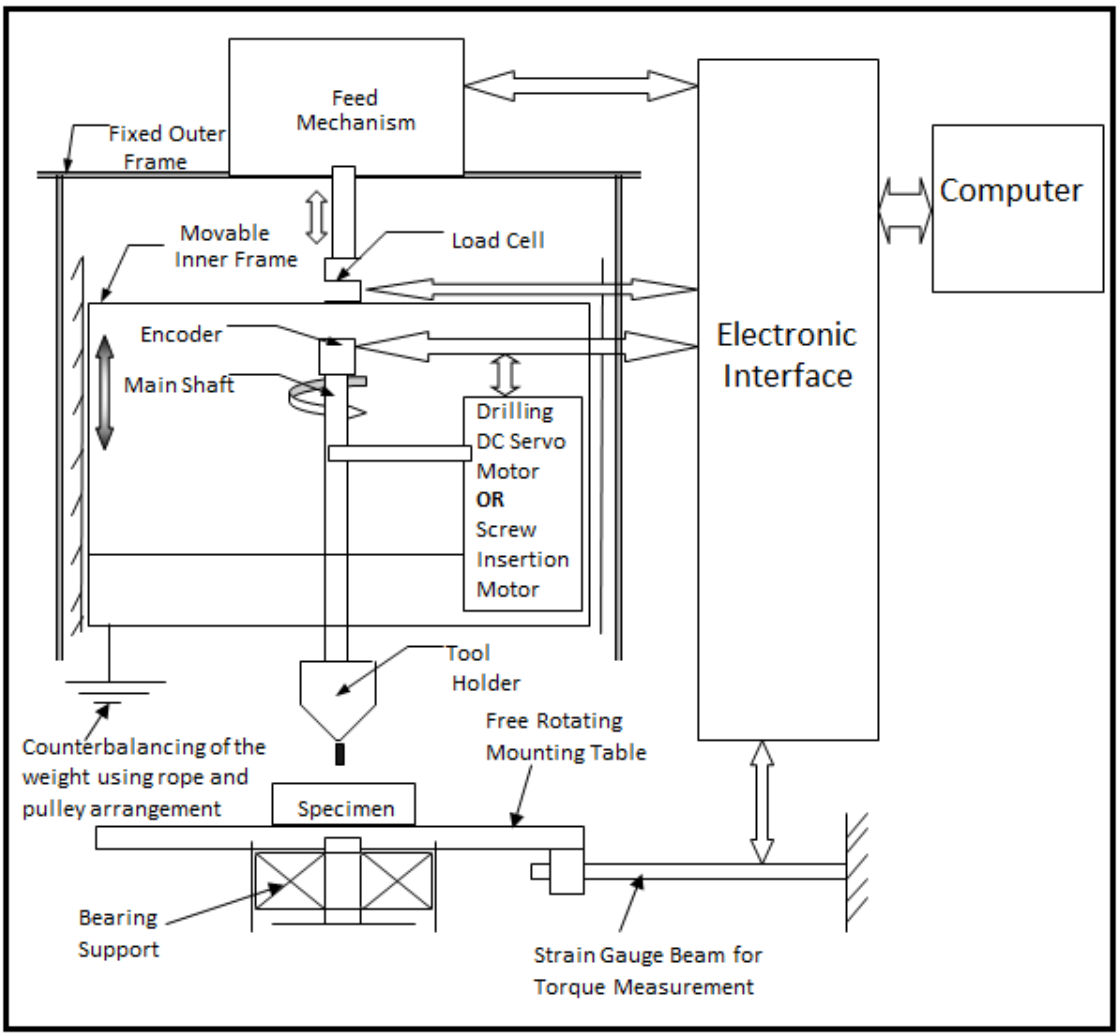

Figure 3-3 Schematic Diagram of the Electromechanical Test Rig [136]

The ball screw is directly connected to the stepper motor shaft through a coupling; therefore the rotational speed of the stepper motor shaft is the same as that of ball screw. Rotary motion is converted by the ball screw mechanism into a linear motion of the actuator arm. In case of screw pullout, the torque from motor shaft is transfer to ball screw through two gear pairs to meet feed rate requirement. The actuator arm pushes the inner frame through a load cell (LC_{Drill} or $LC_{pullout}$); thus transferring the feed motion to the inner frame. A load cell is used to record the force

profiles during drilling and screw pullout. The inner frame moves linearly on two linear bearing shafts.

The required speed for drilling is provided by a DC servo motor, which is part of the drilling motor assembly mounted on the inner frame. A tachometer is used to provide speed feedback to control the drilling speed. The drilling motor shaft is attached to the main shaft which encompasses a chuck at the free end. The weight of the inner frame is counter balanced. The specimen to be drilled is mounted on a plate which is part of the specimen mounting assembly. The specimen mounting assembly is free to rotate on the ball bearings and its rotation is restricted using a torque sensing cantilever beam. The two limit switches, upper and lower, limit the linear movement of the inner frame for safety purposes. Drill bushes are used to ensure that the drill bit is driven into the specimen at an angle of 90 degree.

For tapping and screw insertion the inner frame is disconnected from the ball screw mechanism assembly and is free to move in the vertical direction on linear bearing shafts as shown in Figure 3-5a. The vertical movement of the inner frame is controlled by counterbalancing its weight using wire rope and pulley arrangement. A chuck attached to the main shaft is used to hold the screw driver bit. To have a constant engagement of the screw driver bit into the screw, a constant pressure on the screw head has to be applied by the screw driver bit. As the chuck moves with the inner frame therefore, a weight added on to the inner frame will apply a constant load on the screw head. A constant load of 1.14 Kgf has been used in accordance with the ASTM F543-02. A stepper motor (SMSc_Ins) provides the driving torque for screw insertion or screw tightening. The screw insertion mechanism assembly is engaged with the main shaft using a gear pair.

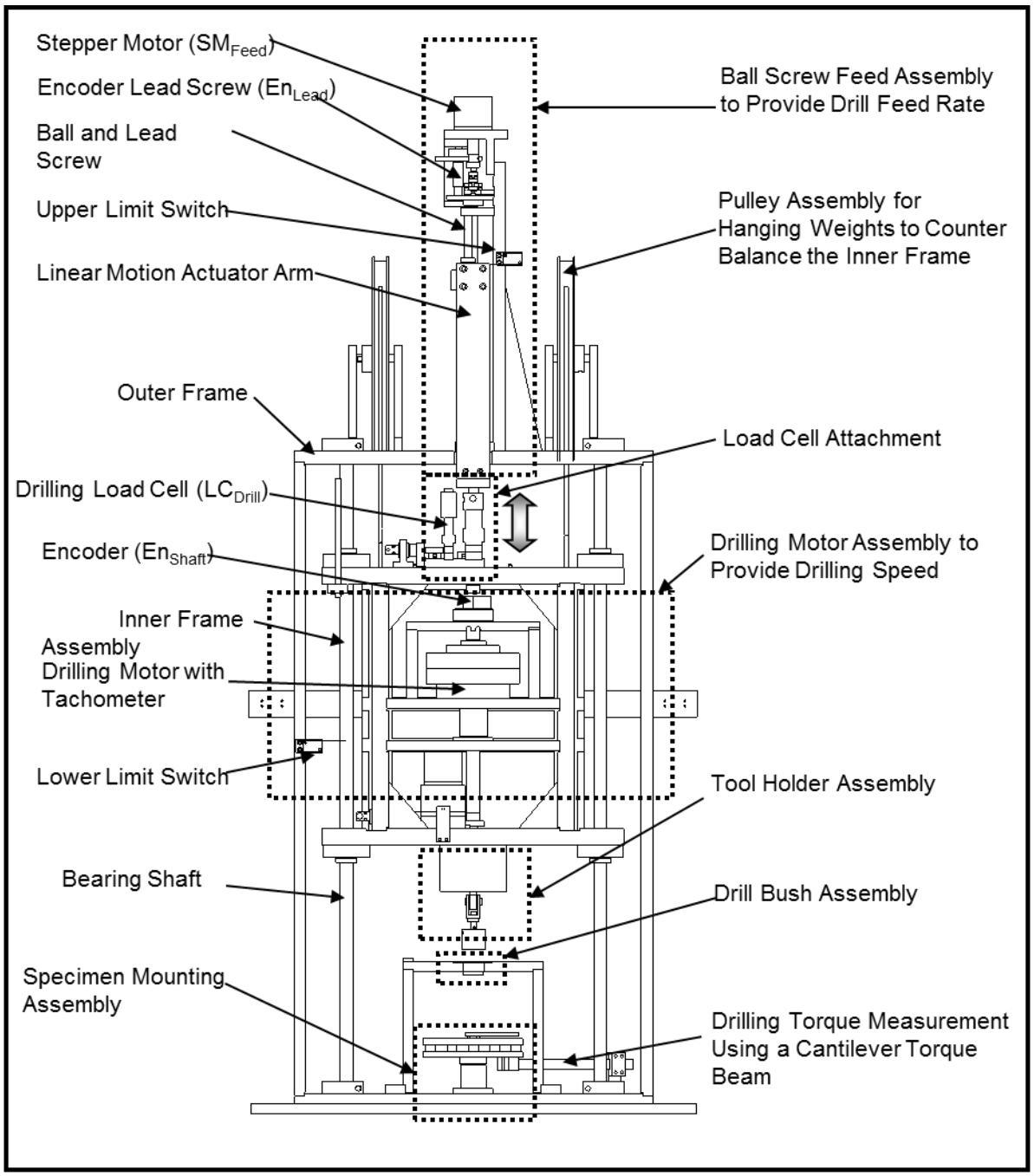

Figure 3-4 Test Rig Components used during Drilling/Screw pullout Operation

[136]

A microcontroller PICI8F6620 is used for interfacing the test rig with the computer. A 12-bit, eight channel data acquisition system is used for data acquisition. Figure 3-5b shows different component of test rig.

(a)

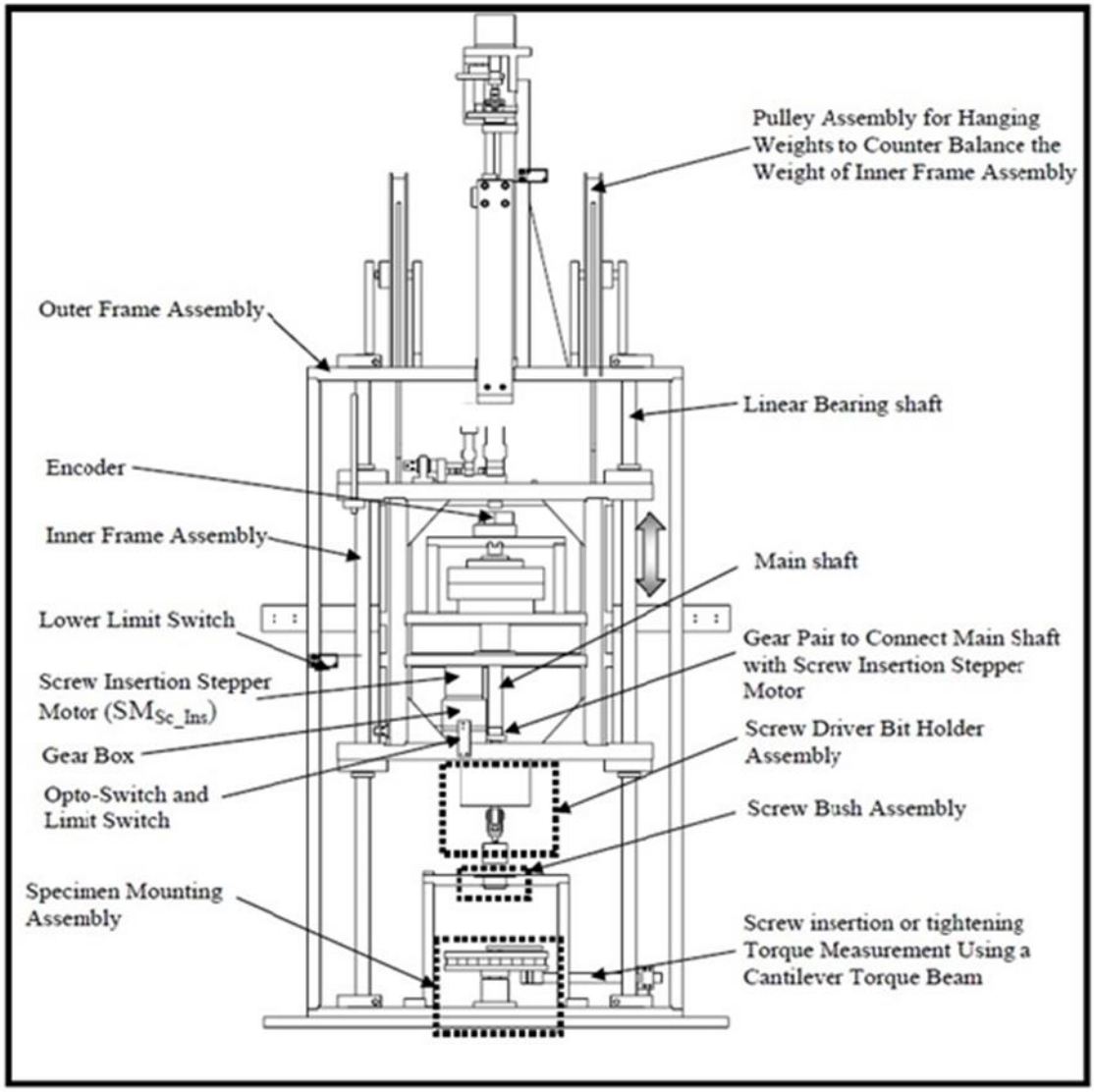
Pulley Assembly for Hanging Weights to Counter Balance the Weight of Inner Frame Assembly
Outer Frame Assembly
Linear Bearing shaft
Encoder
Inner Frame Assembly
Main shaft
Lower Limit Switch
Gear Pair to Connect Main Shaft with Screw Insertion Stepper Motor
Screw Insertion Stepper Motor (SM_{Sc_Ins})
Screw Driver Bit Holder Assembly
Gear Box
Opto-Switch and Limit Switch
Screw Bush Assembly
Specimen Mounting Assembly
Screw insertion or tightening Torque Measurement Using a Cantilever Torque Beam

(b)

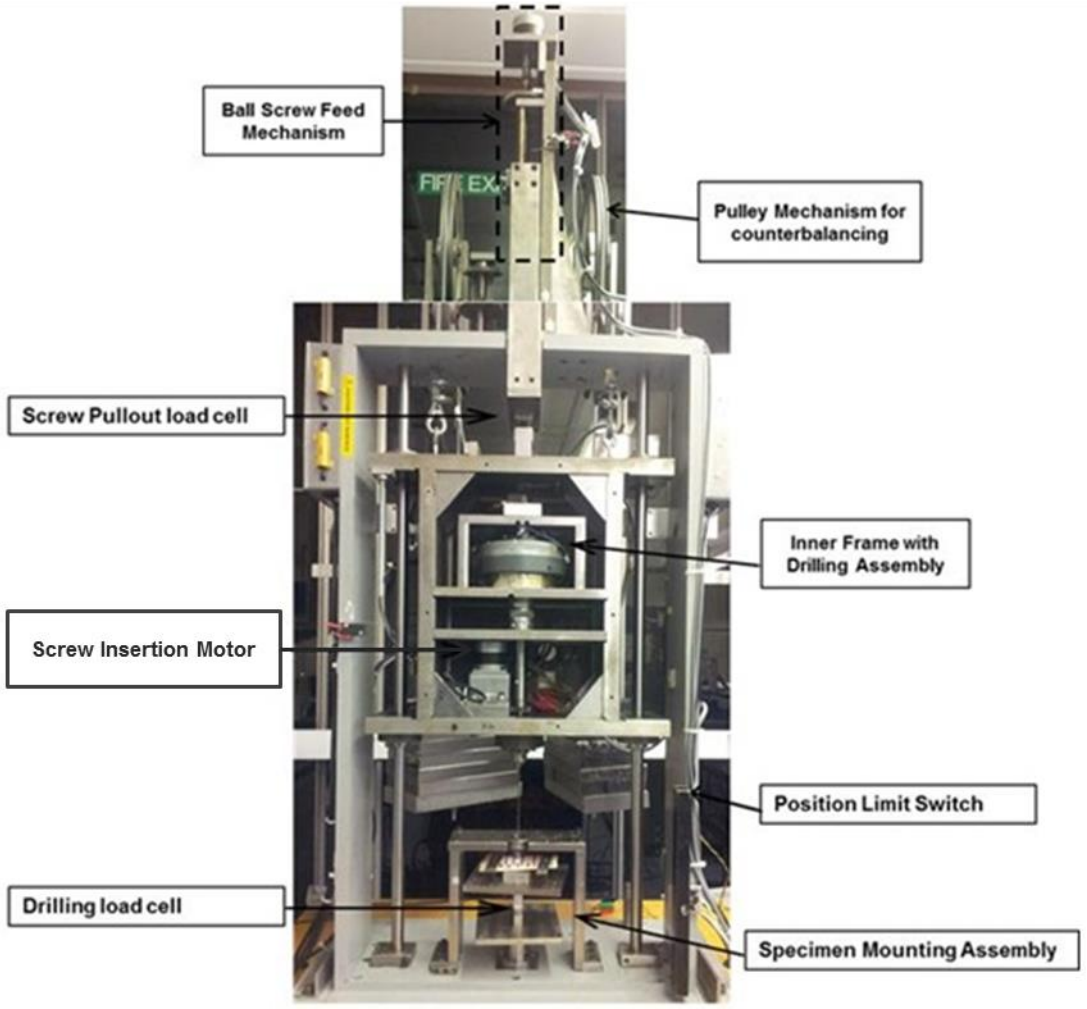

Figure 3-5 (a) Test Rig Components Used During Screw Insertion [136]**, (b) Test Rig**

3.3 Drilling Experiments

3.3.1 Aims

- *To investigate the effects of dryness and anatomic positions on the drilling thrust force.*
- *To investigate the effects of different drilling conditions on thrust force.*
- *To investigate the effect of material density on thrust force.*

3.3.2 Drilling Procedure

Drilling of femur bone and foam samples was carried out at feed rates between 40 mm/min and 282 mm/min, based on the assumption made about the approximate drilling time that a surgeon would take to perform drilling in clinics. The required drilling speed was provided by a speed feedback controlled DC servo motor. Drilling in the cortical bone specimens was carried out at drilling speeds of 800rpm, 1200rpm and 1500rpm, using 2.5 mm diameter industrial drill bits (Model A9762.2X95 Dormer UK). The speed range was chosen to reduce the generation of high temperature during drilling. All the experiments were performed at room temperature without cooling as in real orthopaedic surgery. The specification of the drill bit used is given in Figure 3-6. Industrial drill bits were used because they are inexpensive and easily available as compared to surgical drill bits. A diameter of 2.5 mm drill bits was used because it is a common size in orthopaedic surgery. The drilling force data was recorded at a sampling rate of 500Hz. Mounting arrangement for drilling is shown in Figure 3-7.

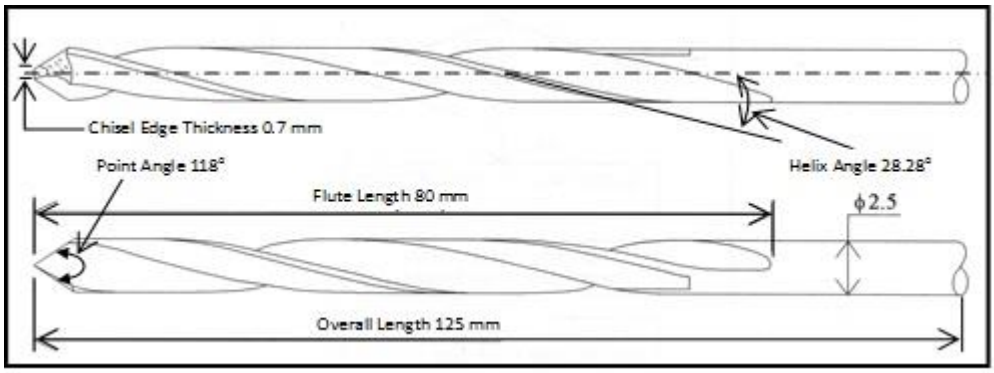

Figure 3-6 Drill Bit Specification

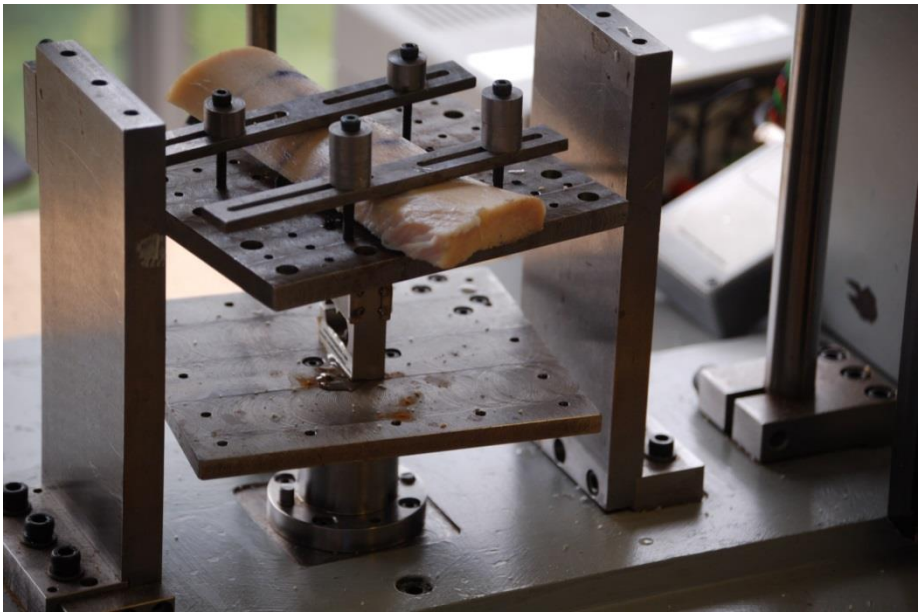

Figure 3-7 Specimens Mounting for Drilling

The sample size for the drilling experiments on each anatomical location and every foam density was calculated using Equation 3-1 [138].

$$n1 = \left(\frac{\bar{\sigma} z_{\alpha/2}}{e_r}\right)^2 \qquad 3\text{-}1$$

where $n1$ is number of drilled holes for each anatomical location, e_r is the margin of error, $z_{\alpha/2}$ is the critical value of the standard normal distribution (found in tables of standard normal distribution) and $\bar{\sigma}$ is the standard deviation of data.

The standard deviation of our experimental set up was calculated by drilling five holes in PU foam FR-6725 with the following conditions:

Drilling Feed = 150 mm/min,

Drilling speed = 800rpm, and

Sampling rate = 500 Hz.

The mean and standard deviations of the recorded averaged drilling force profile was calculated as:

$\bar{X} = 4.05,\ \bar{\sigma} = 0.06, \qquad z_{\alpha/2} = 1.96$

The margin of error acceptance was calculated as 0.05 N, and then the minimum number of holes (sample size) required for testing was calculated as:

$n = 2.35$

Hence, three holes drilled into one particular density of foam or one location of bone will give an accurate measurement of the drilling force. As bone thickness and structure are not homogeneous and vary from sample to sample, the mid-shaft region of the femur, which is more homogeneous, was selected for this research.

It is critical to know after how many holes the drill bit gets blunt and should be changed, and as there is no standard which gives such information a procedure was developed to identify when there is a need to change the drill bit. According to the adopted procedure, the drilling force recorded for the first hole in foam sample FR-6725 was taken as the reference drilling force value. After drilling ten holes into the different bone, a hole is then drilled into the foam sample FR-6725 and the recorded drilling force is compared with the reference value. If a significant difference was found between the two drilling forces, the drill bit was replaced; otherwise the same drill bit was used to drill another ten holes. In general, the drill bit was changed after 20 drilled holes.

3.4 Screw Pullout Testing

3.4.1 Aim

- *To investigate the efficacy of using thrust force to predict quality of the bone.*

Mechanical strength at the bone screw interface is an important factor in fracture treatment to obtain a rigid fixation. Fixation strength is described in terms of pullout strength of the screw, which is determined by the screw pullout test. Screw pullout strength is directly proportional to shear strength of material [144], therefore, a good correlation between pullout strength and thrust force will endorse the use of thrust force as predictor of bone quality.

3.4.2 Pullout Procedure

The same foam and femur cortical samples used in drilling were used for screw pullout. Surgical cancellous screws (Model No. 206.045, Synthes Ltd., UK) were used for foam sample, and surgical cortical screw (Model No 204.045, Synthes., UK) were used for cortical bone. The key dimension of surgical screws were measured using an optical microscope of 1 µm least count and are given in Figure 3-8.

Tapping of pilot holes (2.5 mm diameter) were done using a tap supplied by the manufacturer for the corresponding screw types used in this study. Both tapping and screw insertion were done at a constant speed of 10 rpm. The same method, as described above for drilling test in section 3.3.2, was used to calculate the minimum sample size required for screw pullout testing. The maximum force required to pullout the screws was recorded at a sampling frequency of 200 Hz. The screws were pulled out at a rate of 5 mm/min. Figure 3-9 shows mounting of bone specimen for screw pullout operation

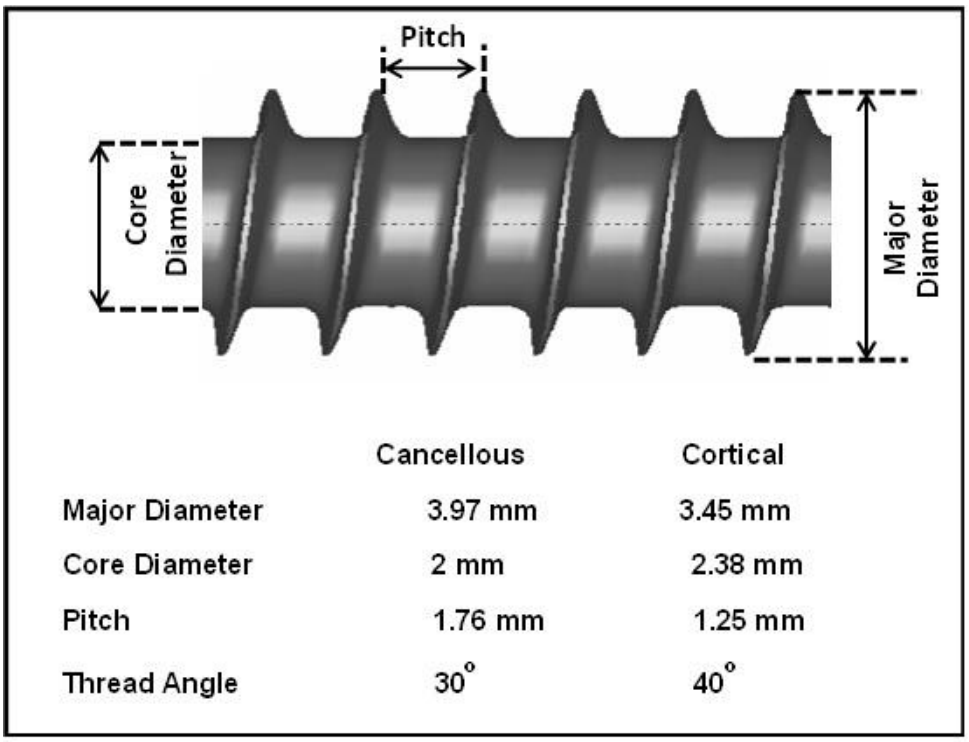

	Cancellous	Cortical
Major Diameter	3.97 mm	3.45 mm
Core Diameter	2 mm	2.38 mm
Pitch	1.76 mm	1.25 mm
Thread Angle	30°	40°

Figure 3-8 Dimensions of Surgical Screws

.

Figure 3-9 Mounting of Bone Specimen for Screw Pullout

3.5 Material Characterisation

The machining process involves high strain and high strain rate in very small deformation zones [139-141]. This causes the mechanical behaviour of the work piece material during drilling to be far different from that observed in quasi static tests. Therefore, the reliability of numerical modelling for drilling is heavily dependent upon accurate material constitutive law which depicts the above conditions. In this research the mechanical properties at high strain were obtained using split Hopkinson pressure bar apparatus.

3.5.1 Specimen Preparation

Bone samples were core drilled from the anterior portion of diaphysis in the both longitudinal and transverse direction of the bone axis. The samples were then machined on a lathe to a cylindrical shape of 10mm diameter and 5mm length. The thickness of the cylindrical specimen was small as compared to typical quasi-static test specimen, to facilitate dynamic stress equilibrium. These specimens were kept moist using saline solution of 4% to preserve the integrity of the bone. Figure 3-10 shows the cortical bone specimen for SHPB.

Figure 3-10 SHPB bone specimen

3.5.2 Dynamic Experimental Set-up

A split Hopkinson pressure bar (SHPB) was used to conduct the dynamic compressive experiments. A schematic of SHPB facility is shown in Figure 3-11. For cortical bone, steel bars were used and for PU foam magnesium alloy ZK 60 bars were used. The lengths of bars used for experiments were 1 m each for the incident and transmitter bars, with a common diameter of 12 mm. Deviating from the original Kolsky specification, a pre-loading bar of lower strength has been added prior to incident bar to reduce the presence of Pochhmammer-Chree oscillations [142]. These arise due to Fourier components of pulse suffering elastic wave dispersion as consequence of fact that the velocity of wave in a bar depends on its wavelength relative to the bar diameter. Therefore, after sufficient time of propagation along the bar, the higher frequency components of pulse will begin to lag behind the leading edge, resulting in these high frequency oscillations being superimposed on the original wave front. Due to these oscillations the localised regions of the specimen may experience stress and strain histories that differ substantially when compared to the average behaviour of the sample as whole. Thus the addition of a pre-loading bar of lower strength has the effect of damping the oscillations before they can reach the incident bar. At the terminus of the apparatus layout, a final bar has been placed in direct contact with the transmission bar. The function of this bar is to convey the momentum remaining after the initial stress wave propagation away from the experimental field. Failure to achieve this would result in multiple unwanted tensile and compressive waves continuing to travel in pressure bars.

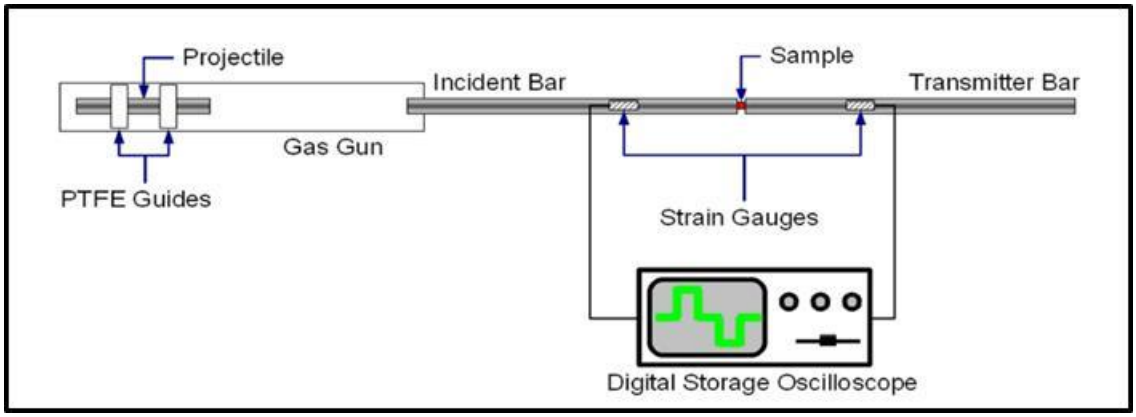

Figure 3-11 Schematic of SHPB Apparatus

Transient stress pulses are generated in the apparatus by the ballistic impact of the projectile, fired from the adjoining gas gun. The projectile consists of a 25 mm cylinder, surrounded by a PTFE carriage that is closely fitting in the gas gun barrel whilst still allowing easy movement. PTFE is used in order to ensure a relatively frictionless passage of the projectile along the length of the gas gun, which is itself a steel tube. A vacuum is created in the gas gun by means of a rotary pump and associated conduits, together with a series of valves that enable each section to be isolated independently.

Measurements of pulses propagating in the pressure bars are made by two pairs of strain gauges affixed on both bars, at equidistant points 40 cm on each side of the specimen position. The gauge pair located on the incident bar observes both the incident compressive pulse generated by impact, together with any reflected pulse after interaction with the sample. The pair of gauges on the transmission monitors any of the pulse that transmitted through the sample. A constant current of 20 mA is maintained across the gauges by stabilized voltage supply and resulting voltage deflections representing compressive or tensile pulse are generated by simple potential divider circuits.

3.5.3 Theory of SHPB

In order to determine the stress-strain behaviour of the material, both the pulse reflected from, and the pulse transmitted through the sample must be observed. This was achieved using strain gauges, and implies that the pulses recorded were that of strain in the bars.

The one dimensional theory of elastic wave propagation has been used by Kolsky [143] in derivation of equations (3-11 and 3-15) to calculate engineering strain and stress with the following assumptions:

1. Wave dispersion is negligible.

2. The stress and strain fields in specimen are homogeneous.

3. The radial inertia and friction effects are negligible.

4. The end surfaces of specimen are flat and in perfect contact with bars for the duration of experiment.

$$\sigma = \rho c_0 \dot{u} \qquad 3\text{-}2$$

and thus

$$\dot{u} = \frac{\sigma}{\rho\, c_0} \qquad 3\text{-}3$$

where $\dot{u}$ is the particle velocity, σ is the stress, ρ is the density and c_0 is the elastic wave velocity. As $c_0 = \sqrt{E_b/\rho}$, in which E_b is the elastic modulus of the pressure bars, this leads to:

$$\dot{u} = \frac{\varepsilon E_b}{\rho\sqrt{E_b/\rho}} = c_0 \varepsilon \qquad 3\text{-}4$$

3-4 integration with respect to time (t) therefore yields displacement (u):

$$u = c_0 \int_0^t \varepsilon dt \qquad 3\text{-}5$$

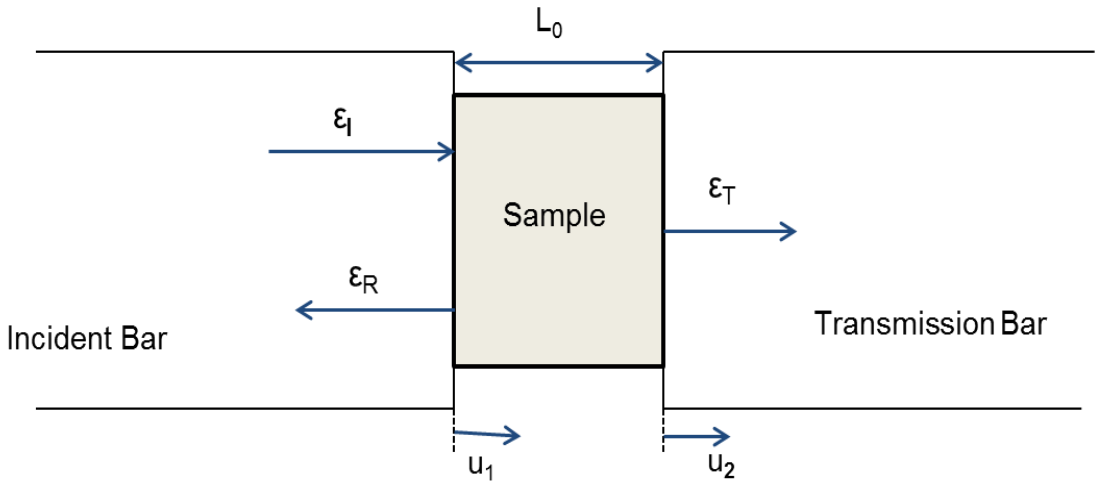

Figure 3-12 Schematic of Strain Pulses on a Sample

Figure 3-12 depicts the sample during a typical experimental scenario. ε_l, ε_R and ε_T correspond to the incident, reflected and transmitted pulses of strain respectively, whilst u_1 and u_2 refer to the displacements of the ends of the two pressure bars. L_0 is the initial length of the sample.

The displacement of the face of the incident bar (u_1) is the result of the both the incident pulse, travelling in positive direction, and the reflected pulse travelling in opposite direction.

$$u_1 = c_0 \int_0^t (\varepsilon_l - \varepsilon_R) dt \qquad 3\text{-}6$$

Displacement u_2 of the face transmitter bar is due to the transmitted pulse, and can be represented as:

$$u_2 = c_0 \int_0^t \varepsilon_t \, dt \qquad 3\text{-}7$$

The engineering strain (ε_e) of the specimen is therefore:

$$\varepsilon_e = \frac{u_1 - u_2}{L_0} \qquad 3\text{-}8$$

and substitution yields:

$$\varepsilon_e = \frac{c_0}{L_0} \int_0^t (\varepsilon_l - \varepsilon_R - \varepsilon_T) dt \qquad 3\text{-}9$$

As L_0 approaches zero, it can be assumed that the stress across the sample becomes constant. By neglecting time delay due to wave propagation implies that the forces acting perpendicular to the bar faces are equal. Hence it can be assumed that:

$$\varepsilon_T = \varepsilon_l - \varepsilon_R \qquad 3\text{-}10$$

The relationship can be applied to equation 4.8 resulting in:

$$\varepsilon_e = \frac{2c_0}{L_0} \int_0^t \varepsilon_R \, dt \qquad 3\text{-}11$$

Thus the sample engineering strain can be determined through integration of the reflected pulse and application of the constants c_0 and L_0.

Similarly, the forces F_1 and F_2 applied to both faces of the specimen are given by:

$$F_1 = E_b A_0(\varepsilon_l + \varepsilon_R) \qquad 3\text{-}12$$

and

$$F_2 = E_b A_0 \varepsilon_T \qquad 3\text{-}13$$

where A_0 is the cross-sectional area of the pressure bar.

The engineering stress (σ_e) within the sample is therefore:

$$\sigma_e = \frac{E_b A_0}{2A_s}(\varepsilon_l + \varepsilon_R + \varepsilon_T) \qquad 3\text{-}14$$

here A_s is the cross-sectional area of the sample. Again considering the equation 3-4, this becomes:

$$\sigma_e = \frac{E_b A_0}{A_s}\varepsilon_T \qquad 3\text{-}15$$

Thus it can be seen that engineering stress is directly proportional to the transmitted strain. Once engineering stress and strain of the specimen had been established, true stress and strain was achieved as:

$$\varepsilon_t = \ln(1 \pm \varepsilon_e) \qquad 3\text{-}16$$

where ε_t and σ_t are the true strain and stress respectively. The ± symbol is included to denote the difference between tensile and compressive deformation characteristics.

$$\sigma_t = \sigma_e(1 \pm \varepsilon_e) \qquad 3\text{-}17$$

3.5.4 SHPB Experimental Procedure

When conducting the experiment, it was first necessary to ensure the axial alignment of the bars. This was achieved by stretching a piece of string along the

entire length of the apparatus and adjusting the bar to be as parallel with the string as possible, and also by shining light through the bar interfaces in order to check that no gaps are present.

A thin film of MoS_2 grease was applied to both faces of the specimen in order to minimise the impact of friction. Then, the sample was sandwiched between the incident and transmitter bars. Once the sample had been positioned as desired, the projectile was loaded into the gas gun breech and the system was evacuated. The required apertures were selected and uncovered prior to loading in order to achieve a strain rate in the range required.

With the required vacuum achieved the oscilloscope was set to a single sequence record mode and the gas gun was suddenly opened to atmosphere by rapidly uncovering the aperture plate. The sudden influx of air into the gas barrel propels the projectile, initiating the experiment and data collection.

The duration of an experiment is very much dependant on the material being tested; a typical duration for this experiment would be of the order of 1 ms. For this work a Shimadzu HPV-1 camera was loaned from the Engineering and Physical Sciences Research Council (EPSRC) engineering instrument loan pool. It is capable of recording at speeds of between 30 and 1,000,000 fps and captures a total of 100 greyscale images at a resolution of 312x260 pixels. It consists of a camera recording head to which any lens using the Nikon F-mount SLR format may be attached, and a separate Microsoft Windows XP computer which runs software to receive and store the images from the camera. The CCD (Charge-coupled device) is unique to Shimadzu, and has the capability to store 100 full size images on the chip itself, which are streamed to the computer post capture.

3.6 Concluding Remarks

In this chapter details of the different experimental techniques and materials used as well as reasons for using specific types of bone and foam for different experiments are given. A detailed explanation of the drilling/screw pullout test rig and the Split Hopkinson pressure bar apparatus, as well as details about different conditions used in the drilling and screw pullout experiments and the theoretical background of SHPB, provide in depth information about the experimental set-up. Such set-ups and methods discussed in the chapter are used in the next chapter to carry out the relevant experiments and analyse the results.

CHAPTER 4

Experimental Results

The results of the experimentation carried out for this research are presented in this chapter. The overall experimental programme was described in chapter 3 and consisted of the drilling and screw pullout testing of cortical bone and foam, and characterisation of cortical bone mechanical properties at high strain rate. The results of the cortical bone drilling, at different anatomical positions, in wet and dry conditions, of two different animals (cow and pig) and with different drilling conditions are presented in first part of this chapter. These results are used to investigate the efficacy of thrust force data in the prediction of bone quality. These results are also used to validate the FE and analytical models in chapters 5 and 6. Similarly drilling force results for rigid polyurethane mimicking cancellous bone with different densities are presented in this chapter. Screw pullout results, as a representation of the material's shear stress, and the relationship between drilling force and normalised screw pullout force for the cortical bone and PU foam samples used are also presented in this chapter. The results of the bone high strain rate testing for characterisation of mechanical properties are discussed in the last section of this chapter.

4.1 Drilling of Cortical Bone

The first set of experiments was conducted on locations 1 to 7 of an anterior portion of bovine diaphysis to investigate the variation of drilling results within the same anatomical position, at a constant speed of 800 rpm and a feed rate of 150 mm/min. The drilling force was recorded at a sampling rate of 500 Hz. A typical single cortex drilling force profiles of the bovine femoral shaft is shown in Figure 4-1.

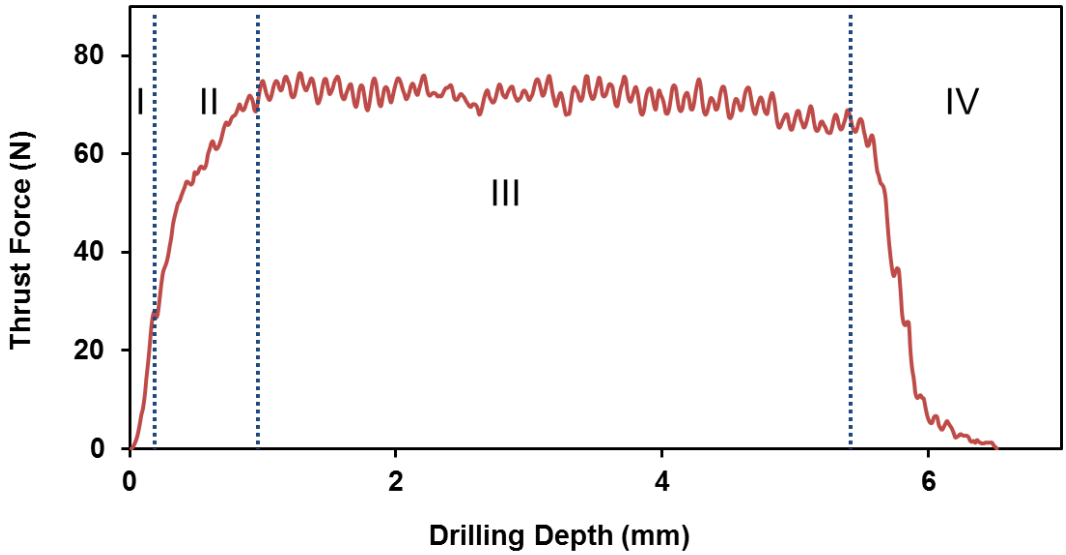

Figure 4-1 Drilling force profile of bovine single cortex at feed rate of 150 mm/min and rotation of 800rpm

The drilling profile is divided into four zones. Zone I shows the penetration of drill bit, which can be seen by a sharp rise in the drilling force. Zone II shows the start of material removal by the chisel edge and the main cutting edge with gradual rise in thrust force upon drill bit entry into the anterior cortex. The Drill bit is fully engaged at the end of zone II and throughout zone III. The average maximum drilling force is calculated in zone III, and Zone IV shows a gradual drop in thrust

force as the drill bit exits the cortex. A small variation in the drilling force magnitude is observed throughout the drilling process, which could be due to the system stiffness, vibration of drill tool and porous nature of bone. Similar drilling force profiles having different drilling force magnitudes were observed for all the drilling conditions considered in this study. Figure 4-2 shows the typical drilling profile for pig femur at feed rate of 150 mm/min and rotation of 800 rpm.

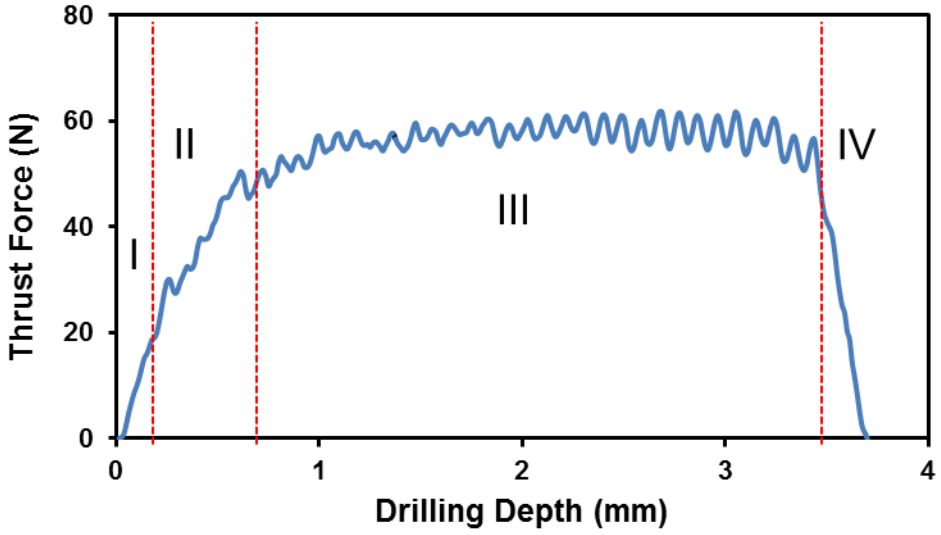

Figure 4-2 Drilling force profile of pig single cortex at feed rate of 150 mm/min and rotation of 800rpm

Figures 4-3 a to g show the drilling force proiles of the anterior portion of bovine cortex for locations 1 to 7 (given in Chapter 3); Figure 4-3a is for location 1, 4-3b for location 2 and so on . As bone is anisotopic in nature, its strength varies from proximal end to distal end within the mid diaphysis. Location 1 is near the proximal end where the bone quality is different from location 4 which is at the centre of the diaphysis. Table 4-1 shows the force at the 1st complete rotation for the drill bit, the average maximum force in zone III and the standard deviation of the average

maximum force. A maximum force of 79N is observed at location 1 (Figure 4-3a). The average maximum force at the proximal (locations 1 and 2) and distal ends (locations 6 and 7) are more than at the centre (locations 4 and 5) of the cortex. The average maximum drilling force from location 1 to location 7 ranges from 64N to 73N. The drilling thrust force at the 1st complete rotation of the drill bit, given in Table 4-1, shows similar trends as the average maximum force. These results also show that the change in bone quality or strength can be easily detected by a change in drilling force with the same drilling conditions, and thus proves the efficacy of using the drilling force for quality prediction. The average thickness of the bone used for the drilling tests is between 5 to 8 mm from locations 1 to 7.

Table 4-1 Drilling force data for anterior cortex at 150 mm/min and 800 rpm

Drilling Location	Drilling Force		
	1st rotation (N)	Average Maximum (N)	Standard Deviation of Average Maximum
1	27 ± 3	73	2.3
2	24 ± 3	71	2.1
3	17 ± 2	70	2.4
4	13 ± 2	68	2.5
5	15 ± 2	64	2.0
6	24 ± 2	70	2.4
7	22 ± 3	72	2.2

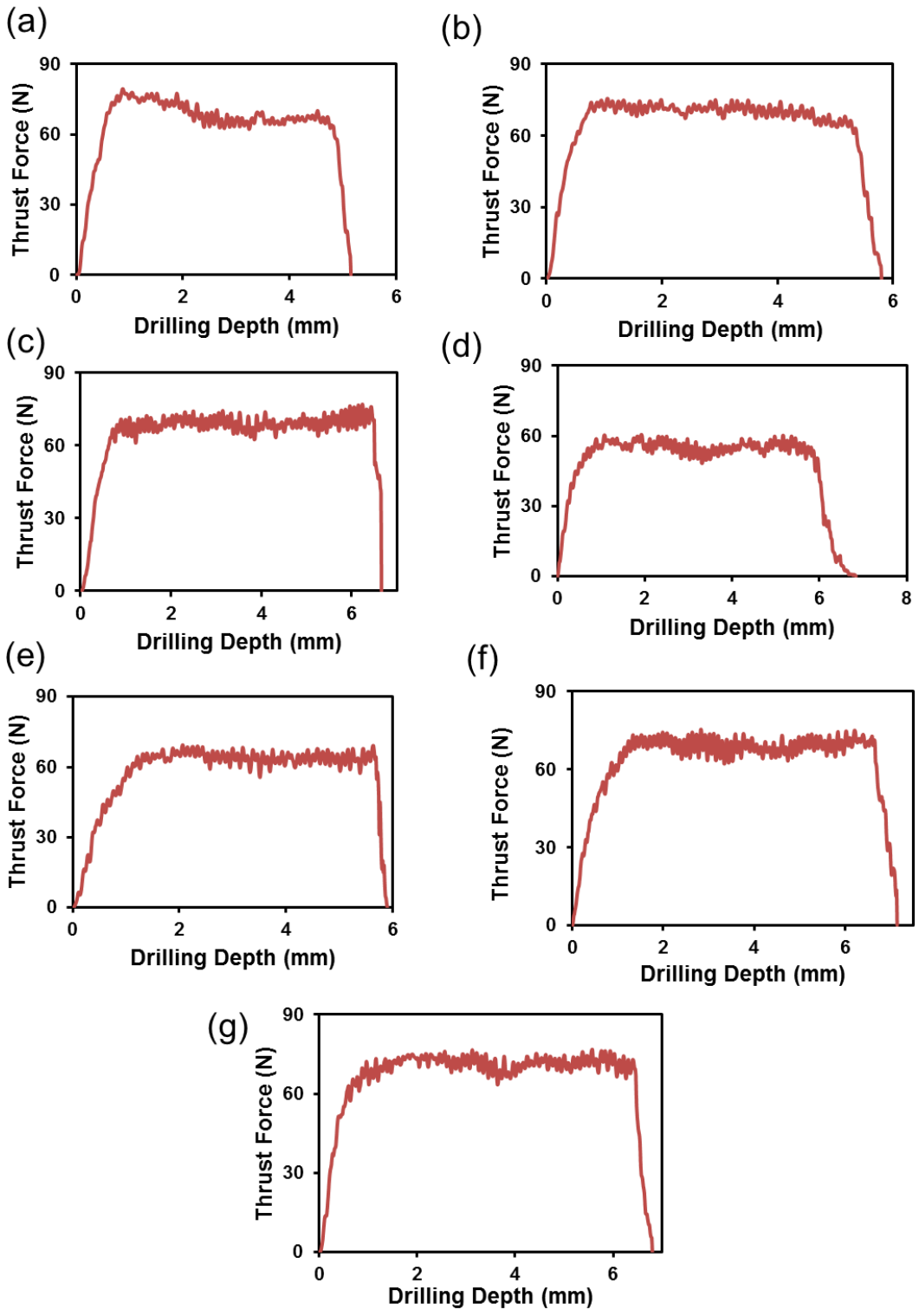

Figure 4-3 Drilling force profiles of anterior bovine cortex at locations 1-7 (a-g) with feed rate of 150 mm/min and rotation of 800rpm

4.1.1 Drilling Force at different Anatomic Positions

Drilling tests were conducted on different anatomic positions of bovine and pig femur bone samples as described in chapter 3, at the same feed rate of 150mm/min and the rotational speed of the 800rpm (i.e. 0.1875mm/rev). Figure 4-4 shows the variation of drilling force for different anatomic positions of the same bovine femur bone. The drilling force at the anterior cortex is the largest, followed by medial and posterior cortices respectively. Similar trends were observed for different anatomic positions of the same pig femur bone as shown in Figure 4-5. The obtained experimental results for the drilling data of the anterior, medial and posterior cortices are well correlated with the literature. Li *et al.* [145] suggested that the anterior and medial locations have a higher stiffness than at the posterior location to sustain a high stress environment. They observed that the changes in the volume fraction of constituents at microstructural level affected considerably the local material properties such as elastic modulus, yield stress, and ultimate strength, which in turn, influenced the drilling force.

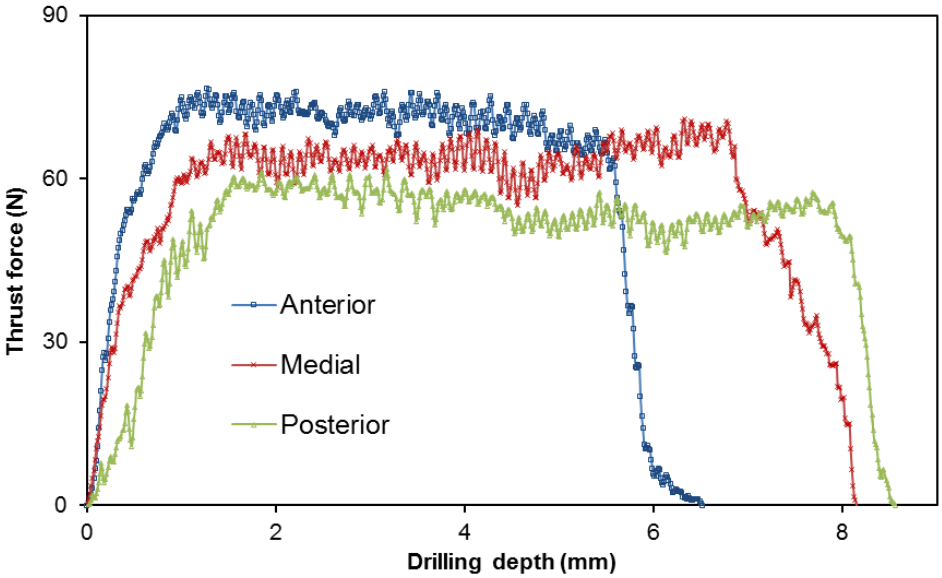

Figure 4-4 Drilling force profile of different anatomic positions of bovine femur at feed rate of 150mm/min and rotation of 800rpm

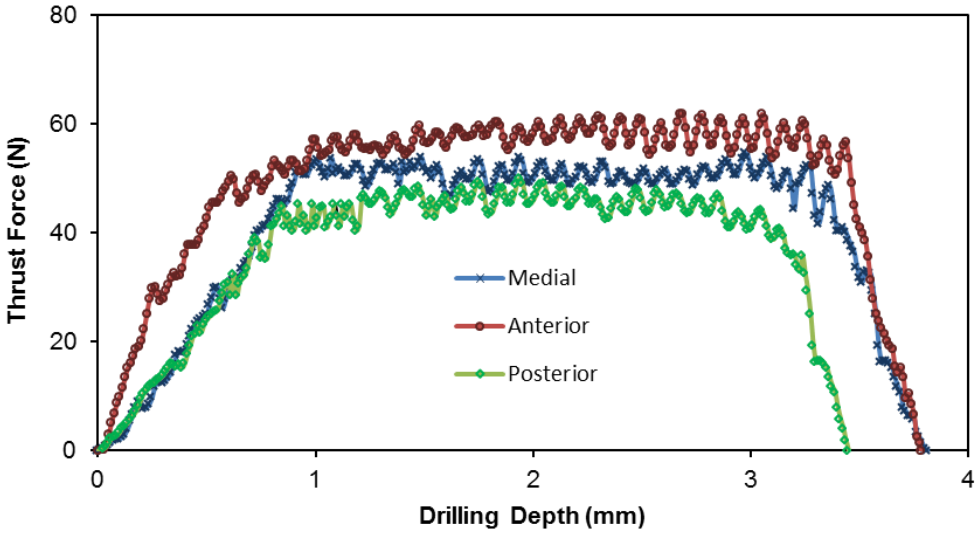

Figure 4-5 Drilling force profile of different anatomic positions of pig femur at feed rate of 150mm/min and rotation of 800rpm

Figure 4-6 shows that the anterior portion of cortex is predominantly occupied by primary osteons; the medial portion has a mixture of both primary and secondary osteons; whereas the posterior portion predominantly consists of secondary osteon together with interstitial matrix. This also demonstrates the capability of drilling force data to predict the quality of bone.

Figure 4-7shows the comparison of the drilling force at feed rate of 150mm/min and rotational speed of 800rpm for different anatomic positions of bovine and pig femur bones. The average maximum thrust force of bovine and pig femur were found to be 75±5 N and 57±10 N for the anterior portion, 70±4 N and 56±5 N for the medial portion, and 62±5 N and 52±5 N for the posterior portion respectively. The thrust force of bovine femur at these drilling conditions is greater than pig femur by 31% in the anterior portion, by 25% in the medial portion, and by 19% in the posterior portion.

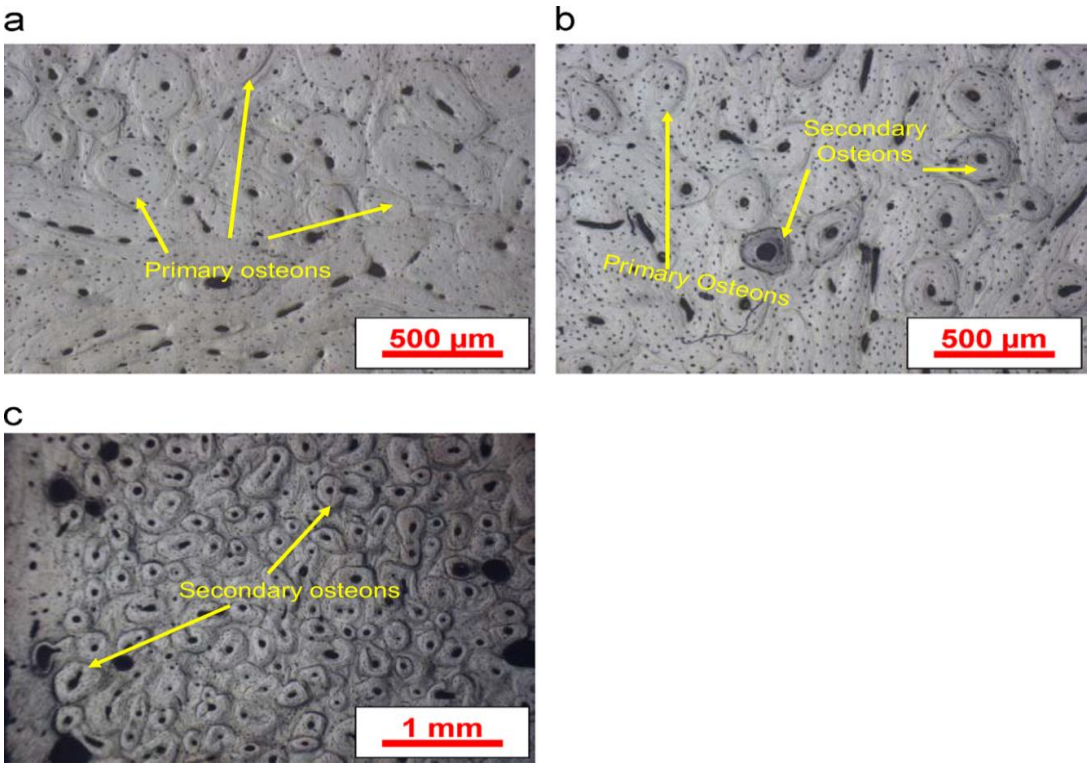

Figure 4-6 Representative microstructural features of different cortex positions: (a) anterior; (b) medial; (c) posterior [146]

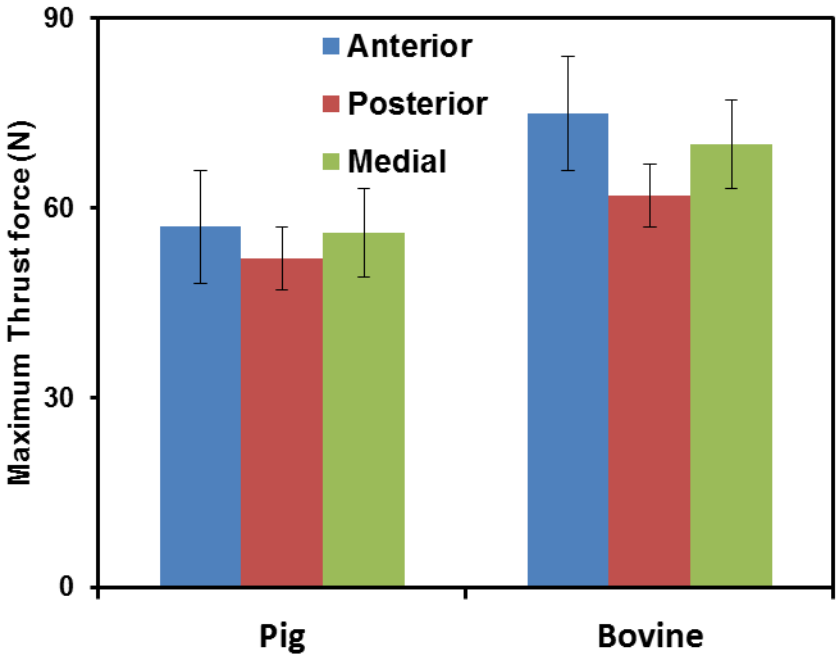

Figure 4-7 Comparison of drilling thrust force at different anatomic positions of pig and bovine femur at feed rate of 150mm/min and rotation of 800rpm

4.1.2 Drilling of Dry Bone

Early studies demonstrated that the stiffness, tensile strength, and hardness increases, whereas the strain at fracture and energy to fracture decreases, following the dehydration of bone tissues. To study this, bone drilling experiments on dry bone have been conducted at the same feed rate and rotational speed, i.e. at a feed rate of 150mm/min and rotational speed of 800rpm. The anterior portion of bovine femur was dried at room temperature for one day before testing. The results are given in Table 4-2. The drilling force at every location of the dry bone is increased by more than 100 % compared to wet bone. Nyman *et al. (2006)* [147] suggested that the water loss caused by drying at room temperature increased the strength of bone.

Table 4-2 Comparison of dry and wet anterior cortex at the feed rate of 150mm/min and rotational speed of 800rpm

Drilling Location	Drilling Force		
	Average Maximum Dry Bone (N)	Average Maximum Wet Bone (N)	Increase %
1	165	73	126
2	162	71	128
3	158	70	125
4	140	68	105
5	133	64	107
6	158	70	125
7	162	72	125

4.2 Effects of Drilling conditions on Thrust force and Torque

To validate the FE and analytical models, drilling experiments on the anterior portion of bovine femur were conducted. The drilling was carried out at feed rates between 40 mm/min to 282 mm/min, based on the assumption made about the approximate drilling time that a surgeon would take to perform drilling in clinics. The required drilling speed was provided by a speed feedback controlled DC servo motor.

Drilling was carried out at drilling speeds of 800rpm, 1200rpm and 1500rpm, using a 2.5 mm diameter industrial drill bit (Model A9762.2X95 Dormer UK). This speed range was chosen to reduce the generation of high temperature during drilling. Drilling parameters used in the experiments are provided in Table 4-3. All the experiments were performed at room temperature without cooling as in real orthopaedic surgery.

Table 4-3 Machining parameters used in drilling of anterior bovine cortex

Drill bit	HSS, ⌀ 2.5 mm, point angle 118°
Spindle speed (rpm)	800, 1200, 1500
Feed (mm/rev)	0.05, 0.1,0.15, 0.1875

Figure 4-8 shows the effect of feed, expressed in drill bit displacement per revolution (mm/rev), on the average maximum thrust force. The thrust force was between 28N and 70N for feeds between 0.05 and 0.1875 mm/rev.. Similar to other studies, the obtained results show that drilling thrust force increases with increasing feed.

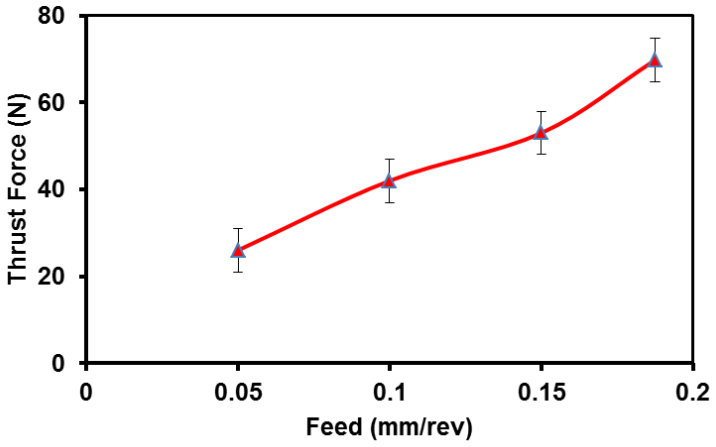

Figure 4-8 Effect of feed on thrust force (with error bar of fixed value ± 5)

It can also be observed from Figure 4-8 that at a feed of 0.1875mm/rev (obtained from a spindle speed of 800rpm and a feed rate of 150mm/min), the average maximum thrust force was the highest, and lowest at a feed of 0.05mm/rev (obtained from a spindle speed of 800rpm and a feed rate of 40mm/min). Comparing the levels of thrust force for different feed values, it was observed that when the feed was increased from 0.05mm/rev to 0.1mm/rev (i.e. from 40mm/min to 80mm/min at 800rpm spindle speed) the thrust force increased by 60% and when the feed was increased from 0.1mm/rev to 0.15mm/rev (i.e. from 80mm/min to 120mm/min at 800rpm spindle speed) the thrust force increased by 83%. The effect of drilling speed on torque and force was also examined. The torque decreased significantly (1.2 to 1.6 N-cm), as the spindle speed was changed from 800rpm to 1500rpm for a feed rate of 150mm/min, as shown in Figure 4-9.

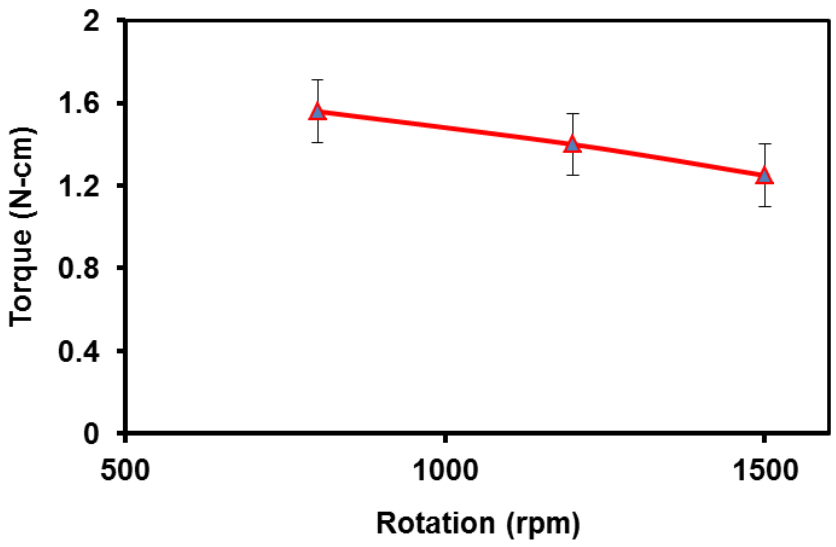

Figure 4-9 Effect of rotation on torque at a feed rate of 150mm/min (with error bar of fixed value ± 0.15)

This trend was observed for all the feed rates used in this study. However, the effect of feed, in mm/rev, on the torque is negligible as shown in Figure 4-10. Comparing the level of torque for different feed values, it was observed that when

the feed was increased from 0.05mm/rev to 0.1875mm/rev (i.e. increased from 40mm/min to 150mm/min at a spindle speed of 800rpm) the torque increased by only 6%.

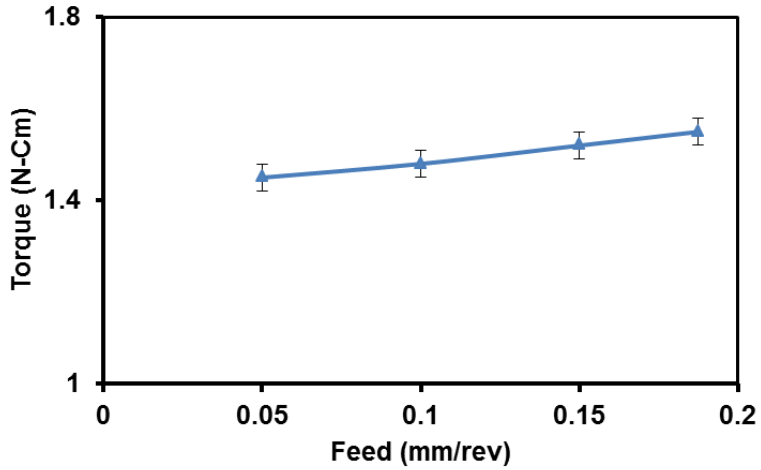

Figure 4-10Effect of feed on torque (with error bar of fixed value + 0.02)

Also, similar to the effect of the spindle speed on the torque, the thrust force decreased as the spindle speed was increased from 800rpm to 1500rpm at a feed rate of 150mm/min, as shown in Figure 4-11. Such a trend was observed for all the feed rates used in this study.

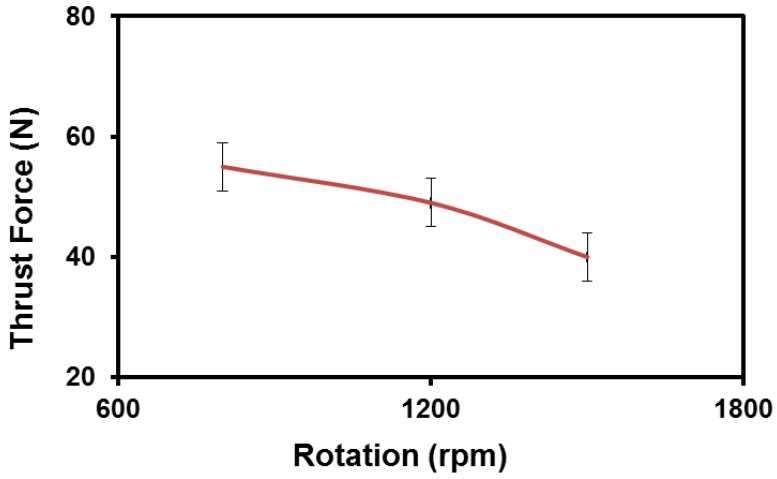

Figure 4-11 Effect of rotation on thrust force at a feed rate of 150mm/min (with error bar of fixed value ± 5)

4.3 Comparison to Previous Studies

Current findings for maximum thrust force and torque have been compared to those reported by others as shown in Table 4-4 (Wiggins *et al.* 1976, Natali *et al.* 1996, Ong *et al.* 1999, 2000, Hillery *et al*. 1999, Tsai et al. 2007, Alam *et al*. 2011, Lee *et al*. 2012, MacAvelia *et al.* 2012) [11, 94, 100, 103, 104,111, 148, 149]. The presented force and torque results overlap with some reports (Alam *et al.* 2011, Lee *et al.* 2012) which have values up to 70N and 3.8Ncm respectively. The difference between the experimental results of various studies arise from the wide variety of test conditions used by researchers regarding drill-bit diameter, drill-bit type, rotational speed, feed rate and bone type.

Table 4-4 Comparison of presented results with respect to previous studies

STUDY	MATERIAL	RESULT
		Force (N)
Present	Bovine femoral shaft	25 to 75
Wiggin and Malkin	Human femoral shaft	2 to 300
Natali et al.	Human tibial shaft	10 to 20
Ong and Bouazza-Marouf	Porcine vertebra	0.6 to 29.6
Tsai et al.	Human femoral trochanter	0 to 5
Ong and Bouazza-Marouf	Porcine femoral trochanter	2 to 24
Ong and Bouazza-Marouf	Porcine femoral head	4 to 32
Alam et al.	Bovine femoral shaft	24 to 70
Hillery and Shuaib	Bovine tibial shaft	24 to 48
Lee et al.	Bovine tibial shaft	0 to 20
Salahi et al.	Human femoral shaft	176 to 198
		Torque (N.cm)
Present	Bovine femoral shaft	1.2 to 1.6
Wiggin and Malkin	Human femoral shaft	0.2 to 12
Tsai et al.	Human femoral trochanter	0 to1
Alam et al.	Bovine femoral shaft	1 to 2.3
Hillery and Shuaib	Bovine tibial shaft	1 to1.45
Allota et al.	Porcine femoral shaft	5.5
Lee et al.	Bovine tibial shaft	0 to 3.8
Salahi et al.	Human femoral shaft	14 to 18

4.4 Drilling of PU Foam (Synthetic Bone)

Drilling of PU foam was conducted at a constant speed of 800 rpm and a feed rate of 150 mm/min was selected based on the discussion in section 3.1.4. The drilling force was recorded at a sampling rate of 500 Hz. A typical drilling profile of the PU foam is shown in Figure 4-12. The noise observed in the experimental data may be due to the porous nature of the foam.

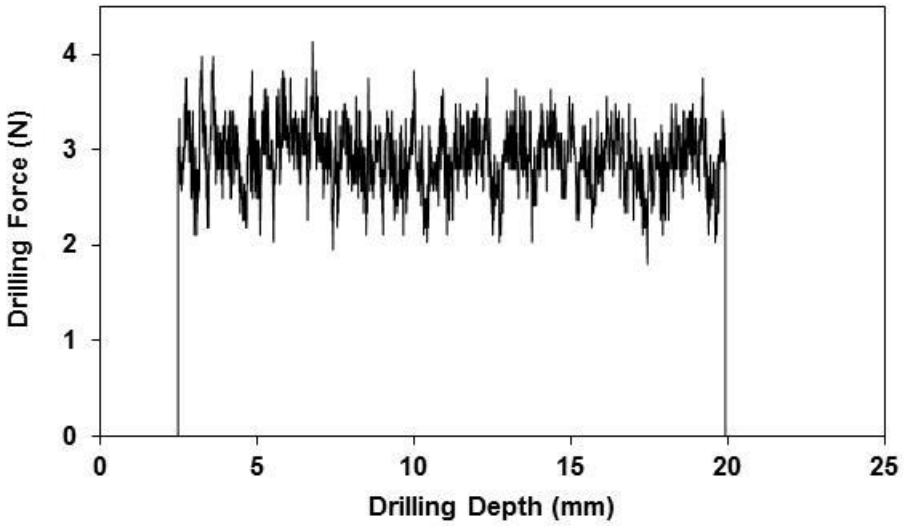

Figure 4-12 Typical drilling Force Profile of FR-6720

Similar drilling force profiles having different drilling force magnitudes were observed for all the ten holes drilled into the foam samples with different densities. The recorded averaged drilling force and shear strength data from the manufacturer (General Plastic) for FR-6700 series PU foams is presented in Table 4-5. The Average drilling force increased with increase of density and shear strength, which mean drilling force is related to the strength of material. According to Jacob *et al.* (1976) [93], Mauch and Lauderbaugh (1990) [120] specific cutting energy is a

function of shear strength. These Results also shows the potential of using drilling force data to detect the quality of bone.

Table 4-5 Averaged Drilling Force of FR-6700 series foam

Sample Model	Sample Density (g/mm^3)	Shear Strength (MPa)	Sample Thickness (mm)	Drilling Force (N)	Standard Deviation
6715	0.2403	3.28	19.00	2.25	0.072
6718	0.2884	4.20	19.10	2.91	0.051
6720	0.3204	4.71	18.80	3.06	0.032
6725	0.4005	6.75	19.10	4.15	0.063

4.5 Screw Pullout of Cortical Bone

From the experimental results presented in the previous section, it is established that drilling is a significantly good predictor of the quality. Foam is a homogeneous material; therefore shear testing and drilling could be done at different locations to find the correlation between the two. However, bone is anisotropic and to avoid non-site specific correlations it is important to do the shear testing at the site of drilling. But, shear testing is destructive in nature and therefore cannot be done at the site of drilling. On the other hand, screw pullout testing, which gives an indication of bone strength, can be performed at the site of drilling. Hence, it is important to investigate the correlation between screw pullout strength and drilling in bone.

Holes drilled in the experiments described in sections 4.1, 4.2 and 4.3 were used as pilot holes for screw insertion. Therefore, the drilling force data as given in those sections is used in this study. Tapping of pilot holes (φ2.5 mm diameter) were

done using a tap supplied by the manufacturer for the corresponding screw type used in this study. Tapping of holes, using a tap, was selected over using the self-tapping screws because pre-tapping decreases the stress and potential damage applied to the surrounding material and decreases the shearing forces on the screw during insertion. Screws were pulled out using the designed test rig according to the process described in the previous Chapter (Section 3.4). The screws were pulled out at a rate of 5 mm/min (as per ASTM F543-02). A typical screw pullout force profile for single cortex is shown in Figure 4-13.

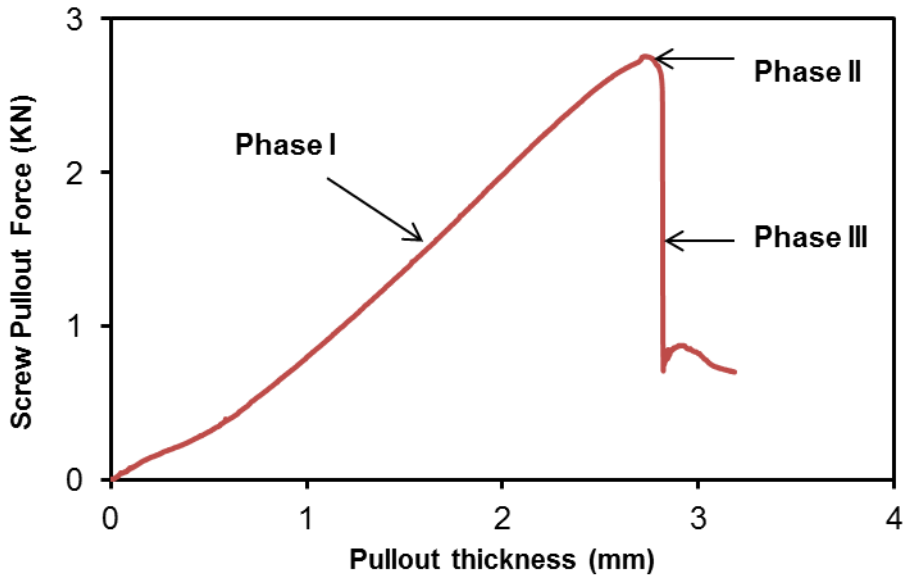

Figure 4-13 Screw pullout profile in bovine cortex at rate of 5mm/min

This curve has three distinct phases; in phase 1 gradual increase of pullout force is observed. In phase 2 a peak force is achieved and thread failure occurs. After failure, in phase 3, there is a sudden drop of force. A slight rebound of screw is observed; this is due to a sudden movement of the screw and test rig immediately after failure. Similar types of curves, with different magnitudes, were observed for each bone sample. The maximum screw pullout force depends upon the specimen

thickness; therefore it was normalised by dividing the force by the specimen thickness. Table 4-6 give a summary of the averaged maximum screw pullout force, average thickness at the specific location of the hole, and the normalised screw pullout force of the anterior portion of bovine bone. The table shows that the pullout force increases with increase of thickness, because the number of thread contacts increases with increase in thickness. The normalised screw pullout force (F_{NSP}) with respect to the thickness is ranges between 444-456N. Figure 4-14 shows the comparison of the normalised screw pull out force at a pullout rate of 5mm/min for different anatomic positions of bovine and pig femur samples.

The average normalised screw pullout force of bovine and pig femur were found to be 450±20 N and 238±12 N for the anterior portion, 430±25 N and 214±10 N for the medial portion, 422±20 N and 205±20 N for the posterior portion respectively. The normalised screw pullout force of bovine femur at these conditions is greater than pig femur by 47% in anterior portion, by 50% in medial portion, and 51% in posterior portion. These results suggest that anterior portion of femur has more fixation strength than medial and posterior. Figure 4-15 shows the comparison of normalised screw pullout force results of dry and wet anterior femur with same pulling conditions. Normalised pullout force of dry bone is larger than wet bone by more than 6%.

Table 4-6 Screw pullout force for anterior portion of bovine femur

Cortical Bone	Screw Pullout Test Results		
Thickness (mm)	**Screw Pullout Force** (N)	**Standard Deviation** (N)	**Screw Pullout Force/ Thickness** (N/mm)
6.15	2756	5.1	448
5.5	2447	6.7	444.9
6.2	2776	4.5	447
8.5	3806	6.5	455
8.6	3885	6.2	451
8.55	3882	8.3	453
9.0	4106	9.1	456

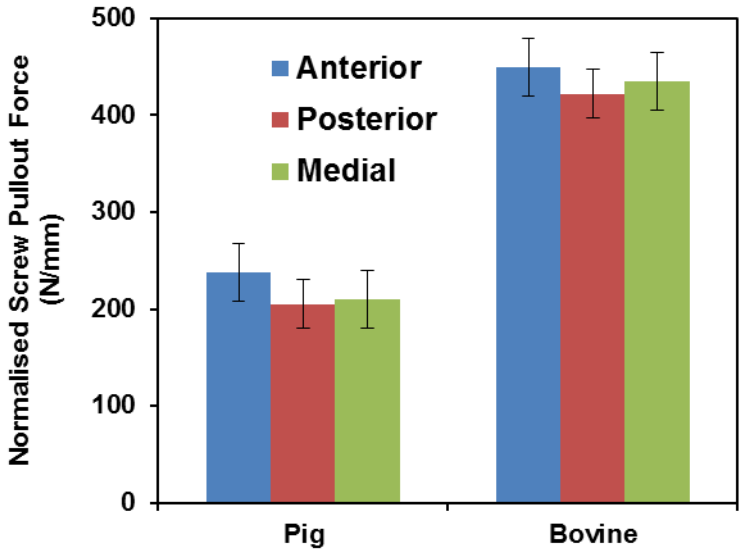

Figure 4-14 Normalised screw pullout force at different anatomic positions of pig and bovine femur at pullout rate of 5mm/min

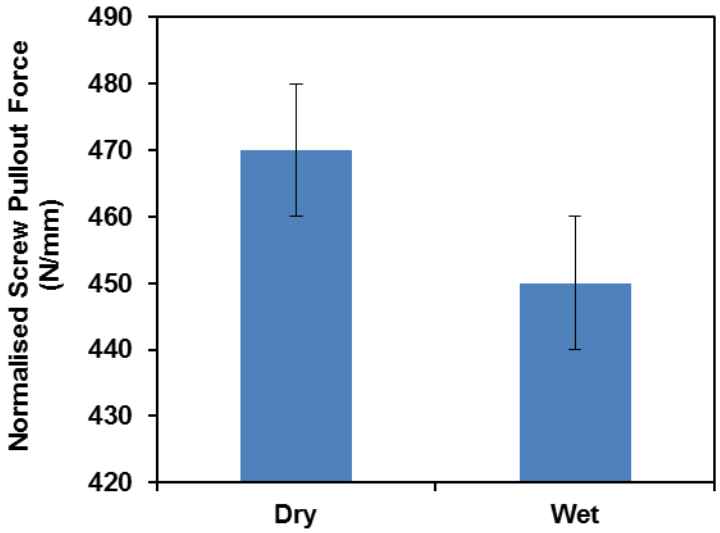

Figure 4-15 Comparison of dry and wet normalised screw pullout force for anterior portion of bovine femur

4.5.1 Correlation between Normalised Pullout Force and Drilling Force

Graphs generated, based on the experimental data, to evaluate the relationship between the drilling force and normalised screw pullout force for bovine and pig cortical bones are given in Figures 4-16 and 4-17, respectively. In both animals femur, good linear relationships ($r^2 > 0.95$) were found at all anatomical positions, between the drilling force and normalized screw pullout force. This shows that bone drilling data can be used as a means to estimate bone quality.

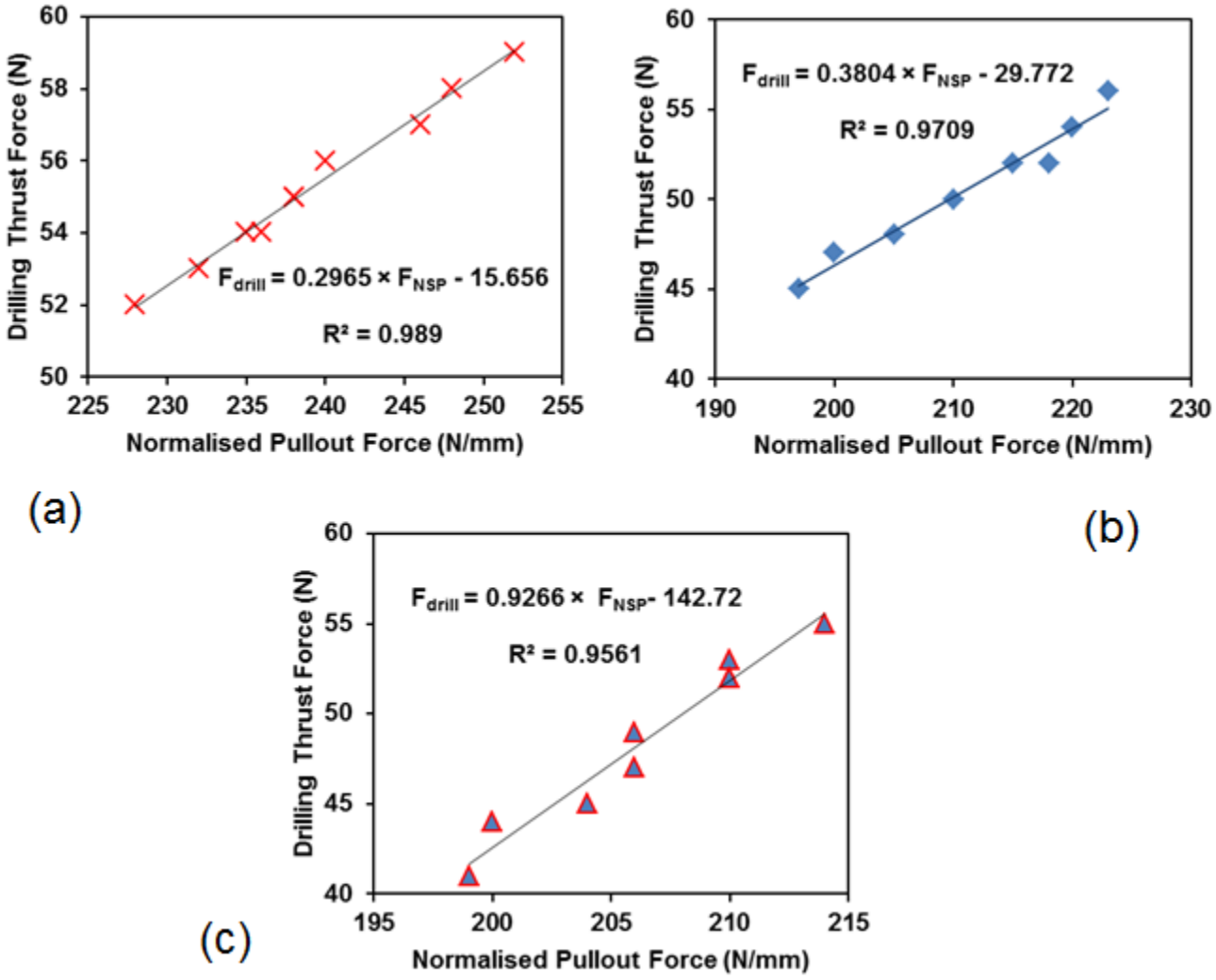

Figure 4-16 Relationship between maximum drilling force and normalised Screw pullout force for pig femur (a) Anterior (b) Medial (c) Posterior

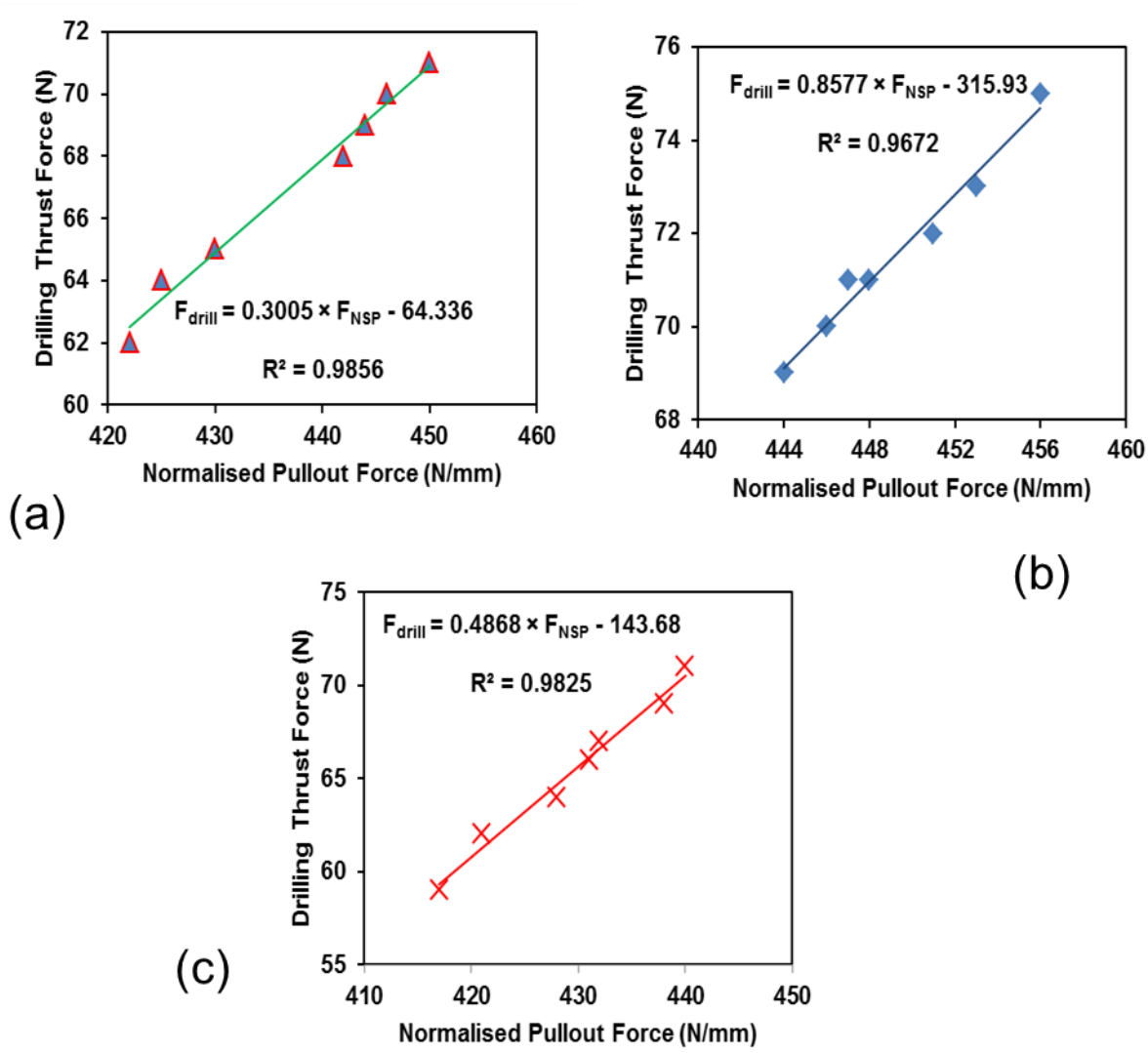

Figure 4-17 Relationship between maximum drilling force and normalised Screw pullout force for bovine femur (a) Medial (b) Anterior (c) Posterior

4.6 Screw Pullout Testing of PU Foam (Synthetic Bone)

The same foam samples and drill bit, as used in section 4.6 were used for the investigation of the relationship between screw pullout force and drilling force. Synthes surgical cancellous screws and taps were used, and both tapping and screw insertion were carried out at a constant speed of 10 rpm using the test rig. The screw pullout force profile for PU foam was found to be similar to the profiles obtained for

cortical bone, i.e. there is a gradual increase in force, then a failure load followed by a sudden force dropand minimal resistance. Table 4-7 summarises the averaged maximum screw pullout force and normalised screw pullout force with respect to different thicknesses of FR-6700 series polyurethane foam.

Table 4-7 Screw pullout force for FR-6700 series foam

Foam Samples Used			**Screw Pullout Test Results**		
Foam Model	**Density of Foam** (g/cm^3)	**Specimen Thickness** (mm)	**Screw Pullout Force** (N)	**Standard Deviation** (N)	**Screw Pullout Force/Specimen Thickness** (N/mm)
6715	0.2403	19.00	385.5	12.2	20.28
6718	0.2884	19.10	510.5	8.1	26.72
6720	0.3204	18.80	595.3	3.2	31.66
6725	0.4005	19.10	850.2	13.2	44.51

The graph generated in Fig 4-18 is based on the data presented in Table 4-7 to evaluate the relationship between the normalised screw pullout force with respect to the sample thickness and drilling thrust force. The normalised force showes a linear relationship with the drilling force, and a strong correlation ($r^2 > 0.985$) was found for the foam material. This shows that bone drilling data can be used as a means to estimate bone quality.

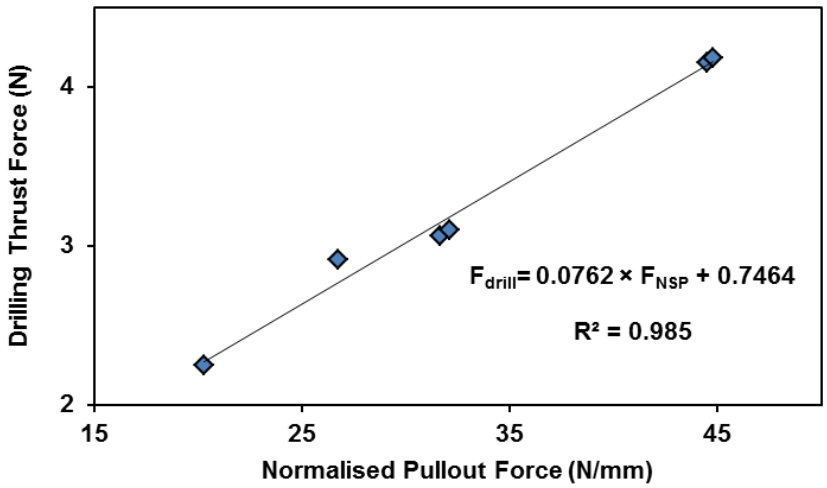

Figure 4-18 Relationship between drilling force and normalised Screw pullout force for PU foam

4.7 Characterisation of Bovine Cortical Bone at High Strain

High strain testing of the anterior portion of bovine cortex was conducted on split Hopkinson pressure bar apparatus as discussed in the Chapter 3 (Section 3.5). Dry and wet bone results were compared first, and then wet bone data was recorded in both longitudinal and transverse directions.

4.7.1 Dry Bone Testing

Bone specimens were dried at room temperature for a week. Figure 4-19 shows the incident (I), transmitted (T) and reflected (R) pulses obtained from the SHPB set up. The loading and transmitted pulses generated by the impact of the projectile were used to calculate the engineering strain as explained in Section 3.5. The two signals have been normalised so that all the pulses are compared from zero volts. . If the recording is started at a reasonable time before the incident pulse begins, an accurate value of the offset may be obtained by simply calculating the average value of the data up to this point. This may then be subtracted from the data and the normalisation is complete. To ensure that stress and strain began at the

origin when plotted against one another, an offset in the start time of the pulses was introduced. This had an effect of overlaying the two pulses. Without such correction it would appear that the sample was being strained without the application of any stress, or vice versa that there was an application of stress without any resulting strain. Figure 4-19 shows a long enough rise time to achieve dynamic equilibrium. The incident pulse has 20 μs rising time and 114 μs pulse width.

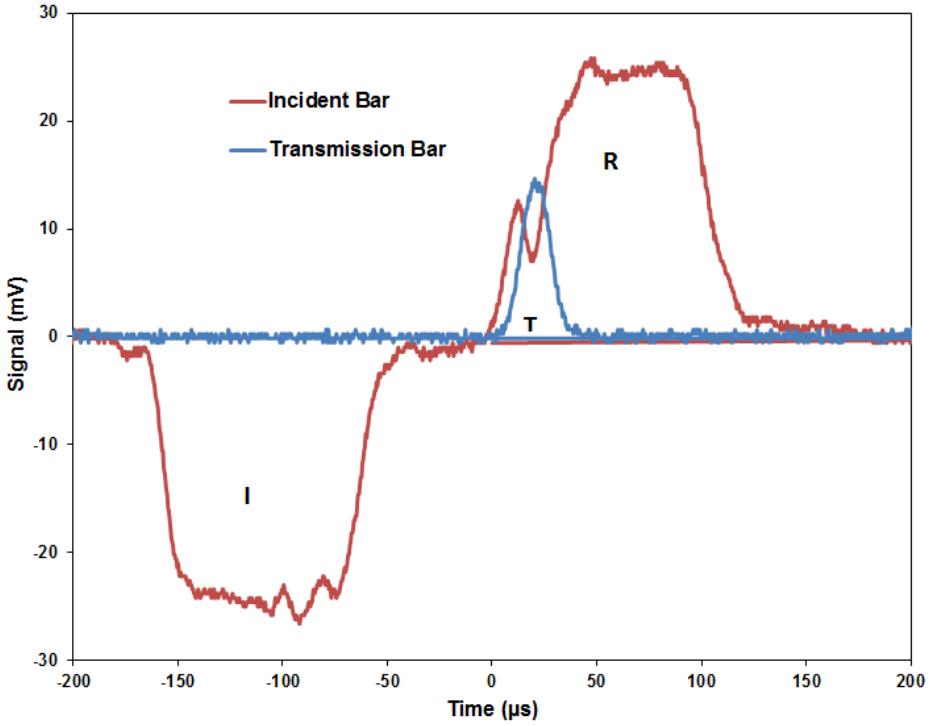

Figure 4-19 Output signal from SHPB for dry bone

A stress-strain curve was produced as explained in Chapter 3 (Section 3.5.3). Defining the yield stress of a material from its stress-strain curve can be quite difficult, particularly for materials like bone. Perhaps the simplest technique to locate the turning point of the stress-stain curve is defined as the maximum value of the second derivative of stress with respect to strain. This is not possible when the stress-strain curve being analysed contains any noise, as any deviation from the general shape of the curve may result in incorrect identification of the point of yield. This can be

overcome by producing an approximation of the stress-strain curve, making it as simple as possible without losing its general shape. In the work presented in this thesis, this has been performed using the following method:

- The stress-strain data between the start and the point of maximum stress is selected. This allows for the approximation to be created more easily than for the full stress-strain curve.
- A 20th order polynomial is fitted to the reduced data set.
- The first and second derivatives of stress with respect to strain are calculated.
- The first point at which the second derivative is greater than or equal to zero, denotes the turning point of the stress-strain curve, and hence the point of yield.

While it is perfectly possible to estimate values of Young's modulus, E, with the split-Hopkinson pressure bar experiments, some considerations must be made in order to get reliable results. As discussed in Section 3.5.3, the measurement of stress in SHPB experiments is defined by

$$\sigma_e = \frac{E_b A_0}{A_s} \varepsilon_T \qquad 4.1$$

where A_0 and A_s are the cross-sectional areas of pressure bar and sample respectively, E_b is the elastic modulus, ε_T and σ_e correspond to transmitted strain and engineering stress respectively.

While there is no one correct way of measuring strain rate, perhaps the simplest technique, and that used throughout this work, is to calculate the strain rate at the point of maximum stress.

Figure 4-20 shows high speed images of dry bovine bone specimen during the SHPB test. These images clearly show that the response of bone due to impact load is quasi brittle. Fragmentation of the bone specimen in the longitudinal direction is seen in Figure 4-20.

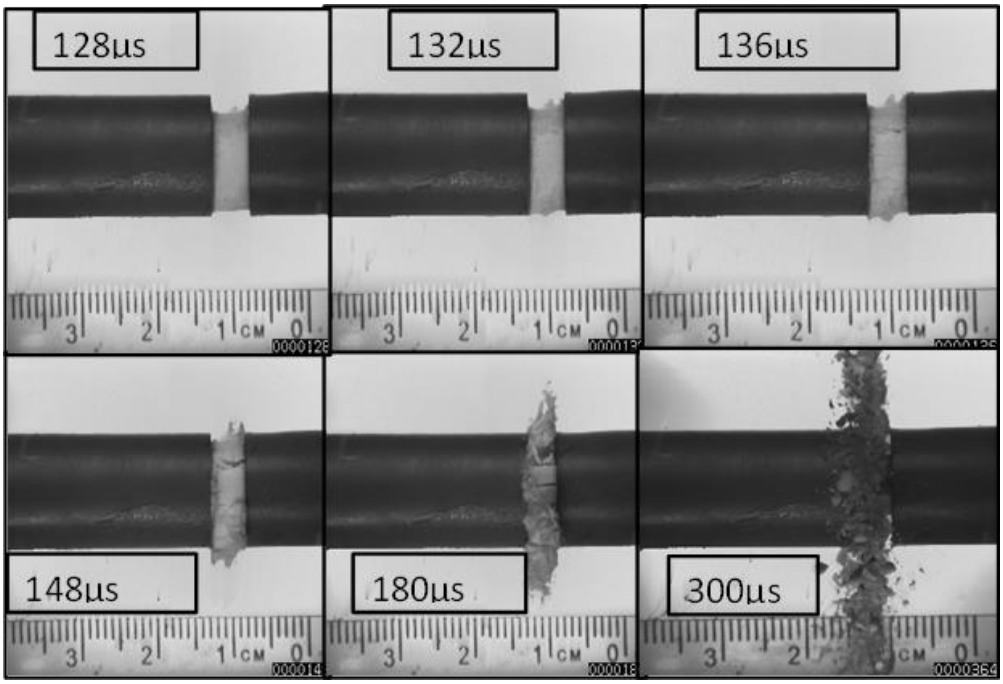

Figure 4-20 High speed Images of dry bone specimen in SHPB

Failure is characterised by the appearance of a multitude of discrete discontinuities. After attainment of failure stress the samples collapse violently. Bone contains numerous pores, voids and micro-cracks along the cement line; these pre-existing flaws act as tensile stress producers in the lateral direction of compression. Cracks propagate and open in the direction of compression due to hoop stress. Macroscopic formations of columns of bone bounded by long cracks under compression were observed, which was the result of coalescence of many micro-cracks.The typical stress-strain response observed in this study for dry cortical bone specimen at a strain rate of 4500/s can be seen in Figure 4-21. The curve shows

three distinct zones, up to the initial stress threshold the behaviour is linear elastic but after initiation and propagation of many cracks the behaviour is non-linear, in the damage zone, due coalescence of micro-cracks and attainment of failure, stress crushing occurs. The first significant departure from linearity of the true stress-strain relationship is observed at the stress level of about 308 MPa and a corresponding strain level 2.1 %. The elastic modulus (E_o) is, therefore, calculated to be 15.61 GPa. Damage started at a stress level of about 401 MPa, and a corresponding strain of 3.3 %. The average value of yield stress (σ_o), ultimate stress(σ_{yo}), elastic modulus (E_0), and strain at damage initiation ($\bar{\varepsilon}_0^{pl}$) at failure stress of 5 dry bone specimens tested at strain rates of 3800/s and 4500/s are given in Table 4-8. Figure 4-22 shows the strain rate effect on the stress-strain curve. As the strain rate increased from 3800/s to 4500/s the peak stress of the dry bone increased from the average value of 350 MPa to 410 MPa, but the strain at failure decreased from 3.6% to 3.4%. The failure energy density in both cases is around 13 MJ/m^3.

Table 4-8 Material properties of Dry Bone

Strain Rate (1/s)	σ_o (MPa)	E_o (GPa)	σ_{yo} (MPa)	$\bar{\varepsilon}_0^{pl}$ (%)
3800	245	13.1 ± 3	350	3.6
4500	312	13 ± 3	410	3.4

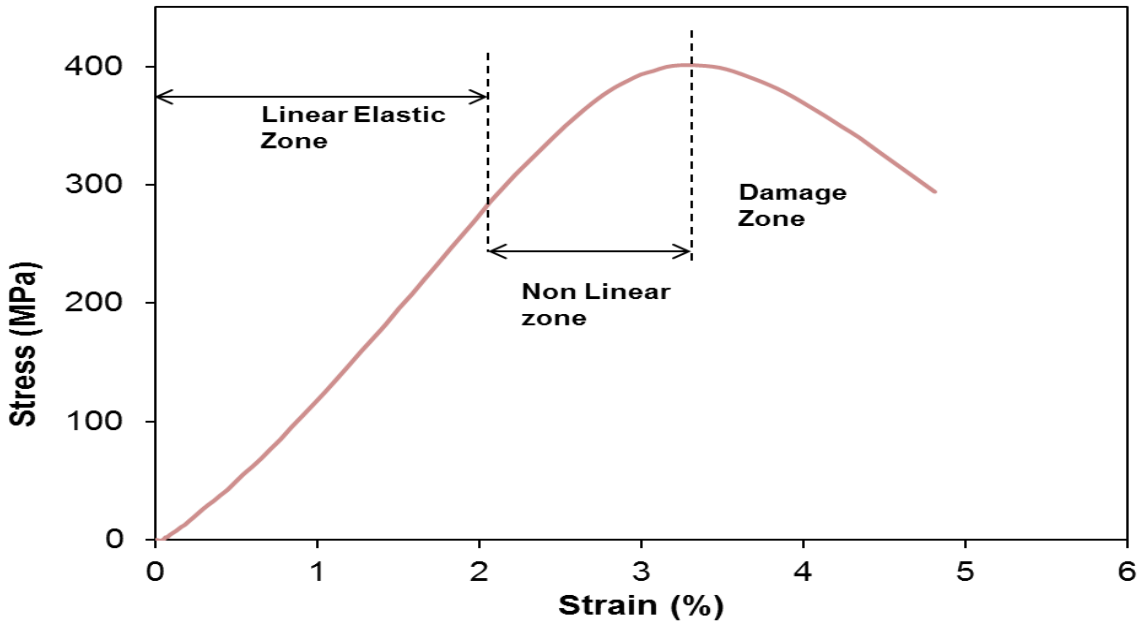

Figure 4-21 Stress-strain response of dry bone (transverse direction)

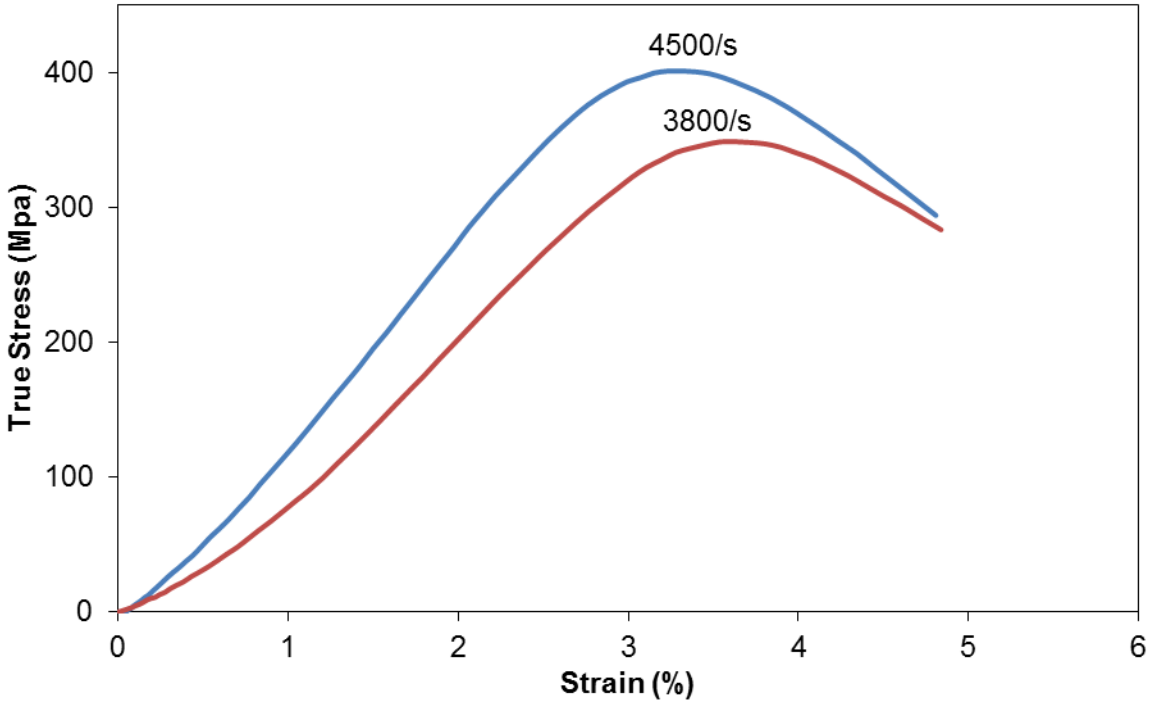

Figure 4-22 Effect of strain rates on dry bone (transverse direction)

4.7.2 Wet Bone Testing

The specimen used for these tests were kept moist in a saline solution at room temperature. The loading and transmitted pulses obtained from SHPB, set up

for wet specimen testing, are shown in Figure 4-23, which shows a long enough rise time to achieve dynamic equilibrium. The incident pulse has 22 µs rise time and 120 µs pulse width. High speed images of wet bone specimens during the SHPB tests indicate a brittle response to dynamic loading as shown in Figure 4-24. The images show that wet specimen failure occurs by propagation of cracks. Crack appearance on the surface of the specimen was observed at 116 µs. As the load is applied the mushrooming of material is observed at one end.

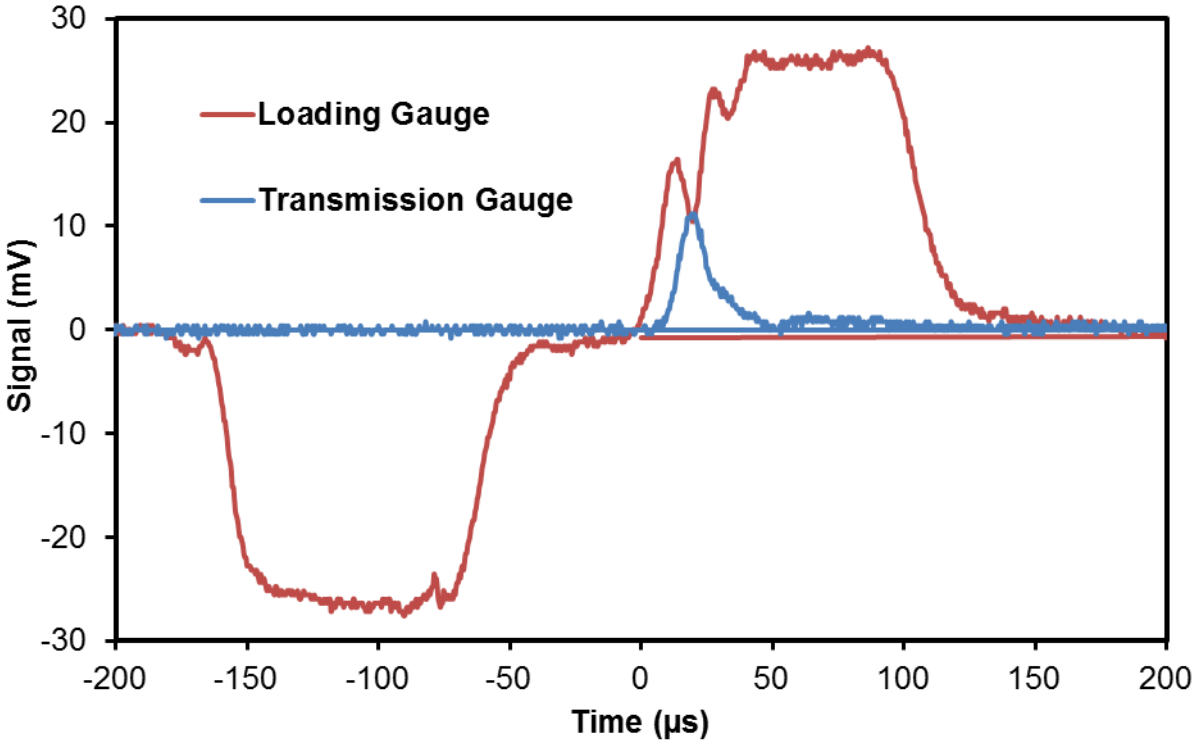

Figure 4-23 Output signal from SHPB for wet bone

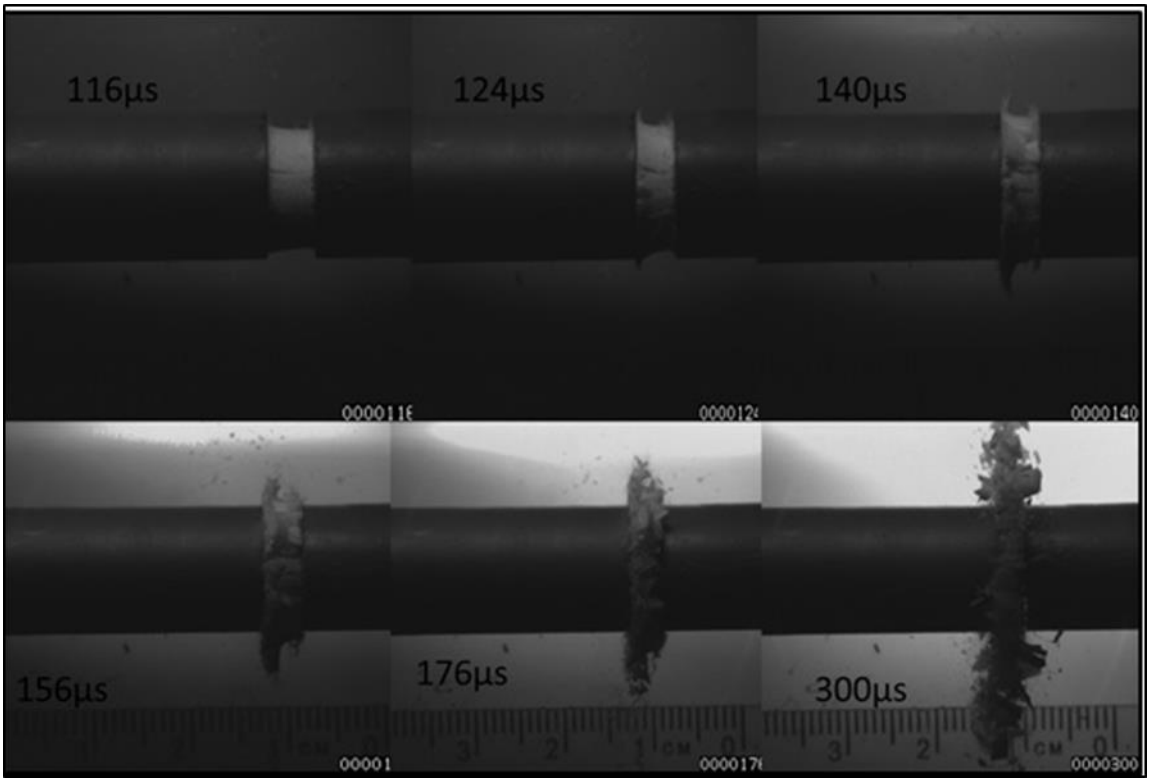

Figure 4-24 High speed Images of wet bone specimen in SHPB

The typical stress-strain response observed in this study for wet cortical bone specimen at a strain rate of 4500/s can be seen in Figure 4-25. The curve shows brittle behaviour; up to crack initiation the behaviour is linear elastic, then nonlinear with crack propagation up to failure stress, and after attainment of failure stress the specimen crushes due to the coalescence of micro-cracks. The first significant departure from linearity of true stress-strain relationship is observed at a stress level of about 205 MPa and a corresponding strain level of 2.2 %. The initial elastic modulus (E_o) is, therefore, calculated to be 10 GPa. The failure occurred at the stress level of about 269 MPa, and a corresponding strain of 3.57 %. The average value of the yield stress (σ_o), ultimate stress (σ_{yo}), elastic modulus (E_0), strain at damage initiation ($\bar{\varepsilon}_0^{pl}$), of a wet bone specimen tested in the longitudinal (L) and transverse (T) directions at strain rates between 3800/s and 7100/s are given in Table 4-9. Figure 4-26 shows the strain rate effect on the stress-strain curve. As the

strain rate is increased from 3800/s to 4500/s the peak stress of the wet bone increased from an average value of 255 MPa to 270 MPa, but the strain at failure decreased from 4.2% to 3.6%.

Table 4-9 Material properties of wet bone in longitudinal and transverse directions

Direction	Strain Rate (1/s)	σ_o (MPa)	E_o (GPa)	σ_{yo} (MPa)	$\bar{\varepsilon}_0^{pl}$ (%)
T	3800	162	08 ± 2	255	4.2
T	4500	205	08 ± 2	269	3.6
L	7100	260	14 ± 2	370	14
L	6100	255	14 ± 2	350	16

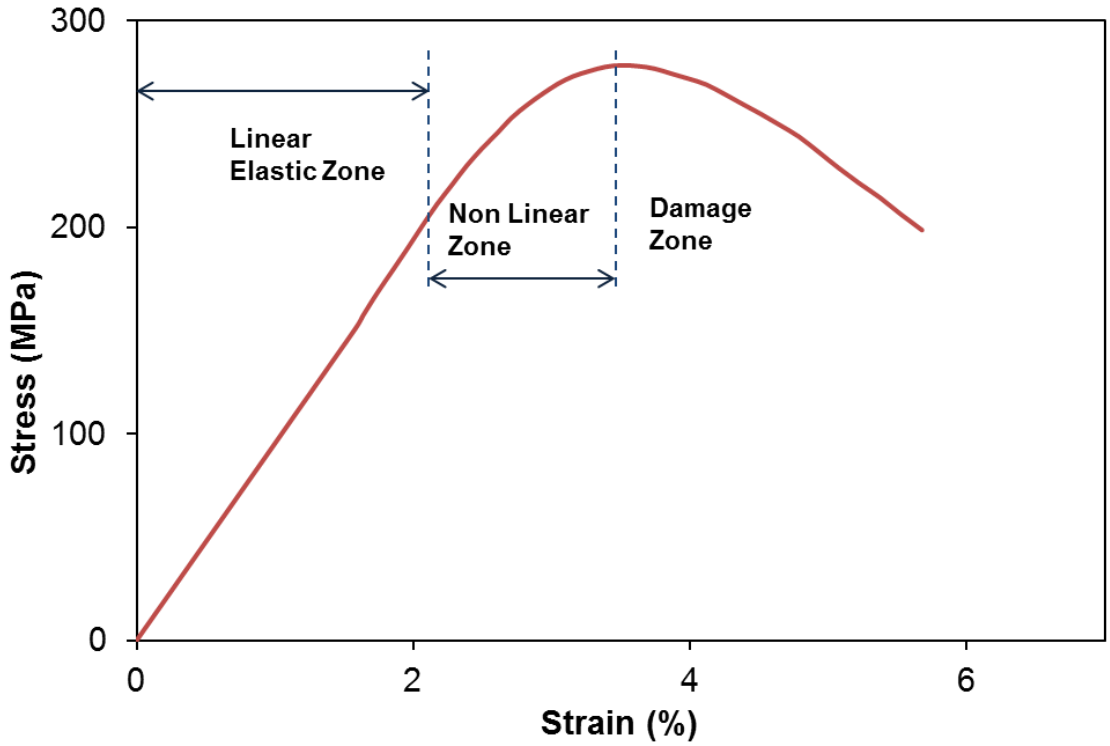

Figure 4-25 Stress-strain response of wet bone (transverse direction)

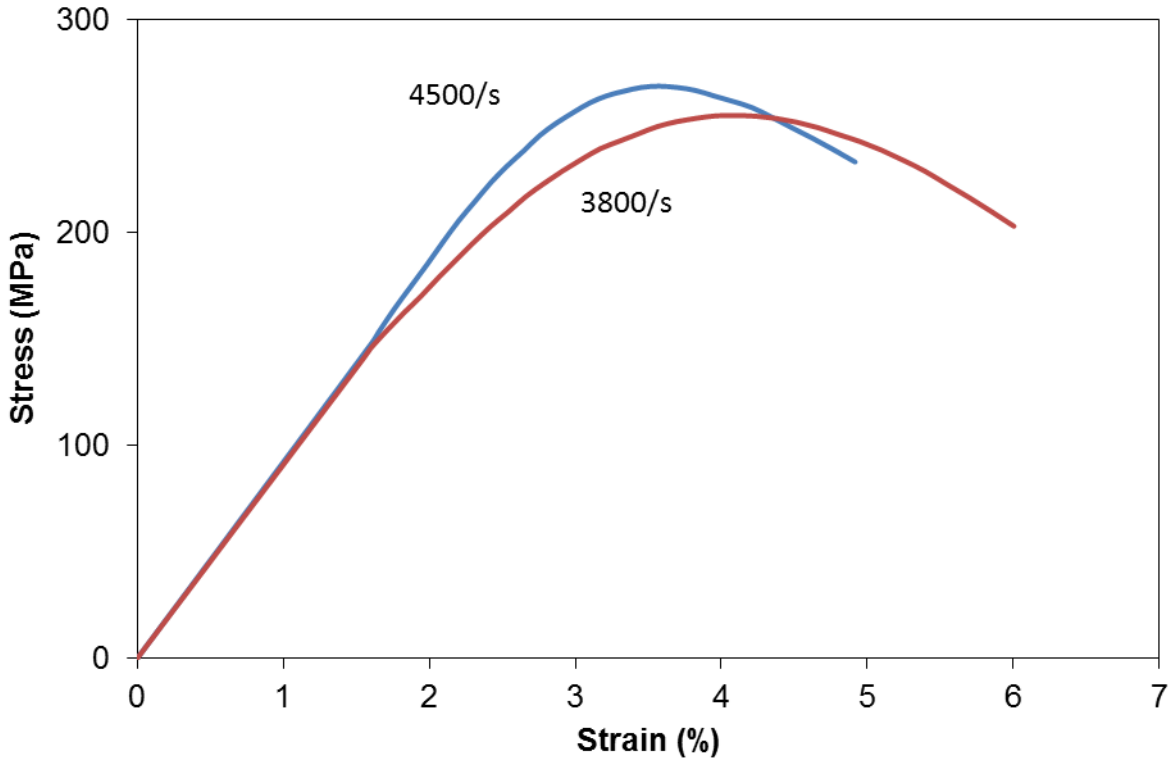

Figure 4-26 Effect of strain rates on wet bone (transverse direction)

4.8 Concluding Remarks

The results of the experimental programme carried out in this study have been presented in this chapter. Drilling tests were performed on bovine and pig femur bones to investigate the efficacy of using drilling thrust force data to predict the quality of the bone. The drilling results on different anatomic positions on the same cortex show that the thrust force varies across different positions for the same drilling conditions. This indicates the ability of drilling force to detect structural variability within the cortex. Variability of drilling force in dry and wet bone also proves the effectiveness of using drilling data as a predictor of bone quality. The results at different drilling conditions are also presented in this chapter, and are well in agreement with previous studies. These results will be used for validation of FE and analytical models. Various tests conducted on synthetic bone material covering a density range, simulates osteoporotic and cancellous bone have been presented. A

good correlation ($r^2 > 0.95$) was found between drilling force and screw pullout force in bovine, pig and synthetic bone. All these results suggest that drilling force is a good predictor of the material quality. The mechanical behaviour of dry and wet bone at different strain rates was observed and it showed that failure stress had strain rate dependence. Both wet and dry bone showed quasi brittle behaviour at high strain rate. The next chapter presents the description and results of finite element modelling of drilling in bone.

CHAPTER 5

Finite Element Modelling of Drilling of Cortical Bone

Complex processes such as drilling can often only be accurately modelled using numerical techniques, such as finite element (FE). The FE method breaks down a complex structure into many interconnected sub-regions, called finite elements. Briefly, finite element modelling consists of the discretisation of domain, stiffness matrix derivation, application of boundary conditions, solution and post processing of results. Numerical modelling of drilling was carried out in this research. The aim of the drilling numerical model is to relate drilling force with bone mechanical property based on established material model and damage criteria. This chapter provides details of the FE modelling approach used in this work. The commercially available finite element code ABAQUS CAE was used for the numerical analysis. The 3D geometric model development for drill bits was carried out using the commercial CAD package Pro-Engineer (Pro/E). Meshing and problem setup were carried out using ABAQUS CAE. A consistent system of units based on N, mm, and second was used. The meshing strategy and the selection of element type are also discussed in this chapter. For the simulation of drilling, calculation of an integration step was carried out using the explicit integration method.

5.1 Drill Bit Geometry

For reliable finite element simulation of the drilling process, it is important to establish the true drill bit geometry, which is quite complex. At the centre of the drill bit tip, the cutting speed is close to zero and the work material is ploughed under a high negative rake angle. Along the drill bit cutting edge, the cutting speed and rake angle both vary with respect to the distance from the drill bit centre.

The detailed parameters of the industrial drill bit used in this research are given in Chapter 4, Section 4.3.2; these are used in the CAD software Pro/E. The default coordinate CS0 of Pro/E is taken as the centre point of the drill bit. From the centre point a helix curve is generated using the cylindrical coordinate system (r, z, θ) with the following equations

$$r = r_0 \tag{5-1}$$

$$\theta = -h \times 360 \times n \tag{5-2}$$

$$z = -2 \times h \times l \tag{5-3}$$

where r_0 is the radius of the drill bit, z is the direction and length of the helix curve; l is the pitch of the helix, n is number of helix, and h is a dimensionless parameter varied between 0 and 1 for r, z and θ. The axis of drill bit is generated by using the Cartesian coordinate system as follows;

$$x = 0, y = 0,$$

$$z = -2\pi n r_0 / \tan(\psi) \tag{5-4}$$

where ψ is the helix angle. The flute is generated by cutting along this helix curve. The shape of the flute is generated by using the Cartesian coordinate system and CS0 as the centre point with following equations;

$$r = {}^{w}/_{2} + (r_0 + w/2) \times h \qquad 5\text{-}5$$

$$\theta = \sin^{-1}\left(\frac{w}{2r}\right) + \left(\frac{1}{r_0}\right) \times \sqrt{(r)^2 - \left(\frac{w}{2}\right)^2} \times \tan(\psi) \qquad 5\text{-}6$$

$$\times (1/(\varphi/2)) \times (180/\pi)$$

where w is the chisel edge thickness and φ is half point angle.

Figure 5-1 shows the imported model of the drill bit to ABAQUS. The drill bit is modelled as rigid body with a reference point and reduced flute length to save computing time and resources. This did not affect the overall calculation and aim of this research, which is the evaluation of bone quality. The stable time increment for stiff deformable region can be small, resulting in a very small global time increment. Element level calculations are not performed for elements that are part of a rigid body; therefore, the rigid body (drill bit) does not affect the global time increment. The motion of rigid body is determined completely by attaching a frame of reference at the reference point. This allows constraining the motion of the drill bit to the motion of the reference point. The reaction forces and moments are recovered in all the degrees of freedom with respect to the frame of reference at the reference point.

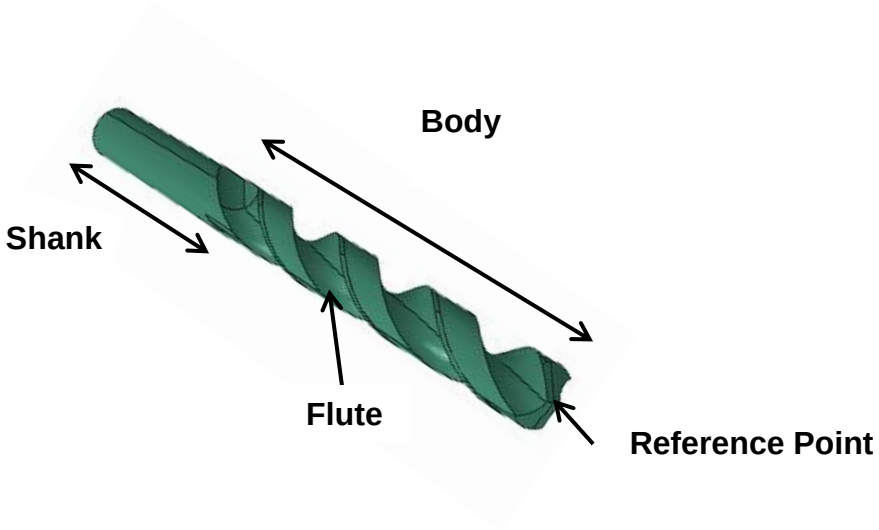

Figure 5-1 Drill Bit

5.2 Geometric Model and Boundary Conditions

A 3D FE model of drilling was developed which consists of a HSS twist drill bit and cortical bone with appropriate boundary conditions as shown in Figure 5-2. A square block of cortical bone with overall dimensions of 5 mm × 5 mm × 2 mm was modelled in Abaqus. These dimensions are selected to allow small computational time with full drill bit engagement profile. A 3D geometry of a 2.5 mm diameter twist drill bit with a point angle of 118^0 and a helix angle of 28^0 was modelled by the procedure described in section 5.1. The drill bit was modelled as a rigid body because the elastic stiffness of the HSS twist drill bit is in the range of 220–240 GPa as compared to 10-20 GPa for the cortical bone, reducing the computational cost involved in the highly resource-consuming drilling simulations. The cortical bone was fixed at all four vertical faces, while the drill bit was constrained to rotate only about its own longitudinal axis with a specified speed and vertically downward feed into the work piece as shown in Figure 5-3. The FE analysis was performed with the drilling parameters listed in Table 5-1.

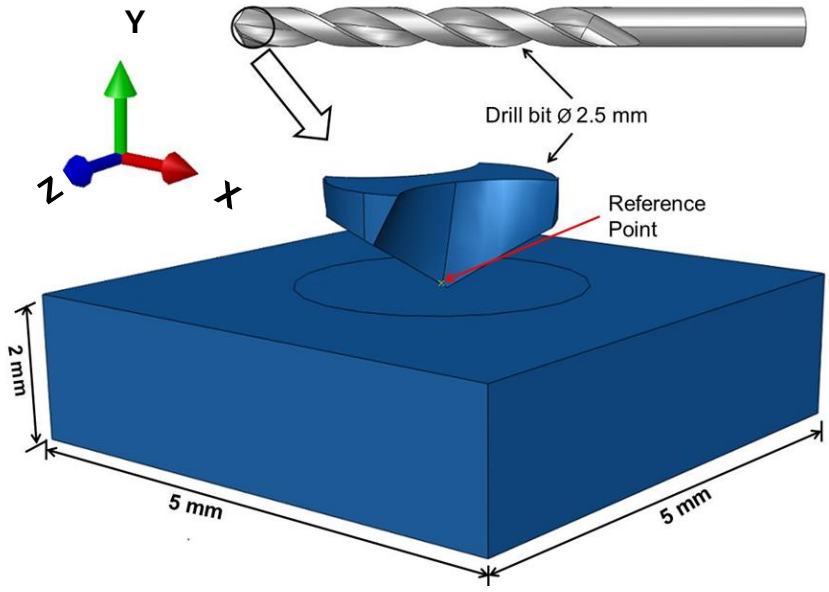

Figure 5-2 Finite element model of bone drilling

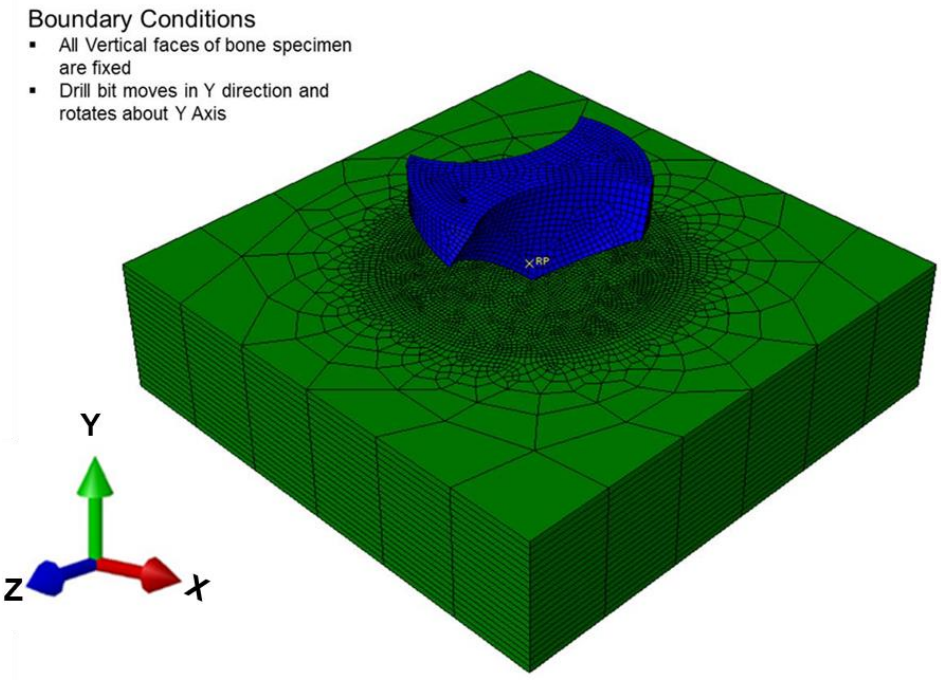

Figure 5-3 Boundary Conditions

Table 5-1 Machining Parameters used in Simulations

Drill bit	HSS, ⌀ 2.5 mm, point angle 118^{o}
Spindle speed (rpm)	800, 1200, 1500
Feed (mm/rev)	0.05, 0.1,0.15, 0.1875

5.3 Meshing Methodology

Due to complexity of the drill bit and the dynamic nature of the problem, drilling simulation is meshing sensitive. Normally, meshing of a physical model depends upon the size and the order of interpolation. The size of interpolation is the smallest sphere that encloses the element, and both the size and the order of interpolation define the degree of polynomial for the shape function of the element. The mesh size for bone was selected in the range of 10µm to 500µm. Different regions of geometry are defined and seeded separately based on the required mesh density to reduce the computational time. Meshing was executed using the sweep meshing scheme in Abaqus [150].

The choice of element selection for drilling of bone depends upon the selection of the integration procedure and response of the material. Eight node linear brick elements (C3D8R) with reduced integration and hourglass control were used to model the bone in the drilling simulation. Each node had four degrees of freedom: three displacements in the X, Y, and Z directions and one nodal temperature. The workpiece mesh was finer near the tool tip, as shown in Figure 5-3, where the largest material deformation was expected to occur. The element size was important for the simulation. If the mesh is too coarse, too many elements experience severe distortion and are deleted, resulting in improper bushing formation. On the contrary, if the mesh is too fine, the computational time increases significantly without improving the results. A balance was achieved between computational time and the amount of workpiece mesh removed by element deletion. A single integration point gives computational efficiency. 3D linear tetrahedral element C3D4 was used for drill bit meshing. Figure 5-4 shows the hexahedral and tetrahedral elements with node number used for bone materials.

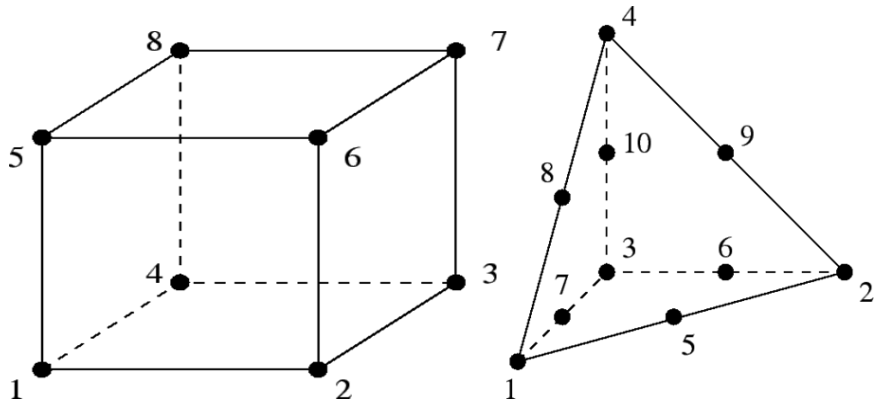

Figure 5-4 Hexahedral (left) and Tetrahedral (right) Element

5.4 Mesh Convergence

As the mesh sensitivity study is very important in simulations involving high deformations and a nonlinear material behaviour, a rigorous mesh sensitivity study was carried out to obtain a computationally accurate finite element mesh. In the current model, due to the complex geometry of the drill bit and removal of material, the history of the force-time signal is used as the criterion of convergence. The number of elements and element size were changed by changing the number of seeds in contact area and through the thickness of bone. Drilling simulations at 150 mm/min and 800rpm were carried out for each mesh. The average thrust force at the reference point was plotted against each combination as shown in Figure 5-5. For every number of seeds, the average thrust force after 12 elements per 1mm thickness remained unchanged. Similarly for a number of seeds above 70 the average thrust forces were very similar. From this analysis, a mesh scheme of 25 elements per 2 mm thickness and 70 seeds for sweep mesh were selected for use in further analysis as it was computationally less expensive.

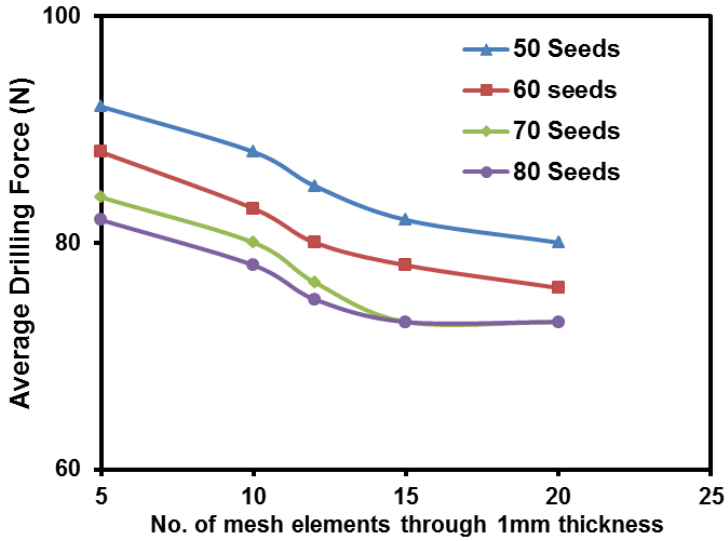

Figure 5-5 Mesh Convergence Analysis for Drilling Simulation

All the results are presented based on simulations performed with an optimised mesh. The cortical bone was meshed with 101320 elements with a smallest element size of 5μm. The drill bit was meshed with 4850 elements. Localised stiffness reduction due to internal damage can cause excessive element distortion that could lead to difficulties in numerical convergence. To resolve this numerical issue, 'distortion control' was used in Abaqus, and damage variables were limited to a maximum value of 0.999. Following a wave stability study it was observed that the smallest element which governs the stability of the solution has a very low stable time increment of the order of 10^{-8}s. This affected the overall solution runtime, and hence a selective variable mass scaling technique was used for the element set in the refined cylindrical zone. The mass scaling increased the mass of the selected elements to 0.5% with a stable time increment of the order of 10^{-7}s. This had minimal effect on the kinetic energy of the model.

5.5 Constitutive Material Model

Bone as an anisotropic material exhibits different yield behaviour in different directions. The present work is based on modeling of anisotropic yield behaviour of cortical bone using yield stress ratios. Bone is clearly a quasi-brittle material relative to ductile metals as shown in Chapter 4. However, Wiggins and Malkin (1978) [151] estimated an apparent toughness of bone from their machining tests by dividing the energy expended in cutting by the area of newly formed surface of segmented chips (they also presented quick-stop pictures of the segmented chip formation),. Their value of 12 kJ/m^2 is of the same order of magnitude as for fibre reinforced plastics, considerably larger than for cast iron (0.2 to 3 kJ/m^2) and much larger than for extremely brittle materials such as ceramics and glass (<0.1 kJ/m^2) (Ashby and Jones,1980) [152]. These relative values support the use of a plastic strain accumulation damage law, coupled with a plasticity analysis, for modelling hole formation in bone drilling simulation. In this study bone material is considered as a transversely isotropic material with five independent elastic constants. The long axis of the bone has been taken as the axis of symmetry. The transversely isotropic model proposed in this work is based on the quadratic yield criterion for anisotropic material by Hill's (Hill 1952, 1990) [153, 154] and non-linear isotropic hardening rule for rate dependent plasticity. The constitutive equations of this model for uniaxial loading are as follows.

The total strain tensor during deformation is the sum of the elastic strain tensor and the plastic strain tensor, given by,

$$\varepsilon = \varepsilon^{el} + \varepsilon^{pl} \qquad 5\text{-}7$$

In this case the yield ratios were defined with respect to a reference yield stress, σ^o, a user-defined reference yield stress specified for the material plasticity definition. For anisotropic yielding, Hill's potential function can be expressed in terms of rectangular stress components as given by,

$$f(\sigma) = (F\left(\bar{\sigma}_{22} - \bar{\sigma}_{33)}\right)^2 + G(\bar{\sigma}_{33} - \bar{\sigma}_{11})^2 + H(\bar{\sigma}_{11} - \bar{\sigma}_{22})^2 + 2L{\bar{\sigma}_{23}}^2 + 2M{\bar{\sigma}_{31}}^2 + 2N{\bar{\sigma}_{12}})^{1/2}$$

$$f(\sigma) = |\sigma^y| + R \qquad 5\text{-}8$$

where F, G, H, L, M and N are constants, obtained from the following equations.

$$F = \frac{1}{2}\left(\frac{1}{R_{33}^2} + \frac{1}{R_{22}^2} - \frac{1}{R_{11}^2}\right),$$

$$G = \frac{1}{2}\left(\frac{1}{R_{33}^2} + \frac{1}{R_{11}^2} - \frac{1}{R_{22}^2}\right),$$

$$H = \frac{1}{2}\left(\frac{1}{R_{11}^2} + \frac{1}{R_{22}^2} - \frac{1}{R_{33}^2}\right),$$

$$L = \left(\frac{3}{2R_{23}^2}\right),$$

$$M = \left(\frac{3}{2R_{13}^2}\right),$$

$$N = \left(\frac{3}{2R_{12}^2}\right), \qquad 5\text{-}9$$

Here $\bar{\sigma}$ is the measured yield stress when applied as the only non-zero stress component, R_{ij} are anisotropic yield ratios and can be calculated from the cortical

bone yield strengths. σ^y is the size of an initial yield surface, while R is the isotropic hardening term given as:

$$R = \sigma^0(\varepsilon^{pl}, \theta^0) \qquad 5\text{-}10$$

Here θ^0 is the temperature of the cortical bone. For 2-3 plane to be the plane of isotropy at every point, transverse isotropy requires that $E_1 = E_p$, $E_2 = E_3 = E_t$, $\nu_{12} = \nu_{13} = \nu_{pt}$, $\nu_{21} = \nu_{31} = \nu_{tp}$ and $G_{12} = G_{13} = G_t$ where p and t stand for in-plane and transverse respectively.

The rate-dependent properties of the cortical bone were also defined using the Cowper–Symonds overstress power law (Cowper *et al*. 1957) [155]:

$$\dot{\bar{\varepsilon}}^{pl} = d\left(\frac{\sigma}{\sigma_0} - 1\right)^n \qquad 5\text{-}11$$

where σ/σ_0 is the yield stress ratio, σ and σ_0 are the yield stress under different strain rates and static strain rate respectively, and d and n are material constants.

5.6 Element Removal Scheme

Here, simulation of the hole-generation process in cortical bone was accomplished with the help of the element removal scheme in Abaqus/Explicit and chip formation was not modelled. Damage initiation in the cortical bone was based on a ductile damage criterion. The ductile criterion is specified by providing the equivalent plastic strain at the onset of damage, $\bar{\varepsilon}_D^{pl}$, which is a function of stress triaxiality and strain rate:

$$\bar{\varepsilon}_D^{pl}(\eta\,, \dot{\bar{\varepsilon}}^{pl}) \qquad 5\text{-}12$$

where η = *p/q* is stress triaxiality, p is the pressure stress, q is Mises equivalent stress, and the criterion for damage initiation is met when the following condition is satisfied by ω_D, a state variable that increases monotonically with plastic deformation, and proportional to the incremental variation in the equivalent plastic strain.

$$\omega_D = \int \left(\frac{1}{\bar{\varepsilon}_D^{pl}(\eta,\ \dot{\bar{\varepsilon}}^{pl})} \right) d(\bar{\varepsilon}^{pl}) = 1 \qquad 5\text{-}13$$

The characteristic stress-strain behaviour of a material under uniaxial loading that undergoes progressive damage is shown in Figure 5-6. In the case of the elastic-plastic material this damage can be decomposed into two parts; softening of the yield stress and degradation of the elastic modulus. The solid curve in Figure 5-6 represents the damaged stress-strain response, whereas the dashed line represents the undamaged behaviour. σ_{yo} and $\bar{\varepsilon}_0^{pl}$ are yield stress and equivalent plastic strain at the onset of damage respectively, while $\bar{\varepsilon}_f$ is the equivalent plastic strain at failure, also known as fracture strain. D is the overall damage parameter: with D= 0 at damage initiation, and D=1 at complete damage. After damage initiation, the residual elastic modulus, E_r, is given as:

$$E_r = (1 - D).E \qquad 5\text{-}14$$

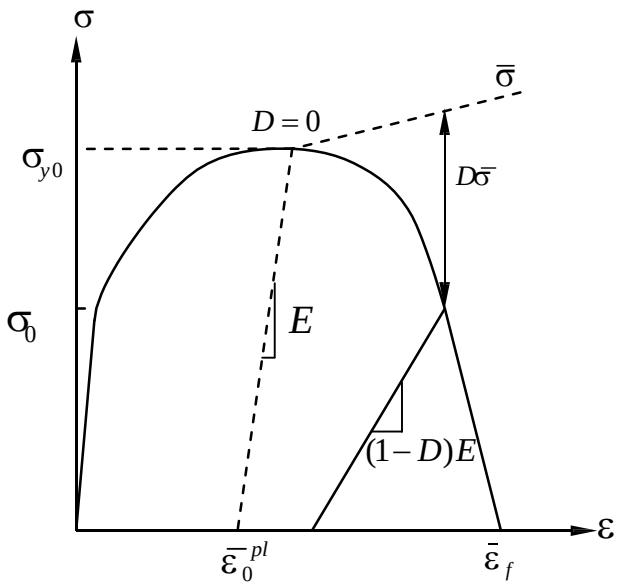

Figure 5-6 Stress-strain curve with damage behaviour

When material undergoes damage, the stress-strain relationship fails to accurately present its behaviour because of a strong mesh dependency linked to the strain localisation. Hence a different approach is required to trace the strain softening branch of the stress-strain curve. Thus, the Hillerborg's fracture energy approach (Hillerborg 1985)[156] was employed in this model, which eventually helped to reduce mesh dependency by formulating a stress displacement response after damage initiation. The fracture energy was idealised as work required to open a unit area of a crack and expressed as:

$$G_f = \int_{\bar{\varepsilon}^{pl}}^{\bar{\varepsilon}_f^{pl}} l\sigma_y \, d\bar{\varepsilon}^{pl} = \int_0^{\bar{u}_f^{pl}} \sigma_y d\bar{u}^{pl} \qquad 5\text{-}15$$

Where $\bar{u}^{pl}$ is the equivalent plastic displacement and can be considered as fracture energy conjugate of yield stress after the damage initiation: $\bar{u}^{pl} = 0$ at damage initiation and $\bar{u}^{pl} = l\bar{\varepsilon}^{pl}$ after it. Here l is the characteristic length of an element in a meshed body that depends on its geometry and formulation.

5.7 Mechanical Properties

As the cortical bone was modelled as transversely isotropic elasto-plastic rate dependent material, the quasi static properties were taken from literature (Reilly et al. 1975) [157]. For rate dependent properties, the split-Hopkinson pressure bar (SHPB) test results are used, and a best-fit curve and constitutive constants for equation 5-11 were generated. The stress-strain curve of a material at a known strain rate could be scaled to determine the material properties at an unknown strain rate by using equation 5-11 with the respective material coefficients (*d* and *n*). The material properties of cortical bone used in FE analysis are listed in Tables 5-2 and 5-3.

Table 5-2 Mechanical Parameters of Cortical Bone

Property	Value
Longitudinal stiffness, E_{11} (GPa)	14
Transverse stiffness, E_{22} (GPa)	08
Poisson's ratio, v_{12}	0.34
Poisson's ratio, v_{23}	0.4
Shear modulus, G_{12} (GPa)	5
Density (kg/m^3)	2000
Materials constants (d/n)	9897/0.65

Table 5-3 Values of Rij for calculating Hill's potential constants

R11	R22	R33	R12	R13	R23
1.2	1	1	0.77	0.77	0.88

The contact and friction parameters used in the simulations were based on a number of experimental factors such as spindle speed, feed rate and drill bit geometry. Contact between the twist drill bit and cortical bone was defined by the general contact algorithm available in Abaqus/explicit. This algorithm generated the contact forces based on the penalty-enforced contact method. The friction coefficient μ is used to account for the shear stress of the surface traction τ with the contact pressure p and can be represented as $\tau = \mu p$. In this case, the frictional contact between a drill bit and cortical bone was modelled with a constant coefficient of friction of 0.7 (Davidson et al. 2003) [87].

5.8 Explicit Solution and Model Formulation

For simulation of a fast dynamic process such as drilling, the calculation of integration step is very important. In general, finite element formulations are based on either quasi-static implicit or dynamic explicit schemes. The former requires convergence at every time step or load increment and the latter solves an uncoupled equation system based on information from previous time steps. The implicit method is too slow for these processes, so the calculation is based on the explicit integration method. Although the minimum time step used in Explicit method is bounded by stability, contact algorithms available in explicit are more robust and straightforward than their implicit counterpart. Implicit method leads to system matrices which often exceeds the available in-core storage capacity. The difference of the two methods is in the way of calculating each time step from equation 5-16. Explicit methods use the differential equation at time t to predict the solution at time $t+\Delta t$, and the implicit methods attempt to satisfy the differential equation at time t after the solution at time $t-\Delta t$ is found.

$$M\ddot{U} + C\dot{U} + KU = F(t) \qquad 5\text{-}16$$

where M is the mass matrix, C is the damping matrix, K is the stiffness matrix, U is the displacement matrix and F is the force matrix. The concept of explicit FEM consists in the use of second Netwon's law that is rewritten in matrix form, equation 5-17, and defined at the beginning of each time step.

$$[a_t] = [M]^{-1}\left[(F_t^{ext}) - \left(F_t^{int}\right)\right] \qquad 5\text{-}17$$

where $[a_t]$ is acceleration vector at time t, (F_t^{ext}) is the vector of external forces applied at time t, and $\left(F_t^{int}\right)$ is the vector of internal forces at time t.

Lagrangian formulation is used for this research. In this formulation, the FE mesh is attached to the bone material and deforms with it. This is useful for relatively low distortion and large deformation. The history of the state of material in each element is known completely. This formulation is close to the physical problem as the geometry of material boundaries does not have to be predetermined, but is developed during the course of the analysis entirely as a function of the physical deformation process, drilling parameters and material properties.

A 3D model of drilling has thousands of elements and is computationally expensive and time consuming to solve. ABAQUS provides the facility of parallel computing, where a single machine with multiple nodes / processors may be used for computing the solution. Thread or MPI (message passing interface) based parallel processing options were available for this study. The model was divided in computing domains according to the number of nodes/processors. Parallel processing was used on a HPC shared memory machine to solve the 3D models. The models required on average 54 hours on 36 Intel quad-core processors with 48

GB RAM each. A High Performance Computing (HPC) facility available at Loughborough University was used.

5.9 Results

To identify the maximum force and maximum torque easily, any noise in the force and torque data was filtered out using the running average function. A typical profile of the drilling force with respect to drill bit displacement for a single hole was obtained as shown in Figures 5-7a and 5-7b. The drilling profile is divided into four zones. Zone I shows the penetration of the drill bit, which can be seen by a sharp rise in the drilling force. Zone II shows the start of material removal by chisel edge and main cutting edge with gradual rise in thrust force upon drill bit entry into the anterior cortex. The Drill bit is fully engaged at the end of zone II and throughout zone III, and the maximum drilling force is calculated in zone III, and Zone IV shows a gradual drop in thrust force as the drill bit exits the cortex. Similar drilling force profiles having different drilling force magnitudes were observed for all the drilling conditions considered in this study.

The noise observed in the simulations results is due to the continuous make-and-break of contact between the drill bit and bone upon removal of material. Such inherent noise caused by the “Alternating in and out” of drill bit is due to the removal of material and the small stable time increment in the “explicit solver” used. The noise could be reduced through inducing artificial damping, but this will reduce the stable time further which results in high computational costs. The torque profiles, given in Figure 5-7c and 5-7d, show the same increasing and decreasing trends as the thrust force upon drill bit penetration and exit respectively.

The distribution of Von Mises stress of the work piece is shown in the Figure. The maximum Von Mises stress is estimated around 340 MPa. It shows that Mises

stress increased gradually in the entrance stage, then the maximum Mises Stress was obtained in steady state, later it decreased gradually until the hole was drilled throughout the bone.

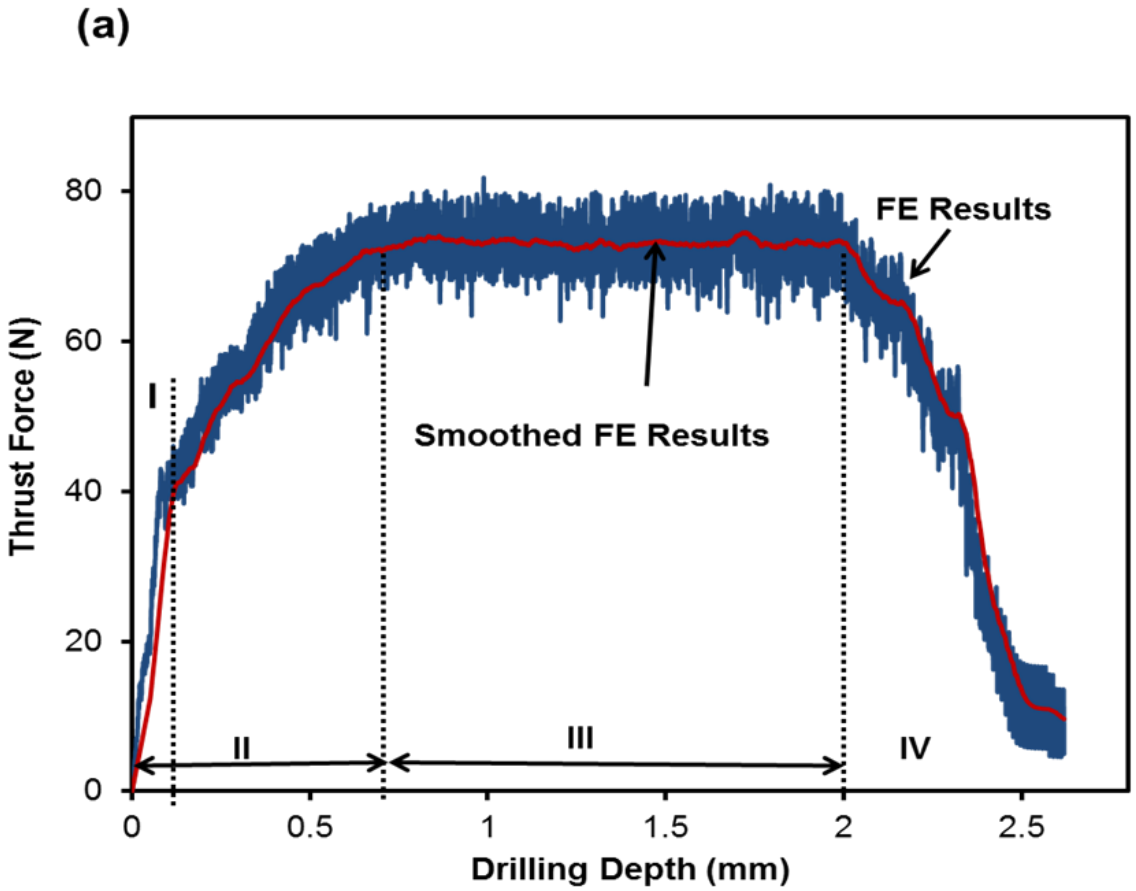

(b)

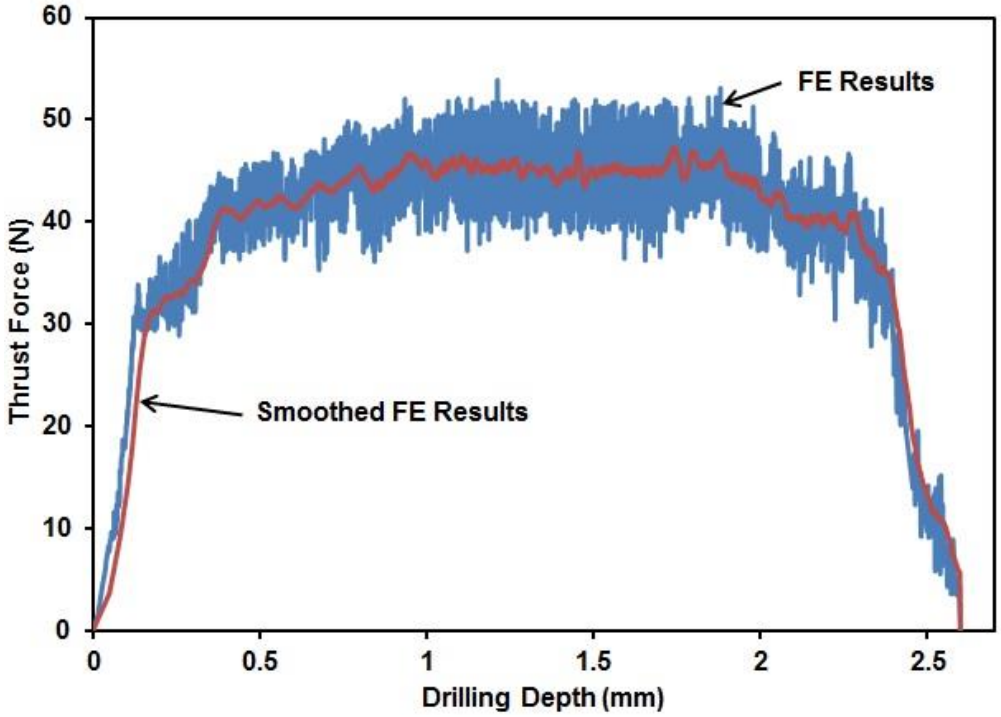
60
50
40
30
20
10
0
Thrust Force (N)
FE Results
Smoothed FE Results
0
0.5
1
1.5
2
2.5
Drilling Depth (mm)

(c)

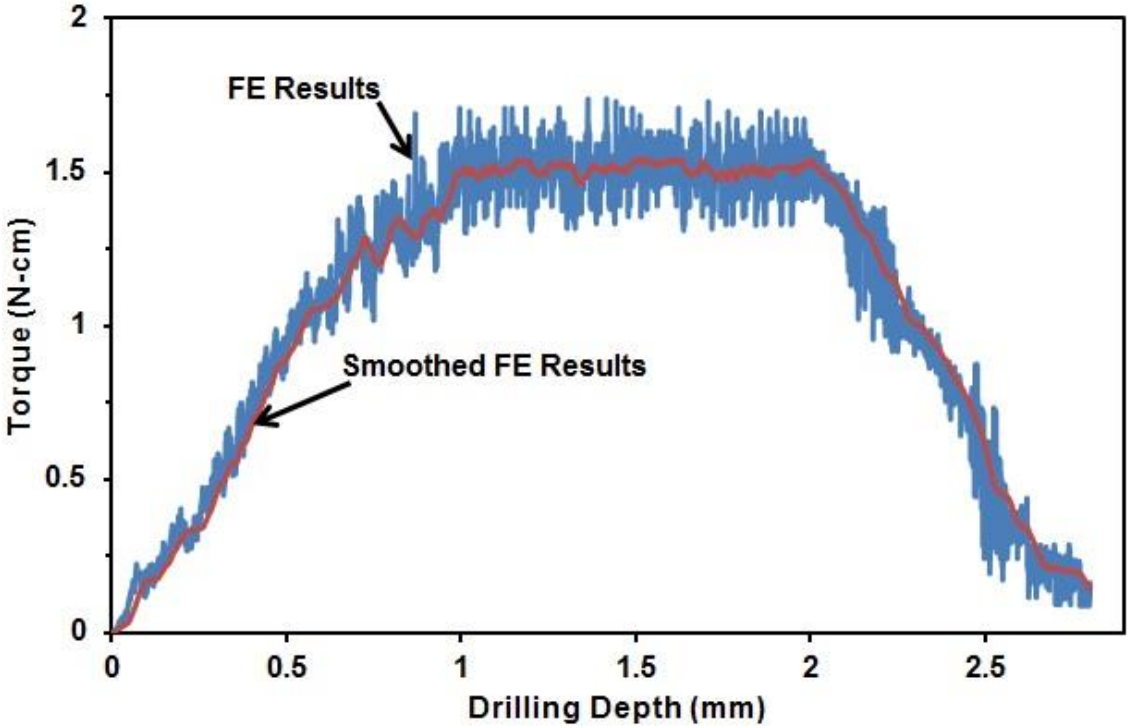
2
1.5
1
0.5
0
Torque (N-cm)
FE Results
Smoothed FE Results
0
0.5
1
1.5
2
2.5
Drilling Depth (mm)

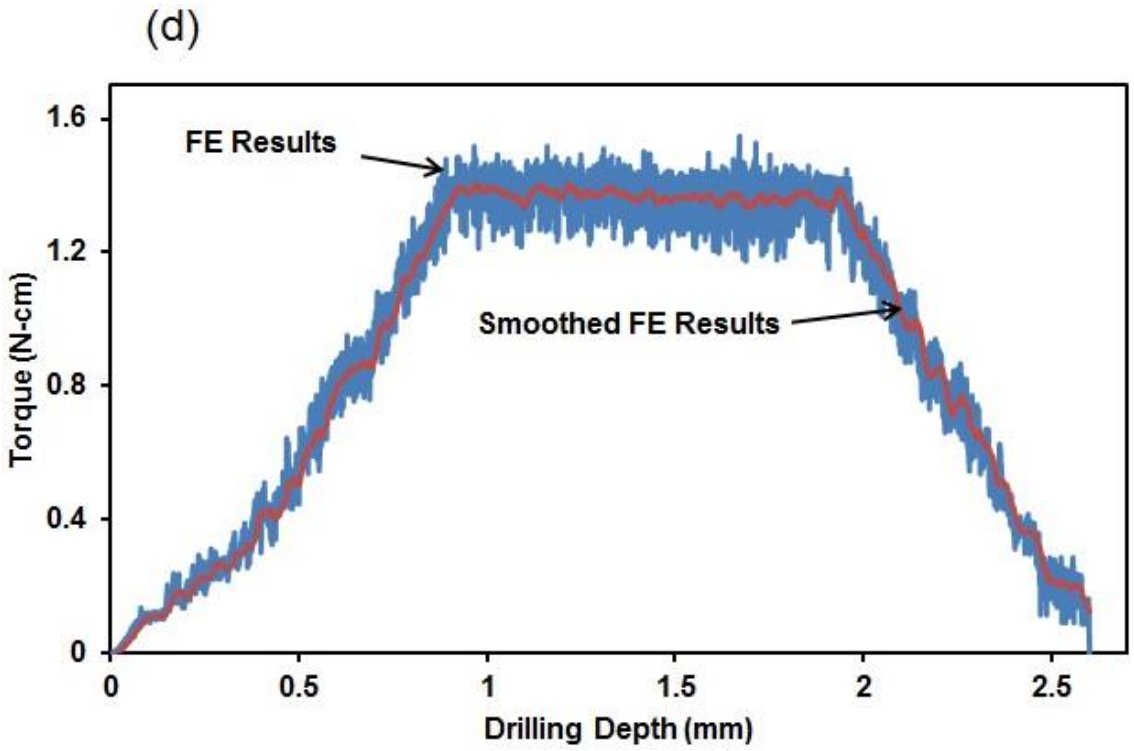

Figure 5-7 FE Drilling Results (Smoothed using the moving average function) (a) Thrust Force at 150 mm/min and 800 rpm, (b) Thrust Force at 80 mm/min and 800 rpm, (c) Torque at 150 mm/min and 800rpm, (d) Torque at 80 mm/min and 800 rpm

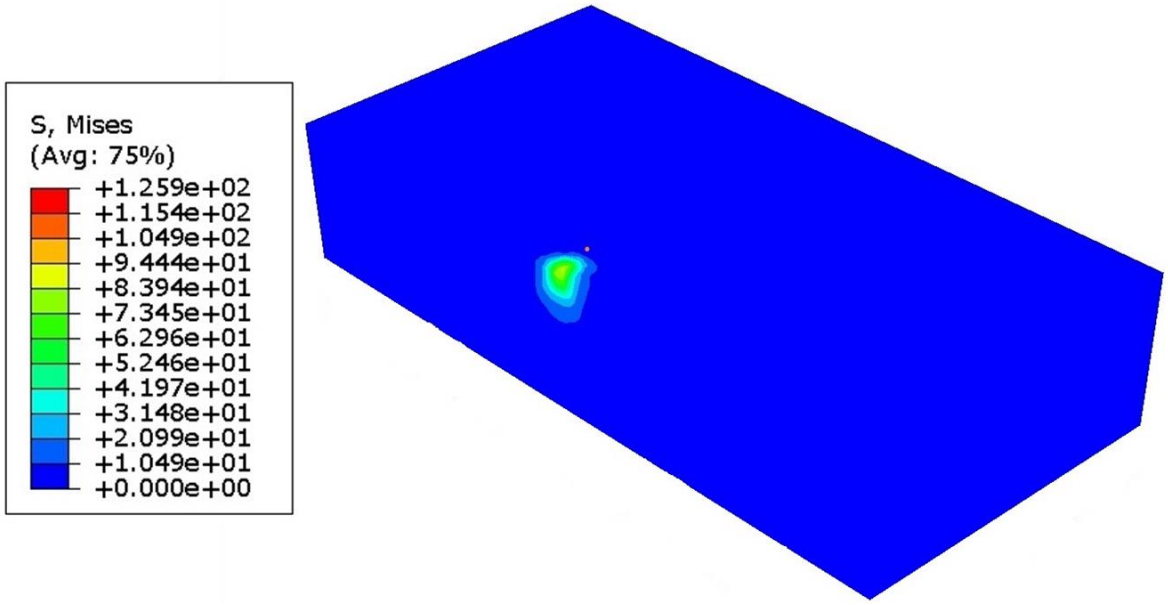

Figure 5-8 Cross-sectional view of bone sample at Drill bit initial contact (800 rpm and 150 mm/min)

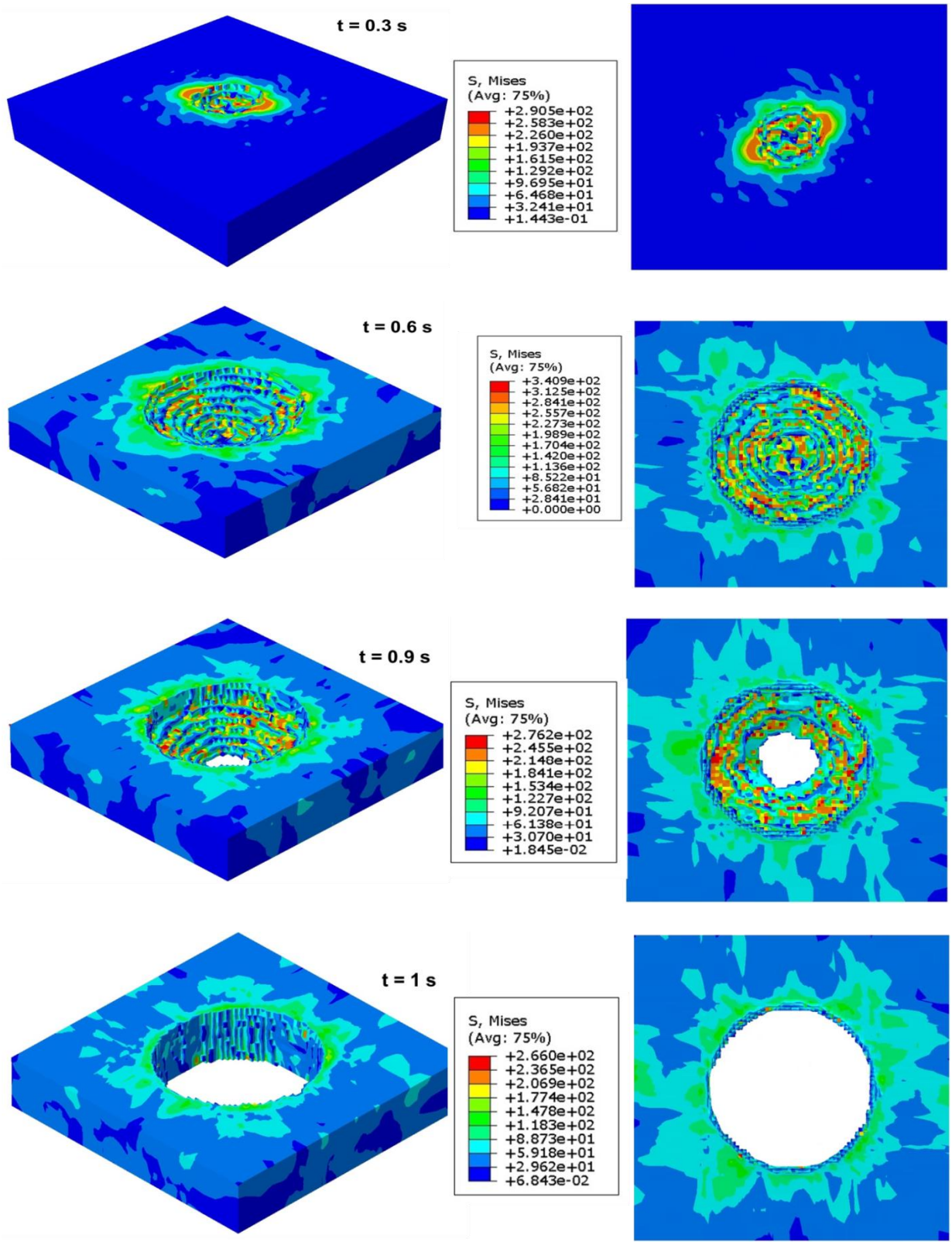

Figure 5-9 Stress distribution of FE model (800 rpm and 150 mm/min)

5.10 FE Model Validation

In order to allow a better comparison of the experimental and simulated thrust force and torque in drilling cortical bone, a feed rate of 150 mm/min was chosen from the experimental feed data with a spindle speed of 800 rpm, which gives a feed with respect to the rotational speed of 0.1875mm/rev. The FE simulations were carried out using these process parameters, which were subsequently used to predict the thrust force and torque for other feed rates and rotational speeds. Figures 5-8a and 5-8b show the experimental results and simulated data of the drilling thrust force and torque in cortical bone. The noise in the FE simulated force and torque data has been filtered out using the running average function. The average maximum thrust force (obtained for the period of complete drill engagement) in the experimental trials was 70-75N whereas the FE model estimated 73N. The experimentally measured torque was 1.54-1.62 N-cm compared to a predicted torque value of 1.5 N-cm by FE simulation. This shows that the FE model estimated the thrust force and torque accurately, with 2.9% and 6% deviation with respect to the respective test results.

(a)

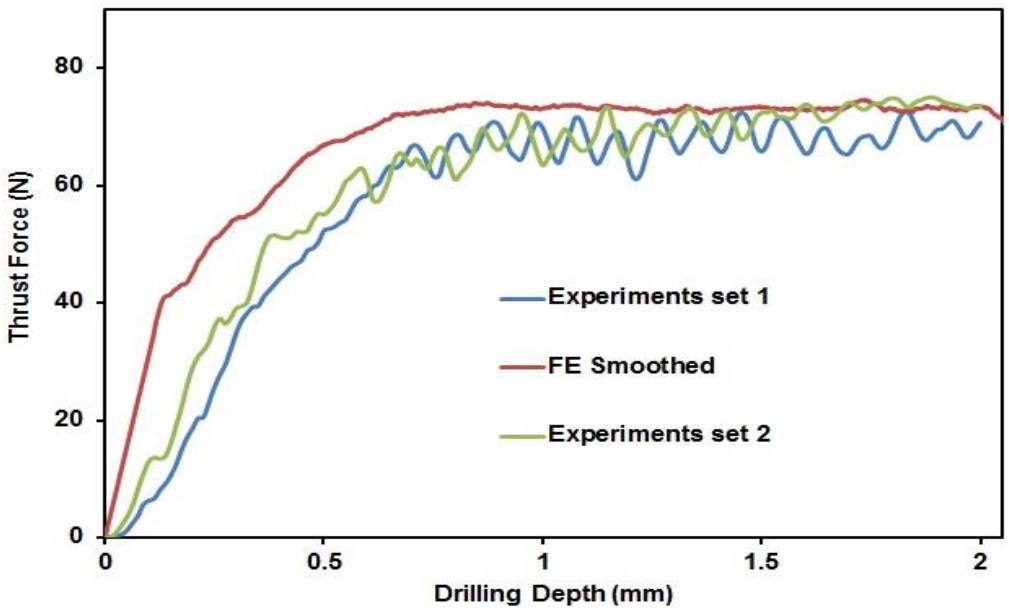

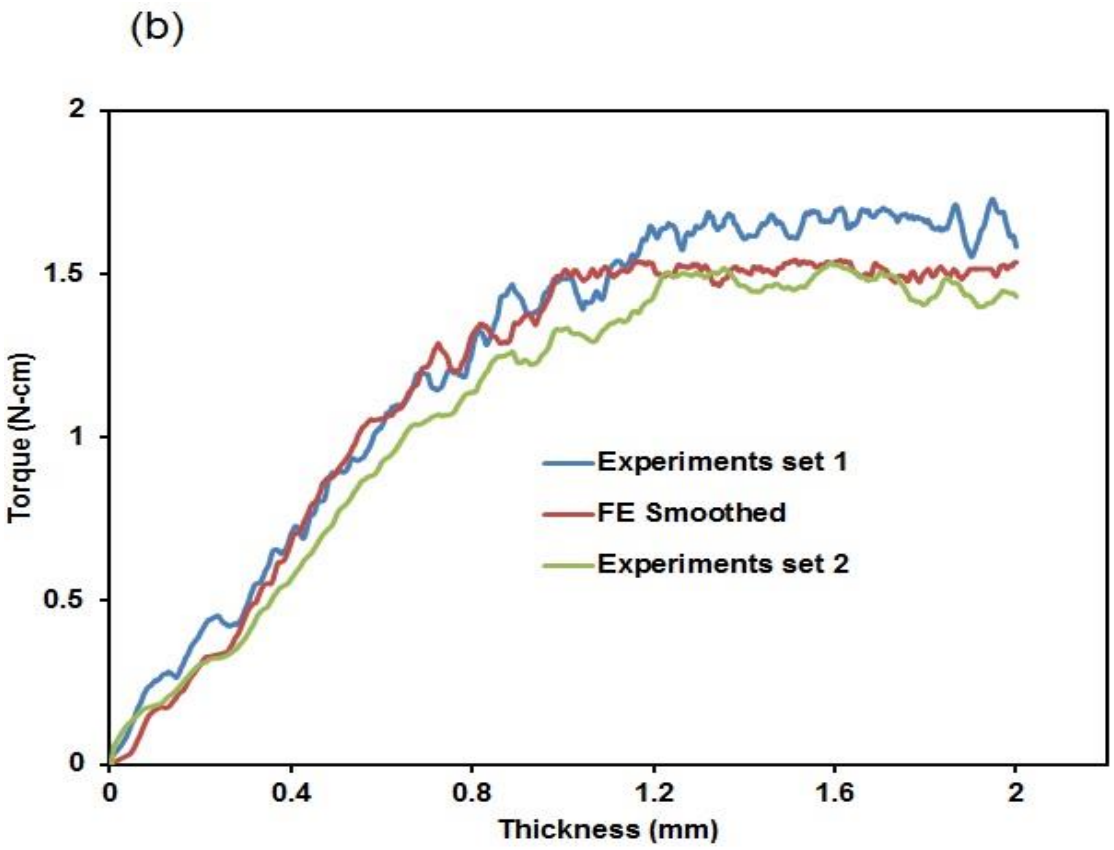

Figure 5-10 Experimental validation of FE model at 150 mm/min and 800 rpm (a) Thrust force (b) Torque. (The FE data is smoothed using the moving average filter)

5.11 Prediction of Thrust Force and Torque

Figure 5-9a shows the effect of drilling conditions on the average maximum thrust force. Both FE modelling and experimental tests give similar results. The FE model estimated the thrust force between 28 N and 76 N and the experimental results gave a thrust force between 23 N and 75 N for the range of feed rates modelled. The obtained results indicate that the drilling thrust force increases with increasing feed rate. It can also be observed from Figure 5-9a that at a constant spindle speed of 800 rpm, the average maximum thrust force was the highest at a feed rate of 150 mm/min (i.e. at 0.1875 mm/rev), and lowest at a feed rate of 40

mm/min (i.e. at 0.05mm/rev). Comparing the levels of thrust force for different feed rates, it was observed that when the feed rate was increased from 40 mm/min to 80 mm/min (i.e. from 0.05 mm/rev to 0.1 mm/rev) the thrust force increased by 60% and when the feed rate was increased from 80 mm/min to 120 mm/min the thrust force increased by 83%. The effect of drilling speed on torque and force was also examined. The torque decreased significantly as the spindle speed was changed from 800 rpm to 1500 rpm at all the feed rates used in this study as shown in Figure 5-9b. Similarly, the thrust force decreased as the spindle speed was changed from 800 rpm to 1500 rpm at the feed rates used in this study. Figure 5-9c shows the effects of spindle speed at a feed rate of 120 mm/min.

The effect of feed rate on torque is negligible as shown in Figure 5-9d. Comparing the level of torque for different feed rates, it was observed that when the feed rate was increased from 40 mm/min to 150 mm/min (i.e. from 0.05 mm/rev to 0.1875 mm/rev) the torque increased by only 6%. All other combinations of feed rates and spindle speed show similar trends in simulations.

(a)

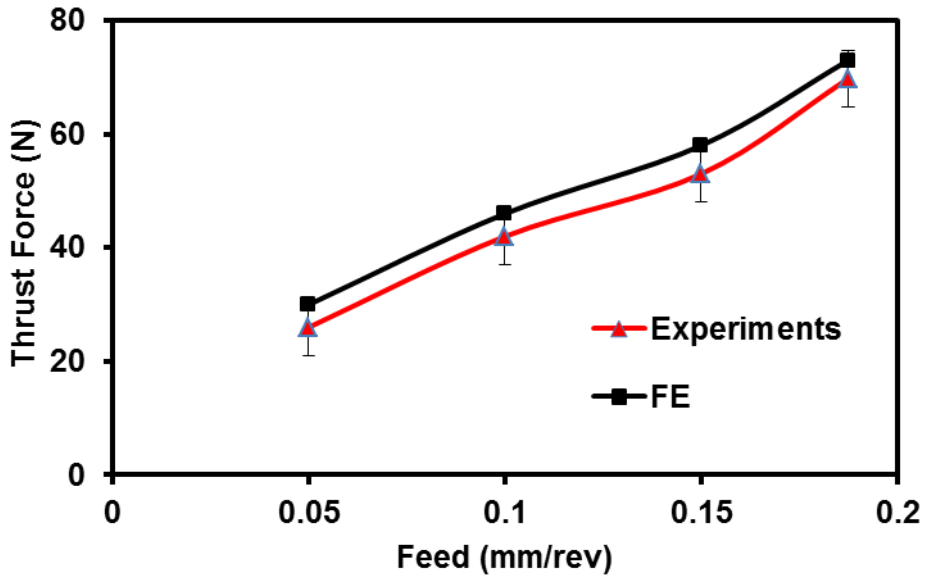
80
60
40
20
0
Thrust Force (N)
0
0.05
0.1
0.15
0.2
Feed (mm/rev)
Experiments
FE

(b)

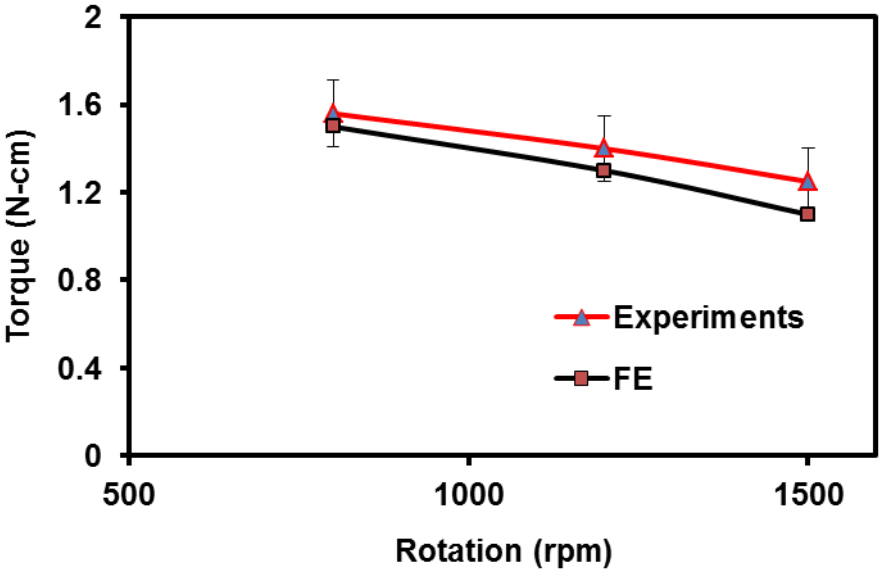
2
1.6
1.2
0.8
0.4
0
Torque (N-cm)
500
1000
1500
Rotation (rpm)
Experiments
FE

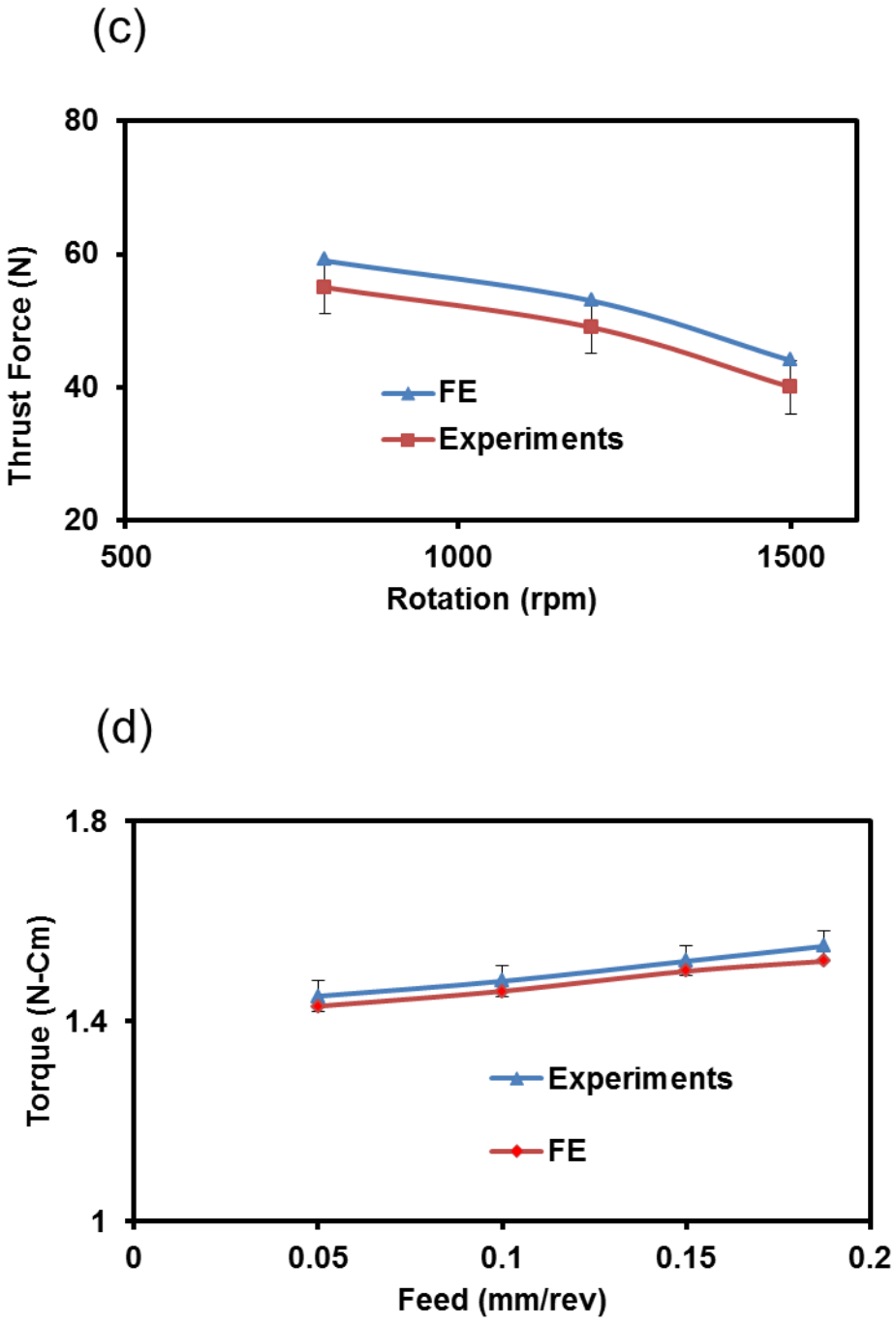

Figure 5-11 Comparison of experimental and FE results at different feed rates and spindle speeds (a) Thrust force (with error bar of fixed value + 5), (b) Torque (with error bar of fixed value + 0.15), (c) Thrust force (with error bar of fixed value + 4), (d) Torque (with error bar of fixed value + 0.02)

5.12 Possible Limitations

It should be noted that several factors could improve the accuracy of the simulation results. Amongst these is the use of a more realistic friction model, chip tool interaction, type of chip, inclusion of thermal effects and accounting for drill bit wear effects. Because of the high elements distortion at the front of the drill bit, the time step decreases and the simulation does not converge; thus the distorted elements at the front of the drill bit need to be deleted. In this study, the chip is not modelled due to the computational cost; therefore the friction between the chip and the drill bit is ignored. Furthermore, in the experiments bone was fully soaked at room temperature, and the maximum time of drilling was 3s, which is below the bone necrosis threshold limit, justifying that temperature does not affect the approach taken in this study; Eriksson et al. 1984 [88] established a threshold of 47 ^{0}C for 1 min to cause thermal necrosis of the cortical bone, and Barbosa et al. 2014 [158] established that increase in temperature without irrigation is 14 ^{0}C. The type of element used to discretize the bone component may also affect the results. A discrepancy in torque predictions may be due to the overly stiff 3D solid elements used with the default reduced-integration scheme available in Abaqus/explicit. Artificially relaxing the stiffness of solid elements may address this issue; this will be a topic for future research and is not addressed in the current study. Only one drill bit diameter was used i.e., 2.5 mm, thereby limiting the present conclusions to this drill bit size. However, the current diameter is within the range reported in previous literature, and the particular drill bit chosen is commonly used in clinics. Only three spindle speeds were used, thereby limiting the conclusion to this range. The current speeds are within the ranges reported earlier in biomechanics reports. Studies carried out by Nam et al. 2006, Matthews et al. 1972 define a range for safe drilling.

5.13 Concluding Remarks

In this chapter the effect of different machining parameters on thrust force and torque in drilling of a cortical bone has been investigated numerically. In this chapter, a three dimensional (3D) Lagrangian FE model of drilling on cortical bone was developed using a commercially available FE software ABAQUS/Explicit. The behaviour of cortical bone in elastic regime was defined using the Hill's potential theory for anisotropic materials together with the rate dependent plasticity criterion. An element removal scheme was used based on ductile damage initiation criterion to replicate the hole making process. The following observations are made in this study:

- This is the first study using 3D FE model with a material damage law to predict drilling forces in cortical bone with experimental validation
- The FE model predicted drilling thrust force and torque with reasonable accuracy when compared to experimental results.
- The validated drilling model was used to determine the thrust force, and torque for different drilling conditions. It was observed that the thrust force increased with an increase in feed rate while the torque decreased with an increase in rotational speed. Similarly the thrust force decreased with an increase in rotational speed while the effect of feed on torque is negligible. The thrust force and torque may be reduced using a combination of low feed rate and high rotational speed while drilling in cortical bone within the range of the drilling conditions investigated in this study. However, care must be taken to avoid bone damage (necrosis) if a very low feed rate with high rotational speed (i.e. very low feed per rotation) is chosen without irrigation, especially when drilling in thick bone. This recommendation is supported in literature as Matthews and Hirsch, 1972 [159] investigated human cadaveric

femora and found that increasing the rotational speed from 345 rpm to 2900 rpm did not have any significant change in the temperature during drilling. But increasing the thrust force was associated with decrease in both maximum temperatures and their duration. They measured the effect of applied force from 19.6 N to 117.6 N along with the drill speeds varying from 345 rpm to 2900 rpm. Nam et al. (2006) [160] proposed that the optimal conditions during experimental testing are a combination of low speed (600 rpm) and high pressure (1000 g), or high speed (1200 rpm) and low pressure (500 g) which produced temperature rise to 40–45 °C.

- The validation of FE model also indicates the efficacy of using drilling data for prediction of quality.

CHAPTER 6

Analytical Modelling for Drilling of Bone Drilling

This chapter proposes an improved theoretical method to predict the thrust force of twist drill bits in bone drilling. The thrust force is calculated analytically without resorting to any calibration experiment, only by tool geometry, cutting conditions and material properties. The validation of the model is also presented in this chapter.

6.1 Analytical Model Formulation

The drilling process has two motions; feed and rotation. These two motions complicate the absolute motion that the drill bit experiences at any point along its cutting edge. At the outer edge the effect of feed is negligible when compared with the rotation component. However, at the centre the drill bit feed is the primary component. For this reason the model of the drill bit was separated into three different zones (indentation, primary cutting and secondary cutting), as shown in Figure 7-1; with each zone being described by a unique cutting model (Section 6.2 & 6.3). The significant parameters that describe the geometry of a conical point drill (Figure 7-1) include the drill bit diameter (D = 2R), point angle (2 φ), helix angle (Ψ), web thickness (w), and chisel edge angle (ϕ). Oxford (1955) [161] identified a small region all around the middle part of the drill (indentation zone) where the material is not cut but extruded. Outside the indentation zone, the chisel edge performs an orthogonal cut with a negative rake angle.

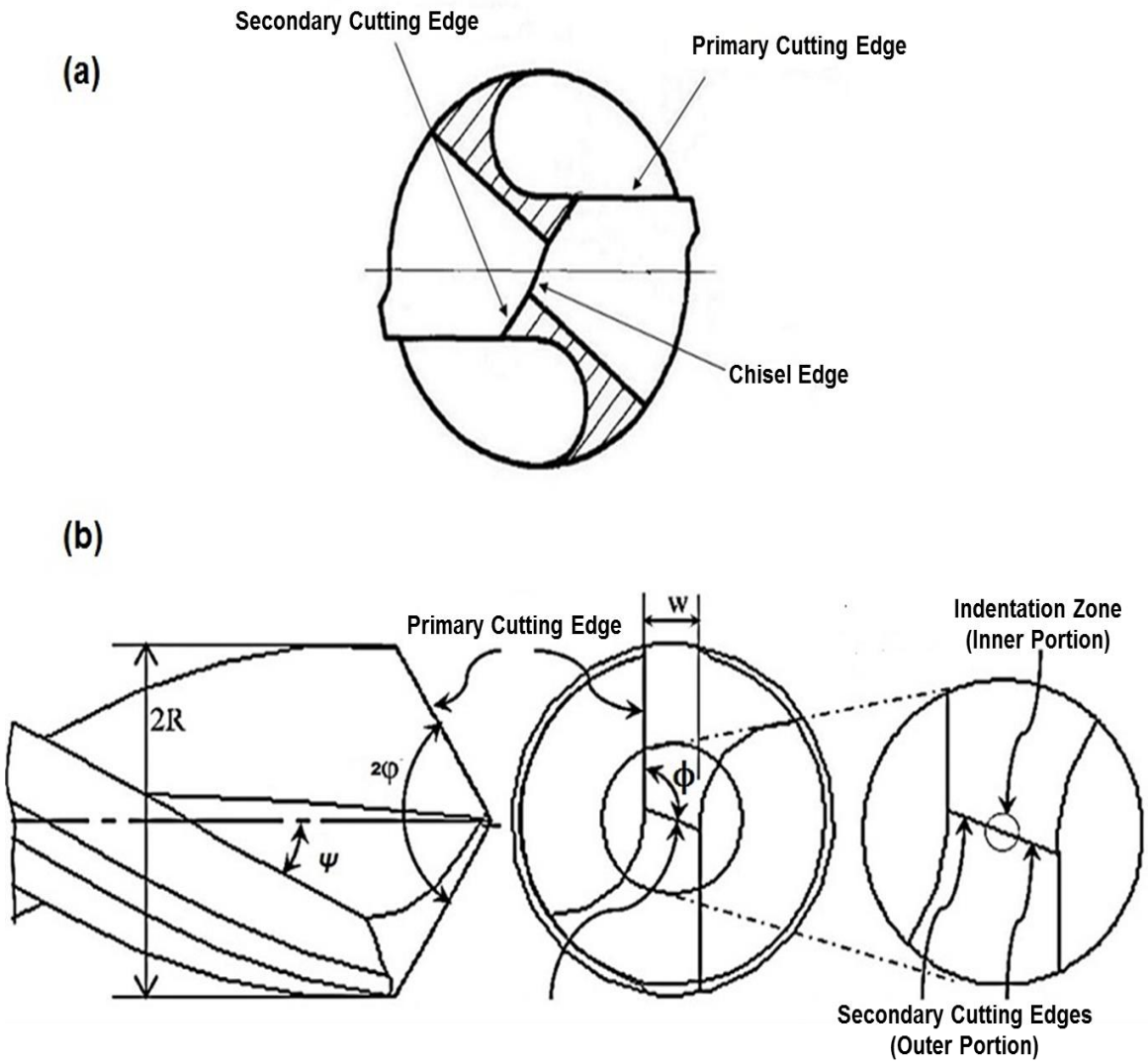

Figure 6-1 (a) End view of Drill bit showing the Cutting Zones (indentation, primary cutting, and secondary cutting), (b) Detailed Description of the Cutting Zones

6.2 Force Model Formulation for Chisel Edge

In the region around the centre of a drill, material removal is assumed to be plastic extrusion. This is called the indentation zone. At the remaining portion of the

chisel edge, termed as the secondary cutting edges, material removal is by orthogonal cutting with a large negative rake angle. Figure 7-1 shows the two regions on the chisel edge. The indentation zone is assumed as a rigid wedge indenting a plastic material with material extruding on both sides of the wedge. To determine the forces on the wedge, it is necessary to find the radius (r_{ind}) of the indentation zone. Bono and Ni (2001) [162] developed an expression for the indentation zone using a three-dimensional mathematical model for the indentation zone geometry and verified its accuracy by experiments. The equation they developed is used in this study, which is shown as:

$$r_{ind} = \frac{f_r \tan k}{2\pi} \qquad 6\text{-}1$$

where k is the half angle of the wedge as shown in Figure 6-2 which is equal to the value of the normal rake angle ($\alpha_{n,ch}$) of the chisel edge (Chandrasekharan, 1996) [163] and f_r is the feed rate.

$$\alpha_{n,ch} = -\tan^{-1}[\tan\varphi \cos(\pi - \phi)] \qquad 6\text{-}2$$

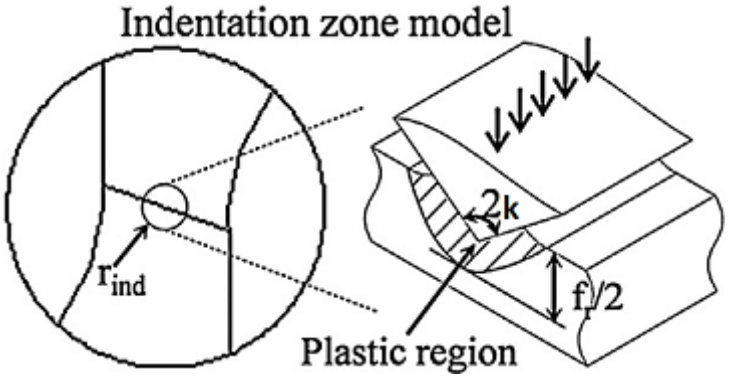

Figure 6-2 Indentation Zone of Chisel Edge

The slip-line field solution developed by Kachanov (1971) for the indentation process with a rigid wedge when the material extrudes along both sides of the wedge is adopted here to determine the cutting forces at the indentation zone. The thrust force (F_{ind}) contributed by the indentation zone is described below:

$$F_{ind} = \frac{2\sigma_y(1+\varepsilon)f_r r_{ind}\sin\alpha_{n,ch}}{\cos\alpha_{n,ch} - \sin(\alpha_{n,ch} - \varepsilon)} \qquad 6\text{-}3$$

where σ_y is the yield stress of the cortical bone, and ε is the solution for the slip lines, determined from the boundary conditions of the problem, which is computed as;

$$2\alpha_{n,ch} = \varepsilon + \cos^{-1}\left[\tan\left({}^{\pi}/_{4} - {}^{\varepsilon}/_{2}\right)\right] \qquad 6\text{-}4$$

In the cutting part of the chisel edge, i.e. in the two secondary edges, The cutting edges are divided into five elements and the method adopted to determine the corresponding elemental drilling thrust forces uses the orthogonal cutting model. The magnitude of the total drilling thrust force along the axis of the drill bit is then obtained by summing the forces at all elements for the chisel cutting edges. Considering that the tangential cutting velocity is small, the effect of the feed velocity is included to compute the dynamic rake angle. The feed angle ϕ_f is defined as the angle between the tangential cutting velocity and the resultant velocity given by

$$\phi_f = \tan^{-1}\left(\frac{f_r}{2\pi r}\right) \qquad 6\text{-}5$$

Therefore, the dynamic rake angle is

$$\alpha_{d,ch} = \alpha_{n,ch} + \phi_f \qquad 6\text{-}6$$

In the case of high negative rake angle as in chisel edge, the shear angle, γ_c, and friction angle, λ_c, could be assumed as (Kita, 1982) [164].

$$\gamma_c = {}^{\pi}/_{2} + 1.2(\alpha_{d,ch} - \lambda_c) \qquad 6\text{-}7$$

$$\lambda_c = {}^{\pi}/_{4} + {}^{2\alpha_{d,ch}}/_{3} \qquad 6\text{-}8$$

The thrust force for each element can be expressed as

$$F_{ci} = \frac{t\Delta r\tau \sin(\lambda_c - \alpha_{d,ch} + \phi_f)}{\sin(\gamma_c)\cos(\gamma_c + \lambda_c - \alpha_{d,ch})} \qquad 6\text{-}9$$

Where Δr is the length of the element, τ is the shear strength of the material, and t is the uncut chip thickness and is given by Armarego (1997) [165] as

$$t = \frac{f_r \sin\varphi \cos\varepsilon}{2} \qquad 6\text{-}10$$

Integrating elemental force along the radius of the drill bit on the chisel edge region, we obtain the following equation for the drilling thrust force on the chisel edge.

$$F_c = 2\int_{r_{ind}}^{w} dF_{ci} \qquad 6\text{-}11$$

6.3 Force Model Formulation for Cutting Lips

The cutting action along the cutting lips is a three-dimensional oblique cutting process (Figure 6-3). The cutting velocity V_c, as well as the inclination angle (***i***) and normal rake angle (δ), vary with the radial distance (r) along the cutting lips of the drill bit. The radial distance is the distance of the considered point on the cutting lips from the drill bit axis measured in a plane that is normal to the axis.

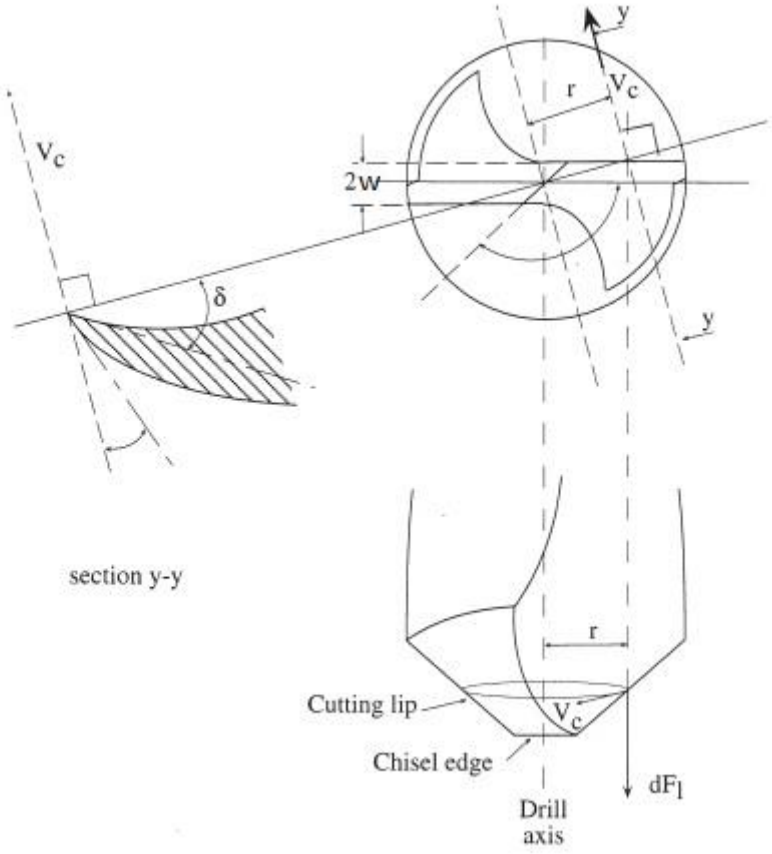

Figure 6-3 Cutting Edge Geometry

The variations in the normal rake angle and cutting velocity cause the forces to vary on the cutting lips of the drill. The cutting action is much more efficient at the outer regions of the cutting lips with large positive normal rake angles and higher cutting velocities than at the inner regions of the cutting lips with negative normal rake angles and lower cutting velocities. Therefore, a model to predict the cutting lip forces should account for the variation of the cutting parameters. To account for this variation, the cutting lips are divided into a number of cutting elements. The cutting forces that are acting along the primary cutting edge are represented as a series of oblique cutting elements. The elemental forces are then integrated to determine the overall thrust force in terms of the basic geometrical features of the drill bit, the cutting conditions and the properties of the machined material.

From the available Oxley force model [166] for oblique cutting, the elemental thrust force $\mathbf{dF_L}$ can be determine based on the elemental forces $\mathbf{dF_R}$, $\mathbf{dF_C}$ and $\mathbf{dF_T}$ given in Figure 6-4.

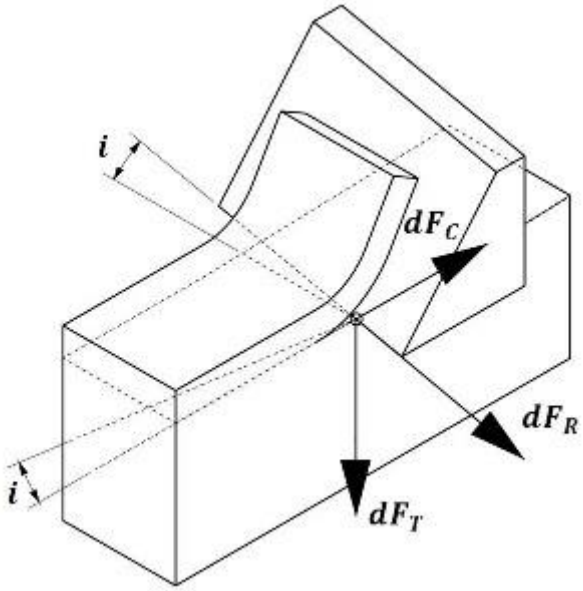

Figure 6-4 Oxley oblique cutting [6]

The elemental force $\mathbf{dF_C}$ at any given point on the cutting edge is parallel to the direction of the cutting velocity, the elemental force $\mathbf{dF_T}$ is perpendicular to the direction of the cutting velocity and to the cutting edge, and the elemental force $\mathbf{dF_R}$ is perpendicular to the both $\mathbf{dF_C}$ and $\mathbf{dF_T}$.

The presented CAD model has shown in Figure 6-5 depicts the projections of each elemental force in each direction.

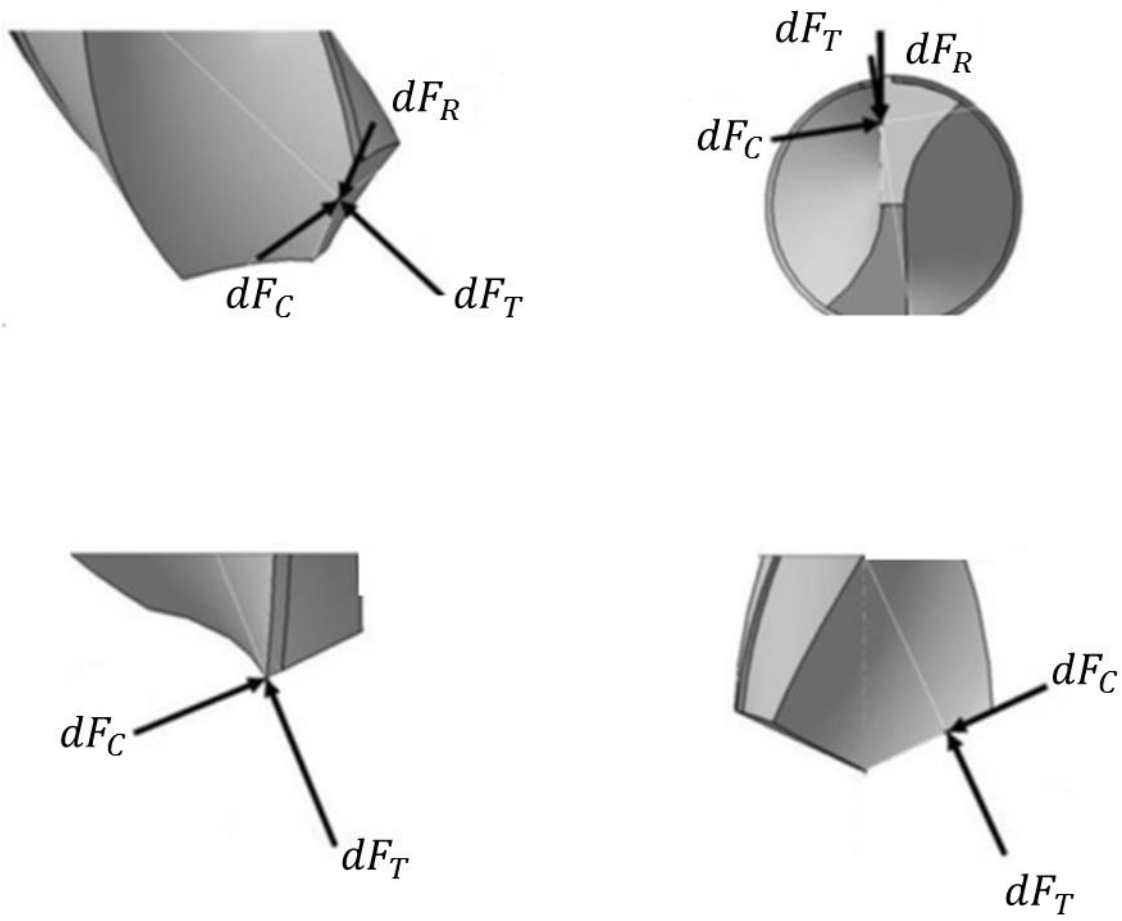

Figure 6-5 Projections of the elemental forces

The total elemental forces $\overline{\boldsymbol{dF}_T}$, $\overline{\boldsymbol{dF}_R}$ and $\overline{\boldsymbol{dF}_C}$ in the normal direction, radial direction and in the direction of the cutting velocity respectively can be calculated as

$$\overline{dF_T} = dF_T \cos\varepsilon - dF_C \sin\varepsilon \qquad 6\text{-}12$$

$$\overline{dF_R} = dF_R \cos i - dF_C \sin i \qquad 6\text{-}13$$

$$\overline{dF_C} = dF_C \cos i - dF_R \sin i \qquad 6\text{-}14$$

Here i and ε are inclination and reference angles as shown in Figure 6-6.

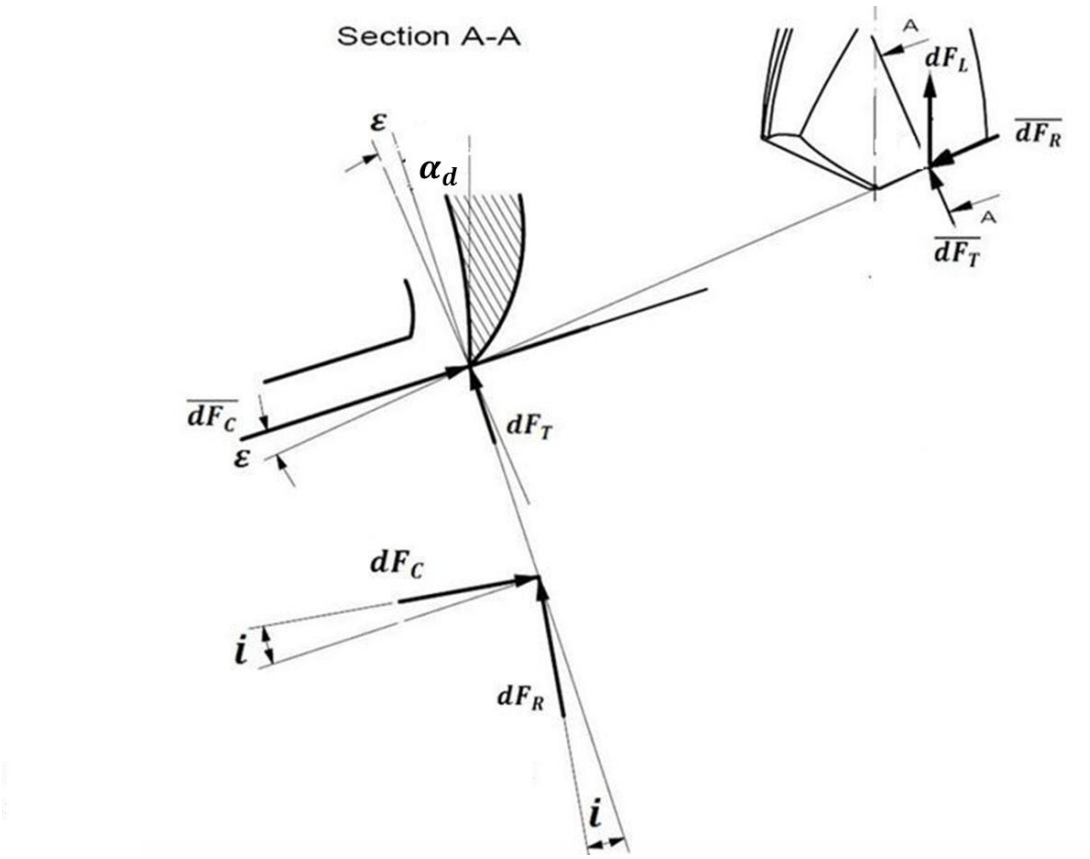

Figure 6-6 Model for Force Prediction along the Primary Cutting Edge

Thereby

$$dF_L = \overline{dF_T} \sin\varphi - \overline{dF_R} \cos\varphi \qquad 6\text{-}15$$

So the total elemental thrust force can be expressed as

$$dF_L = dF_T \cos\varepsilon \sin\varphi - dF_C \sin\varepsilon \sin\varphi - dF_R \cos i \cos\varphi + dF_C \sin i \cos\varphi \qquad 6\text{-}16$$

Using the Oxley model [6], dF_T and dF_R can be found as

$$dF_T = dF_C \tan(\lambda - \alpha_d) \qquad 6\text{-}17$$

$$dF_R = \sqrt{dF_C^2 + dF_T^2}\,\sin\lambda\cos\alpha_d\tan i \qquad 6\text{-}18$$

Here λ and α_d are the friction and dynamic rake angles respectively. Substituting 6-17 and 6-18 into 6-16 gives

$$dF_L = dF_C\left(\tan(\lambda-\alpha_d)\cos\varepsilon\sin\varphi - \frac{\sin\lambda\cos\alpha_d\sin i\cos\varphi}{\cos(\lambda-\alpha_d)} - \sin i\cos\varphi + \sin\varepsilon\sin\varphi\right) \qquad 6\text{-}19$$

The Armarego et al [167] define dF_C as

$$dF_C = \frac{f.dl.\tau.\cos(\lambda-\alpha_d)\cos\varepsilon\sin\varphi}{2\sin\gamma\cos\theta} \qquad 6\text{-}20$$

Here the *dl* is the differential element of the length of the cutting edge, f is the feed rate, γ is the shear angle of oblique cutting and θ is the angle of resulting force.

The total thrust force in the two primary cutting edges is defined as

$$F_L = 2\int_{r_A}^{r_B} dF_L \qquad 6\text{-}21$$

where $[r_A, r_B]$ is an interval, which is defined by the radial distance from the drill bit axis to the beginning and the end of the primary cutting edge. All the parameters for the total thrust force equation depend only on the radial distance of the cutting edge element from the drill bit axis and on the drill bit geometry; they can be found from the equations given below [168].

$$i = \sin^{-1}(\sin\omega\sin\varphi) \qquad 6\text{-}22$$

$$\omega = \sin^{-1}\left(\frac{w}{r}\right) \quad \text{6-23}$$

$$\delta_r = \tan^{-1}\left(\frac{2r}{D}\tan\psi\right) \quad \text{6-24}$$

$$\alpha_d = \tan^{-1}\left(\frac{\tan\delta_r}{\sin\varphi}(\cos\omega + \sin\omega\tan\omega\cos^2\varphi) - \tan\omega\cos\varphi\right) \quad \text{6-25}$$

$$\lambda = \tan^{-1}\left(\frac{\cos\gamma - \cos\gamma_n + \tan(\gamma_n - \alpha_d)\sin\gamma_n}{\sin\gamma}\right) + \alpha_d \quad \text{6-26}$$

$$\gamma = \cot^{-1}(\cot\gamma_n\cos i - \tan\alpha_d(1 - \cos i)) \quad \text{6-27}$$

$$\varepsilon = \tan^{-1}(\tan\omega\cos\varphi) \quad \text{6-28}$$

$$\theta = \gamma + \lambda - \alpha_d \quad \text{6-29}$$

$$\lambda_n = {}^{\pi}/_{4} + {}^{2\alpha_d}/_{3} \quad \text{6-30}$$

$$\gamma_n = {}^{\pi}/_{2} + 1.2(\alpha_d - \gamma_c) \quad \text{6-31}$$

The next important step in this calculation is the necessity to determine the shear stress τ, which essentially affects the values of the total thrust force.

6.4 Shear Strength of Cortical Bone

Shear strength of the material at the shear plane is another challenge in calculating drilling forces since it greatly changes depending on strain, strain rate and cutting conditions. In this study, it is assumed that compressive strength at high strain rate and shear strength of the bone have the same hardening behaviour, given by Equation 6-32 below,

$$\frac{\tau_y}{\tau_{y0}} = \frac{\sigma_y}{\sigma_{y0}} \quad \text{6-32}$$

where τ_{y0} and τ_y are ultimate strength and shear yield respectively, and σ_y and σ_{y0} are compressive yield and ultimate strength of bone at high strain rate.

τ_y, used in the computation of the cutting edge thrust force, is obtained from the octahedral shear stress relationship,

$$\tau_y = \frac{\sqrt{2}}{3}\sigma_y \qquad 6\text{-}33$$

and σ_y is obtained from high strain rate tests results presented in Chapter 4. Table 6-1 shows the drilling conditions, drill bit parameters and material property used in this model.

Table 6-1 Analytical Model input values

Drill Bit	ϕ2.5 mm, point angle 118^o,web thickness 0.7mm,chisel edge angle 116^{o,} Helix angle 28.28^o
Spindle speed (rpm)	800, 1200, 1500
Feed (mm/rev)	0.05, 0.1,0.15, 0.1875
Shear Strength(MPa)	127

Now, we can predict the thrust force from the drill tool geometry, cutting conditions and bone properties. Figure 6-7 shows the flow chart of thrust force computation.

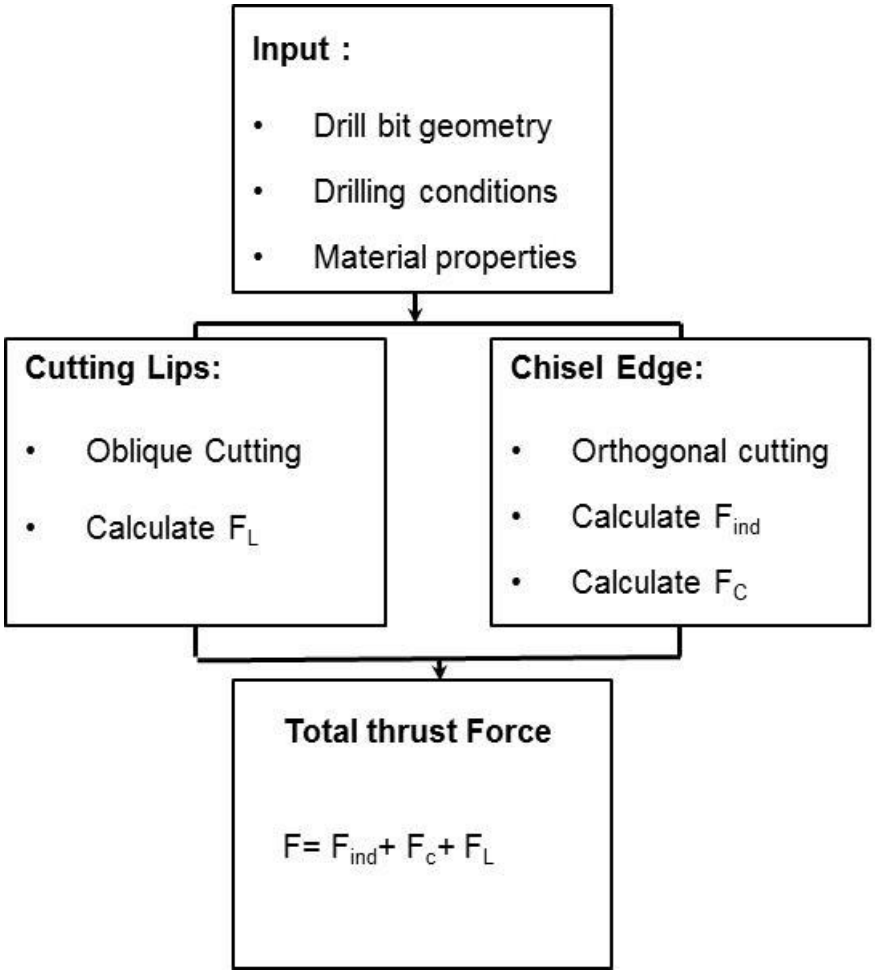

Figure 6-7 Flow Chart of Thrust Force Computation

6.5 Results and Discussion

A computer program in Matlab (2012) is developed to carry out the analysis. The effectiveness of the proposed model for bone drilling is verified by the experimental data presented in chapter 4. Figure 6-8 provides the thrust forces for four cases with feed rates of 150 mm/min, 120 mm/min and 60 mm/min and rotational speeds of 800 rpm and 1200 rpm. First, a considerable variation in experimental data for both within the same bone and between different bones is observed. The variations are smaller within the same anatomic position of bone. This is caused by the inherent variation in mechanical characteristics of different bones. It is seen that the model is able to predict the trend of thrust forces. The model predicts

the average force well upon full engagement at higher feed rates, but it under predicts the average force at 0.05 mm/rev. The main reason for this mismatch is that the gradually compacted chips inside the flutes increase the thrust force as the drill bit is proceeding into the bone, as presented by Mellinger et al., 2002 [169]. Moreover, higher spindle speeds can exacerbate this problem. It is seen that the model is able to predict the trend of thrust forces. Table 6-2 provides the comparison of the predicted thrust forces from different drill bit regions. It shows that, the chisel edge is the major contributor of thrust force. 80% of the predicted thrust force at all drilling conditions was contributed by the chisel edge.

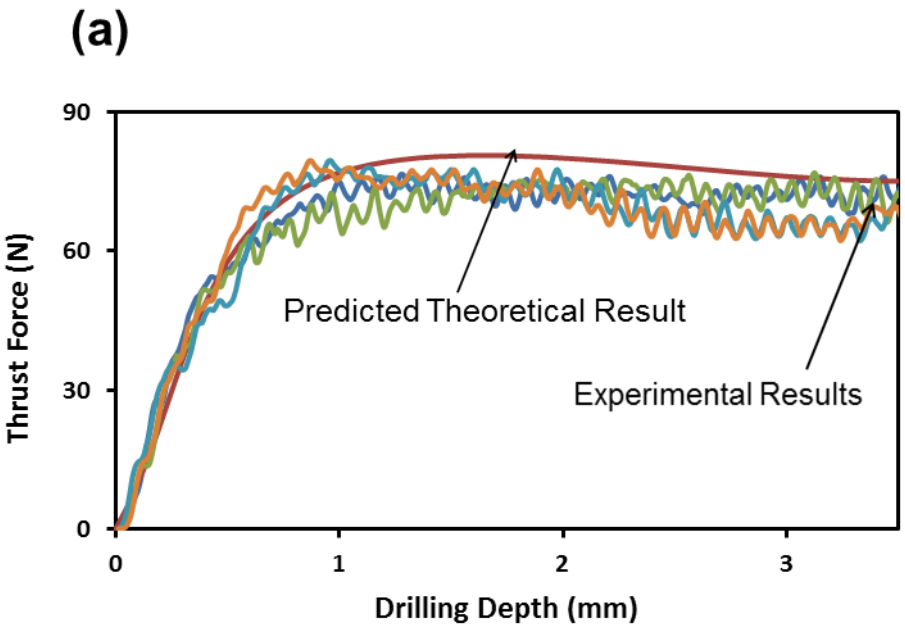

(b)

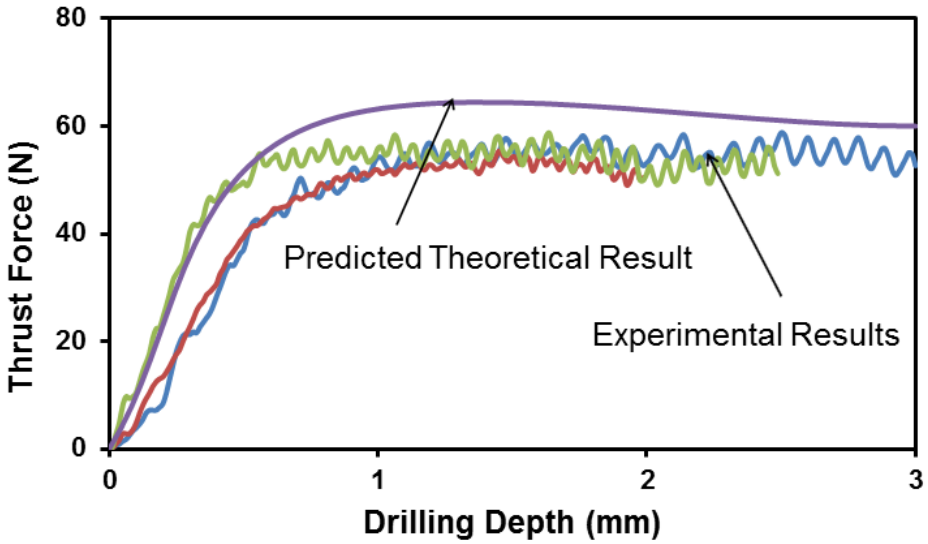
80
60
40
20
0
Thrust Force (N)
0
1
2
3
Drilling Depth (mm)
Predicted Theoretical Result
Experimental Results

(c)

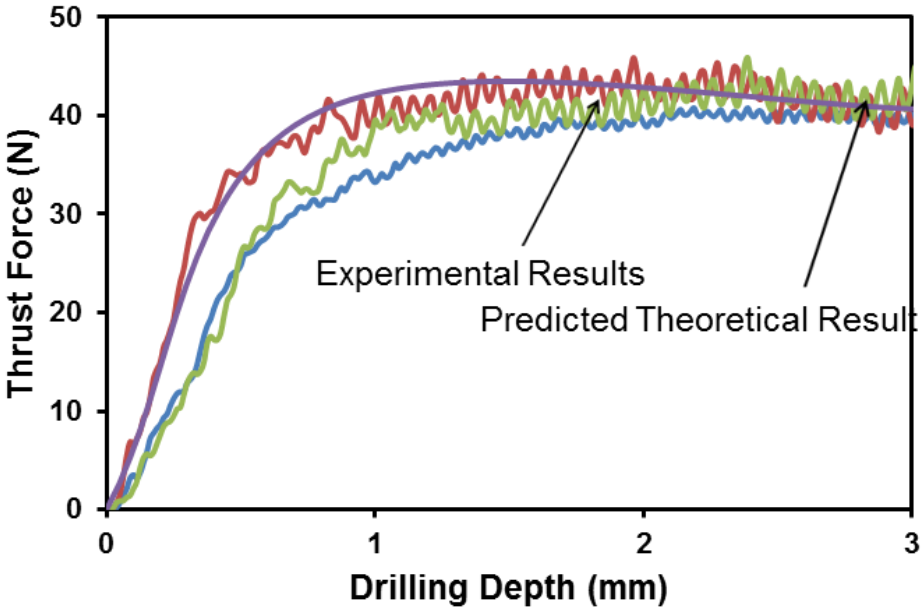
50
40
30
20
10
0
Thrust Force (N)
0
1
2
3
Drilling Depth (mm)
Experimental Results
Predicted Theoretical Result

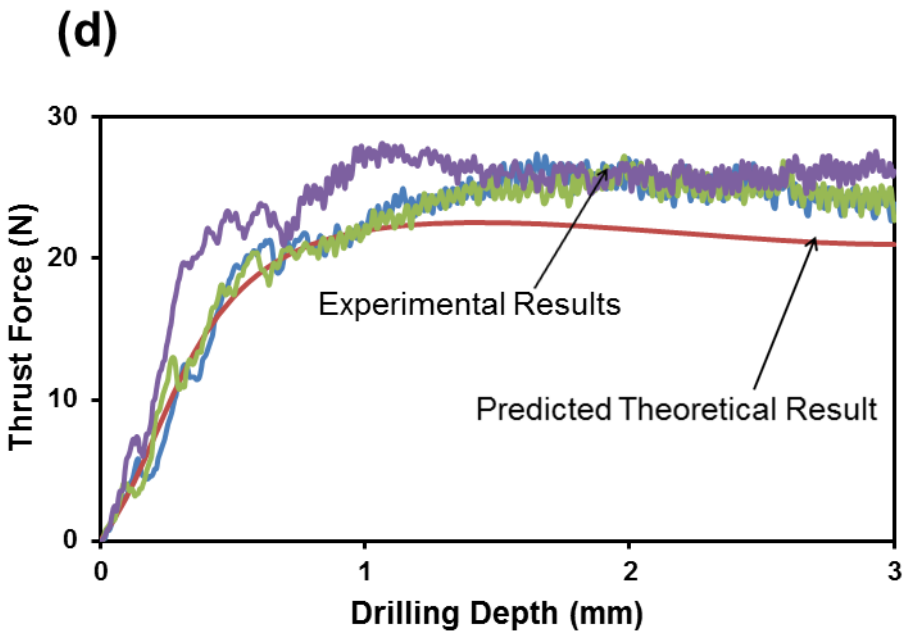

Figure 6-8 Comparison of forces obtained from the model and experiments (anterior portion of bovine femur), (a) 150 mm/min and 800 rpm (0.1875 mm/rev), (b) 120 mm/min and 800 rpm (0.15 mm/rev), (c) 120mm/min and 1200 rpm (0.1 mm/rev), (d) 60 mm/min and 1200 rpm (0.05 mm/rev).

Table 6-2 Comparison of thrust force from different regions

Feed (mm/rev)	Thrust Force (N)		
	Indentation	Secondary Cutting Edge	Primary Cutting Edge
0.05	0.034	16	3.8
0.1	0.133	32	7.6
0.15	0.300	49	11.5
0.1875	0.469	62	14.3

6.6 Concluding Remarks

An improved mechanistic force model for predicting the thrust force, when drilling in cortical bone is developed in this chapter. The cutting action at the drill bit

point was divided into three regions, and models that accounted for the cutting mechanics of each region were formulated. The proposed analytical model consists of three separate machining mechanics for the cutting lips, secondary cutting edges, and indentation zone. The cutting lips and secondary cutting edges are divided into a number of elemental sections, and for each element, the cutting forces are determined using the high strain properties timed by the elemental chip load. The forces from the indentation zone are determined using the slip-line field theory. The predicted results for the cutting lips, chisel edge, and entire drill bit point showed the same trends and agreed well with the experimental results. This model can be used to predict the thrust force without any drilling experiments if the material properties of the bone are in hand, similarly it can be used to predict bone quality if drilling data is recorded in vivo.

CHAPTER 7

Conclusions and Recommendations for Future Work

In this chapter the conclusions that can be drawn from this study are summarised. The chapter aims to show how the objectives presented in Chapter 1 have been met, and concludes with recommendations for further work. A list of published, submitted and proposed publications that are produced as part of this study is also included.

7.1 Contribution of the Research

This research has demonstrated the acquisition of bone quality from drilling force data for the potential application in orthopaedic surgery. Drilling results at different anatomic positions on bone cortex showed that thrust force varies across different positions for the same drilling conditions. This indicated the ability of using drilling force to detect structural variability within bone cortex. Variability of drilling force in dry and wet bone proved the effectiveness of using drilling data as a predictor of bone quality. The results at different drilling conditions also showed agreement with previous studies.

This is the first study using a 3D FE model with a material damage law to predict drilling forces in cortical bone with experimental validation. The advantage of this model is that it can also be used for predicting temperature and mechanical damage during drilling into bone; appropriate experimental information would need to

be obtained for the latter two applications. The validation of the FE model for the prediction of drilling forces also indicates the efficacy of using drilling data for prediction of quality.

An improved analytical model of drilling in bone has also been presented in this study. This model, which showed a direct relationship between drilling force and mechanical property of material, sets the foundation of using drilling force data in quality prediction during orthopaedic surgery using a purposely designed instrumented drill unit.

7.2 Conclusions from this Research

This section aims to show how the objectives presented in chapter 1 have been met. The nine objectives are repeated here for clarity and are defined as:

Objective 1. To critically reviews the use of various direct and indirect bone quality measurements, and identifies the limitations and errors involved in such techniques.

Objective 2. To study and review current progress of the bone drilling process. Also, to identify the range and effect of various drilling parameters. This helps in developing the analytical model of bone drilling.

Objective 3. Characterisation of a cortical bone at high strain rate to determine the mechanical properties for use in numerical models.

Objective 4. Acquiring drilling force data for different cortex positions from pig and bovine bone. This is to verify that the drilling data can capture quality variation within different anatomical sites.

Objective 5. Investigate the effects of drilling conditions on drilling force data for bovine cortex. This is to validate, the finite element model of bone drilling.

Objective 6. Investigate the effects of densities on drilling force data for synthetic bone.

Objective 7. To demonstrate a correlation between the drilling force and screw pullout force by using the data acquired during drilling and screw pullout testing of synthetic bone material and animal bone.

Objective 8. Development of the finite element model to simulate drilling in bone. This is to verify the use of drilling data in predicting quality

Objective9. Formulating an analytical (mechanistic) model of the bone drilling process to establish a relationship between drilling force and bone quality

To support objective 1, a critical literature review of the direct and indirect bone quality measurement methods was conducted. The direct methods are destructive in nature and unavailable noninvasively. The various commercial indirect methods evaluated in this research are not very accurate, effective or reliable methods for in-vivo bone quality prediction. An ideal method of in-vivo bone quality prediction should be cheap, accurate, easy to use and easy to interpret. Hence, the use of bone drilling data as an alternative in-vivo method to predict bone quality has been explored in this research. The following conclusions were drawn from the review:

- Destructive mechanical testing is necessary for direct assessment of bone strength and remains essential to characterization of bone structural performance.
- The direct methods, which are performed in-vitro, measure bone mechanical properties through tensile, compressive, bending, torsion and hardness tests as well as simulating real life bone fracture conditions or screw pullout tests.
- Mechanical properties of the bone specimen can be greatly influenced by the method of bone preservation before conducting any mechanical tests.
- The indirect methods do not give a direct measurement of bone mechanical properties; therefore various correlational studies between direct and indirect methods have been carried out in order to evaluate the efficacy of the indirect methods in predicting bone quality.
- The use of imagining techniques are limited because these are expensive and expose patients to high radiation.
- pQCT has a limited use as it can only be used at the peripheral bone sites and DXA bone density measurements, when performed in-vivo, could lead to an inaccurate or wrong prediction of the bone quality.
- Variation in bone geometry, use of non-site specific bone density measurement, and bone anisotropy affect bone quality prediction using the indirect methods.

To support objective 2, a critical review of bone drilling was conducted. The following conclusions were drawn from the review:

- Drill parameters including geometry, and cutting parameters such as feed rate, cutting speed and the use of coolant have influence over drilling forces, temperature and surface quality.

- Large forces experienced during bone drilling may result in drill overrun; promote crack formation, and are the major contributor of heat generation during bone drilling.
- The limitations of the analytical models include the calibration experiments to determine the coefficients for specific cutting energies, and the assumption of a plastic extrusion mechanism for the bone in the indentation zone.
- Finite element modelling of drilling in bone requires an accurate model of the constitutive behaviour of the bone tissue.
- Data such as drilling force, drilling torque, drill bit displacement and rotational speed could be used in implementing a control algorithm for safety enhancement and/or predicting bone quality.

To satisfy objective 3, high strain testing of anterior portion of bovine cortex was conducted on split Hopkinson pressure bar apparatus. Dry and wet bone was compared first, and then wet bone data was recorded in both longitudinal and transverse direction. Both the wet and dry bone showed quasi brittle behaviour at high strain rate.

To accomplish objective 4, drilling tests were performed on bovine and pig femur bone. The drilling results on different anatomic positions on the same bone cortex show that, thrust force varies across different positions for same drilling conditions. This indicates the ability of drilling force to detect, structural variability within the bone cortex. Variability of drilling force in dry and wet bone also proves the effectiveness of using drilling data as a predictor of bone quality. The results at different drilling conditions are also investigated to satisfy objective 5. These results, which were used for validation of FE and analytical models, are well in agreement with previous studies. Various tests conducted on synthetic bone material covering a

density range to simulate osteoporotic and cancellous bone have been presented to satisfy objective 6.

A strong correlation ($r^2 > 0.95$) was found at all anatomical positions, between drilling force and normalized screw pullout force in both pig and bovine femoral bones. Similarly a strong correlation ($r^2 > 0.98$) was found between the drilling force and normalized screw pullout force in synthetic bone. This verifies that drilling force data can be used to predict bone quality, and achieves objective 7.

Objective 8 was achieved by developing a three dimensional (3D) Lagrangian FE model of drilling in cortical bone using a commercially available FE software ABAQUS/Explicit. The behaviour of cortical bone in elastic regime was defined using the Hill's potential theory for anisotropic materials together with the rate dependent plasticity criterion. An element removal scheme was used based on ductile damage initiation criterion to replicate the hole making process. The validation of the FE model indicates the efficacy of using drilling data for prediction of quality. It was observed that the thrust force increased with an increase in feed rate while the torque decreased with an increase in rotational speed. Similarly thrust force decreased with an increase in rotational speed while the effect of feed on torque is negligible. The thrust force and torque may be reduced using a combination of low feed rate and high rotational speed while drilling in cortical bone within the range of the drilling conditions as investigated in this study. However, care must be taken to avoid bone damage (necrosis) if a very low feed rate with high rotational speed (i.e. very low feed per rotation) is chosen without irrigation, especially when drilling in thick bone.

An improved analytical model was developed to predict the thrust force when drilling bovine bone. This achieves objective 9. The analytical model includes the

description of drilling forces with respect to drill-bit geometry and drilling conditions at each section of a twist drill. This model gives a direct relationship between drilling force and shear strength of the bone. The validation of the analytical model also indicates the efficacy of using drilling data for indication of quality; the model can also be used to control the drilling process in orthopaedic surgery.

7.3 Recommendations for Future Work

This research has successfully demonstrated the efficacy of using drilling force data to give information about the quality of bone. During the process of this research a number of interesting areas worthy of future work have been identified; these are:

1. Using Different Anatomical Bone Samples with a Wide Range of Strength.

   Further research is still required to examine the developed analytical model for different anatomical positions with a wide range of strength. It will be useful to investigate quantitatively the correlation between the behaviour of young and aged, or healthy and diseased bones and the underlying microstructures.

2. Conducting Experiments on Human Bones.

The present investigation has used pig and bovine femur bones to show the correlation between drilling force and screw pullout force. However, the characteristics of drilling force and screw pullout force may be different on human bones. Therefore, sufficient numbers of experiments need to be conducted on human bones in order to establish the relevant relationship. In addition, the experimental rig may have to be modified to cater for human bones. Ethical issues must be considered before the tests are considered. Similarly the present analytical model has only been evaluated using bovine femur, further evaluation using human bone is warranted.

3. Conducting Experiments on Trabecular Bone

In this study, the behaviour of only cortical bone was examined; it will be beneficial to extend these studies to trabecular bones as well.

4. Improved Simulation model

Several factors could improve the range of the proposed model . Amongst these is the use of a more realistic friction model and chip tool interaction model to predict chip morphology, thermal effects and drill bit wear effects.

5. Drill Bit Clogging Problem.

Consideration has to be given to the problem of drill bit clogging due to the large drilling depth in the case of drilling cancellous bone, such as the femoral head. This is to ensure that possible correlations are not adversely affected by the drill bit clogging. In addition, the flow of blood in the proximal femur during drilling may have an effect on the drilling forces.

6. Development of a Handheld Mechatronics Drilling Device.

A handheld mechatronics drill for orthopaedic surgery can be developed to provide in-vivo information on bone quality and to optimize the bone-screw fixation strength. The aim is to assist orthopaedic surgeons in the decision making related to the treatment of a fracture, improvement in the quality of fixation and the management of post-operative treatment. Figure 7.1 shows the concept of using an automatic drilling device.

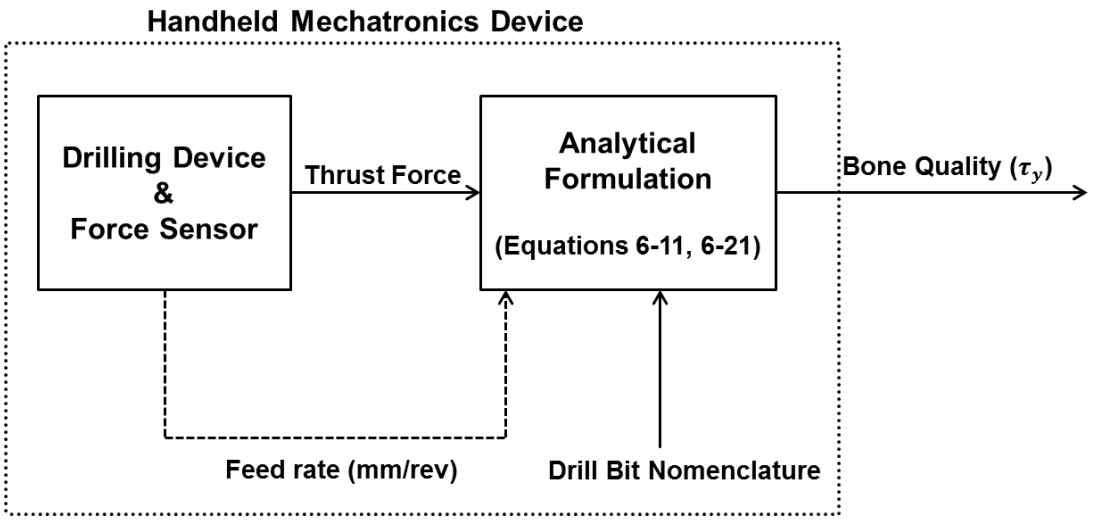

Figure 7-1 Control of Handheld Mechatronics Drilling Device

7.4 Publications

As part of this research published, submitted and planned journal papers are given below.

Published:

WA Lughmani, K Bouazza-Marouf, I Ashcroft (2015), Drilling in cortical bone: a finite element model and experimental investigations**,** Journal of the mechanical behavior of biomedical materials 42, 32-42.

WA Lughmani, K Bouazza-Marouf, I Ashcroft (2013), Finite element modelling and experimentation of bone drilling forces, Journal of Physics: Conference Series 451 (1), 012034

To be submitted:

WA Lughmani, K Bouazza-Marouf, Analytical modelling of bone-drilling process with experimental validation, Journal of biomechanics.

WA Lughmani, K Bouazza-Marouf, Drilling resistance: An indirect method to predict quality of bone, Medical Engineering & Physics.

Planned:

WA Lughmani, K Bouazza-Marouf, High strain rate testing of cortical bone, Acta Biomaterialia.

WA Lughmani, K Bouazza-Marouf, Screw pullout test in cortical bone: Experimental and numerical investigation of anisotropic mechanical behaviour, Medical Engineering & Physics.

WA Lughmani, K Bouazza-Marouf, Prediction of bone quality through bone drilling, IEEE transactions on biomedical engineering.

References

1. Heaney, R. P., 1991, "Effect of Calcium on Skeletal Development, Bone Loss, and Risk of Fractures," The American Journal of Medicine, 91(5) pp. S23-S28.
2. Johnell, O., Kanis, J. A., Oden, A., 2005, "Predictive Value of BMD for Hip and Other Fractures," Journal of Bone and Mineral Research, 20(7) pp. 1185-1194.
3. Guglielmi, G., Diano, D., Ponti, F., 2014, "Quality Assurance in Bone Densitometry," Current Radiology Reports, 2(2) pp. 1-6.
4. Johnell, O., and Kanis, J., 2004, "An Estimate of the Worldwide Prevalence, Mortality and Disability Associated with Hip Fracture," Osteoporosis International, 15(11) pp. 897-902.
5. Harvey, N., Dennison, E., and Cooper, C., 2010, "Osteoporosis: Impact on Health and Economics," Nature Reviews Rheumatology, 6(2) pp. 99-105.
6. Bouxsein, M. L., 2012, "Overview of Bone Structure and Strength," Genetics of Bone Biology and Skeletal Disease, pp. 25.
7. Müller, M.E., Perren, S.M., and Allgöwer, M., 1991, "Manual of internal fixation: techniques recommended by the AO-ASIF group," Springer, .
8. Augustin, G., Zigman, T., Davila, S., 2012, "Cortical Bone Drilling and Thermal Osteonecrosis," Clinical Biomechanics, 27(4) pp. 313-325.
9. Van Brussel, K., Sloten, J. V., Van Audekercke, R., 1996, "Internal Fixation of the Spine in Traumatic and Scoliotic Cases. the Potential of Pedicle Screws," Technology and Health Care, 4(4) pp. 365-384.
10. Carmouche, J. J., Molinari, R. W., Gerlinger, T., 2005, "Effects of Pilot Hole Preparation Technique on Pedicle Screw Fixation in Different Regions of the Osteoporotic Thoracic and Lumbar Spine," Journal of Neurosurgery: Spine, 3(5) pp. 364-370.
11. Ong, F., and Bouazza-Marouf, K., 1999, "The Detection of Drill Bit Break-through for the Enhancement of Safety in Mechatronic Assisted Orthopaedic Drilling," Mechatronics, 9(6) pp. 565-588.
12. Brett, P., Baker, D., Taylor, R., 2004, "Controlling the Penetration of Flexible Bone Tissue using the Stapedotomy Microdrill," Proceedings

of the Institution of Mechanical Engineers, Part I: Journal of Systems and Control Engineering, 218(5) pp. 343-351.

13. Faulkner, K., Gluer, C., Majumdar, S., 1991, "Noninvasive Measurements of Bone Mass, Structure, and Strength: Current Methods and Experimental Techniques," American Journal of Roentgenology, 157(6) pp. 1229.
14. Kowalchuk, R., and Dalinka, M., 1998, "The Radiologic Assessment of Osteoporosis," Orthopaedic Journal, 11pp. 67-72.
15. Cefalu, C. A., 2004, "Is Bone Mineral Density Predictive of Fracture Risk Reduction?" Current Medical Research and Opinion®, 20(3) pp. 341-349.
16. Watts, N. B., 2002, "Bone Quality: Getting Closer to a Definition," Journal of Bone and Mineral Research, 17(7) pp. 1148-1150.
17. Rubin, C. D., 2005, "Emerging Concepts in Osteoporosis and Bone Strength," Current Medical Research and Opinion®, 21(7) pp. 1049-1056.
18. Karasik, D., and Ferrari, S. L., 2008, "Contribution of Gender‐Specific Genetic Factors to Osteoporosis Risk," Annals of Human Genetics, 72(5) pp. 696-714.
19. Rubin, C. D., 2012, "Evaluation and Management of Hip Fracture Risk in the Aged," The American Journal of the Medical Sciences, 343(3) pp. 233-242.
20. Ammann, P., and Rizzoli, R., 2003, "Bone Strength and its Determinants," Osteoporosis International, 14pp. 13-18.
21. Baim, S., and Leslie, W. D., 2012, "Assessment of Fracture Risk," Current Osteoporosis Reports, 10(1) pp. 28-41.
22. Delmas, P. D., and Seeman, E., 2004, "Changes in Bone Mineral Density Explain Little of the Reduction in Vertebral Or Nonvertebral Fracture Risk with Anti-Resorptive Therapy," Bone, 34(4) pp. 599-604.
23. Seeman, E., 2007, "Is a Change in Bone Mineral Density a Sensitive and Specific Surrogate of Anti-Fracture Efficacy?" Bone, 41(3) pp. 308-317.
24. Bolotin, H., and Sievänen, H., 2001, "Inaccuracies Inherent in Dual‐

Energy X‐Ray Absorptiometry in Vivo Bone Mineral Density can Seriously Mislead Diagnostic/Prognostic Interpretations of Patient‐Specific Bone Fragility," Journal of Bone and Mineral Research, 16(5) pp. 799-805.

25. Bolotin, H., 1998, "Analytic and Quantitative Exposition of Patient-Specific Systematic Inaccuracies Inherent in Planar DXA-Derived in Vivo BMD Measurements," Medical Physics, 25pp. 139.
26. Ricci, W. M., Tornetta, P.,3rd, Petteys, T., 2010, "A Comparison of Screw Insertion Torque and Pullout Strength," Journal of Orthopaedic Trauma, 24(6) pp. 374-378.
27. Erhart, S., Schmoelz, W., Blauth, M., 2011, "Biomechanical Effect of Bone Cement Augmentation on Rotational Stability and Pull-Out Strength of the Proximal Femur Nail Antirotation™," Injury, 42(11) pp. 1322-1327.
28. Chagneau, F., and Levasseur, M., 1992, "Dynamostratigraphy, a New Type of Mechanical Test," Materials and Structures, 25(4) pp. 239-247.
29. Ong, F., 2000, "Evaluation of Bone Strength: Correlation between Measurements of Bone Mineral Density and Drilling Force," Proceedings of the Institution of Mechanical Engineers, Part H: Journal of Engineering in Medicine, 214(4) pp. 385-399.
30. Boiadjiev, T., Zagurski, K., Boiadjiev, G., 2011, "Identification of Bone Structure during Automatic Drilling in Orthopedic Surgery," Mechanics Based Design of Structures and Machines, 39(2) pp. 285-302.
31. Bouazza-Marouf, K., 2000, "Development of a handheld Mechatronic drill." Loughborough University, .
32. Faulkner, K. G., 2000, "Bone Matters: Are Density Increases Necessary to Reduce Fracture Risk?" Journal of Bone and Mineral Research, 15(2) pp. 183-187.
33. 'Currey J.D.', 2001, "Bone Strength: What are we Trying to Measure?" Calcified Tissue International, 68(4) pp. 205-210.
34. Evans, F. G., 1969, "The Mechanical Properties of Bone," Artificial Limbs, 13(1) pp. 37-48.

35. An, Y.H., and Draughn, R.A., 2000, "Mechanical testing of bone and the bone-implant interface," CRC Press.
36. Turner, C. H., and Burr, D. B., 1993, "Basic Biomechanical Measurements of Bone: A Tutorial," Bone, 14(4) pp. 595-608.
37. Athanasiou, K., Zhu, C. F., Lanctot, D., 2000, "Fundamentals of Biomechanics in Tissue Engineering of Bone," Tissue Engineering, 6(4) pp. 361-381.
38. Bouxsein, M. L., 2003, "Bone Quality: Where do we Go from here?" Osteoporosis International, 14(5) pp. 118-127.
39. Donnelly, E., 2011, "Methods for Assessing Bone Quality: A Review," Clinical Orthopaedics and Related Research®, 469(8) pp. 2128-2138.
40. Linde, F., and Sørensen, H. C. F., 1993, "The Effect of Different Storage Methods on the Mechanical Properties of Trabecular Bone," Journal of Biomechanics, 26(10) pp. 1249-1252.
41. Hernandez, C., and Keaveny, T., 2006, "A Biomechanical Perspective on Bone Quality," Bone, 39(6) pp. 1173-1181.
42. Goldstein, S. A., 1987, "The Mechanical Properties of Trabecular Bone: Dependence on Anatomic Location and Function," Journal of Biomechanics, 20(11-12) pp. 1055-1061.
43. Morgan, E. F., and Keaveny, T. M., 2001, "Dependence of Yield Strain of Human Trabecular Bone on Anatomic Site," Journal of Biomechanics, 34(5) pp. 569-577.
44. Currey, J. D., 1988, "The Effect of Porosity and Mineral Content on the Young's Modulus of Elasticity of Compact Bone," Journal of Biomechanics, 21(2) pp. 131-139.
45. Currey, J., 1969, "The Relationship between the Stiffness and the Mineral Content of Bone," Journal of Biomechanics, 2(4) pp. 477-480.
46. Burstein, A. H., Zika, J. M., Heiple, K. G., 1975, "Contribution of Collagen and Mineral to the Elastic-Plastic Properties of Bone," The Journal of Bone and Joint Surgery.American Volume, 57(7) pp. 956-961.
47. Carter, D. R., and Hayes, W. C., 1977, "The Compressive Behavior of Bone as a Two-Phase Porous Structure," The Journal of Bone and

Joint Surgery, 59(7) pp. 954.

48. ASTM F543-02. Standard specification and test methods for metallic medical bone screws. 2002.

49. Tseng, K., Bonadio, J. F., Stewart, T. A., 1996, "Local Expression of Human Growth Hormone in Bone Results in Impaired Mechanical Integrity in the Skeletal Tissue of Transgenic Mice," Journal of Orthopaedic Research, 14(4) pp. 598-604.

50. Choi, K., Kuhn, J. L., Ciarelli, M. J., 1990, "The Elastic Moduli of Human Subchondral, Trabecular, and Cortical Bone Tissue and the Size-Dependency of Cortical Bone Modulus," Journal of Biomechanics, 23(11) pp. 1103-1113.

51. Kuhn, J. L., Goldstein, S. A., Choi, R., 1989, "Comparison of the Trabecular and Cortical Tissue Moduli from Human Iliac Crests," Journal of Orthopaedic Research, 7(6) pp. 876-884.

52. Hengsberger, S., Enstroem, J., Peyrin, F., 2003, "How is the Indentation Modulus of Bone Tissue Related to its Macroscopic Elastic Response? A Validation Study," Journal of Biomechanics, 36(10) pp. 1503-1509.

53. Ziv, V., Wagner, H., and Weiner, S., 1996, "Microstructure-Microhardness Relations in Parallel-Fibered and Lamellar Bone," Bone, 18(5) pp. 417-428.

54. Schwiedrzik, J., and Zysset, P., 2014, "Quantitative Analysis of Imprint Shape and its Relation to Mechanical Properties Measured by Microindentation in Bone," Journal of Biomechanics.

55. Hoffseth, K., Randall, C., Hansma, P., 2014, "Study of Indentation of a Sample Equine Bone using Finite Element Simulation and Single Cycle Reference Point Indentation," Journal of the Mechanical Behavior of Biomedical Materials, .

56. Oliver WC, and Pharr GM., 1992, "Improved Technique for Determining Hardness and Elastic Modulus using Load and Displacement Sensing Indentation Experiments." J.Mater.Res., 7pp. 1564-1583.

57. Hengsberger, S., Kulik, A., and Zysset, P., 2002, "Nanoindentation

Discriminates the Elastic Properties of Individual Human Bone Lamellae Under Dry and Physiological Conditions," Bone, 30(1) pp. 178-184.

58. Donnelly, E., Williams, R. M., Downs, S. A., 2006, "Quasistatic and Dynamic Nanomechanical Properties of Cancellous Bone Tissue Relate to Collagen Content and Organization," Journal of Materials Research, 21(08) pp. 2106-2117.
59. Rho, J. Y., Tsui, T. Y., and Pharr, G. M., 1997, "Elastic Properties of Human Cortical and Trabecular Lamellar Bone Measured by Nanoindentation," Biomaterials, 18(20) pp. 1325-1330.
60. Donnelly, E., Baker, S. P., Boskey, A. L., 2006, "Effects of Surface Roughness and Maximum Load on the Mechanical Properties of Cancellous Bone Measured by Nanoindentation," Journal of Biomedical Materials Research Part A, 77(2) pp. 426-435.
61. Follet, H., Boivin, G., Rumelhart, C., 2004, "The Degree of Mineralization is a Determinant of Bone Strength: A Study on Human Calcanei," Bone, 34(5) pp. 783-789.
62. Mazess R.B., Barden H., , Vetter J., , 1989, " Advances in Noninvasive Bone Measurement ," Annals of Biomedical Engineering, 17(2) pp. 177-181.
63. Wahner H.W. and Fogelman I., 1995, " The evaluation of osteoporosis:Dual energy X-Ray absorptiometry in clinical practice." Martin Dunitz, London Anonymous .
64. WHO Study Group, 1994, "Assessment of fracture risk and its application to screening for postmenopausal osteoporosis. " World Health Organization, .
65. Marshall, D., Johnell, O., and Wedel, H., 1996, "Meta-Analysis of how Well Measures of Bone Mineral Density Predict Occurrence of Osteoporotic Fractures," BMJ (Clinical Research Ed.), 312(7041) pp. 1254-1259.
66. Genant, H. K., Engelke, K., and Prevrhal, S., 2008, "Advanced CT Bone Imaging in Osteoporosis," Rheumatology (Oxford, England), 47 Suppl 4pp. iv9-16.

67. Boutroy, S., Bouxsein, M. L., Munoz, F., 2005, "In Vivo Assessment of Trabecular Bone Microarchitecture by High-Resolution Peripheral Quantitative Computed Tomography," The Journal of Clinical Endocrinology & Metabolism, 90(12) pp. 6508-6515.
68. Kazakia, G. J., and Majumdar, S., 2006, "New Imaging Technologies in the Diagnosis of Osteoporosis," Reviews in Endocrine and Metabolic Disorders, 7(1-2) pp. 67-74.
69. MacNeil, J. A., and Boyd, S. K., 2007, "Accuracy of High-Resolution Peripheral Quantitative Computed Tomography for Measurement of Bone Quality," Medical Engineering & Physics, 29(10) pp. 1096-1105.
70. Carballido-Gamio, J., and Majumdar, S., 2006, "Clinical Utility of Microarchitecture Measurements of Trabecular Bone," Current Osteoporosis Reports, 4(2) pp. 64-70.
71. Chung, H., Wehrli, F. W., Williams, J. L., 1995, "Quantitative Analysis of Trabecular Microstructure by 400 MHz Nuclear Magnetic Resonance Imaging," Journal of Bone and Mineral Research, 10(5) pp. 803-811.
72. Majumdar, S., Kothari, M., Augat, P., 1998, "High-Resolution Magnetic Resonance Imaging: Three-Dimensional Trabecular Bone Architecture and Biomechanical Properties," Bone, 22(5) pp. 445-454.
73. Majumdar, S., Genant, H., Grampp, S., 1997, "Correlation of Trabecular Bone Structure with Age, Bone Mineral Density, and Osteoporotic Status: In Vivo Studies in the Distal Radius using High Resolution Magnetic Resonance Imaging," Journal of Bone and Mineral Research, 12(1) pp. 111-118.
74. SINGH, M., Nagrath, A., and Maini, P., 1970, "Changes in Trabecular Pattern of the Upper End of the Femur as an Index of Osteoporosis," The Journal of Bone and Joint Surgery, 52(3) pp. 457.
75. Judex, S., Boyd, S., Qin, Y., 2003, "Combining High-Resolution Micro-Computed Tomography with Material Composition to Define the Quality of Bone Tissue," Current Osteoporosis Reports, 1(1) pp. 11-19.
76. Waarsing, J., Day, J., Van der Linden, J., 2004, "Detecting and

Tracking Local Changes in the Tibiae of Individual Rats: A Novel Method to Analyse Longitudinal in Vivo Micro-CT Data," Bone, 34(1) pp. 163-169.

77. Fielding, K. T., Nix, D. A., and Bachrach, L. K., 2003, "Comparison of Calcaneus Ultrasound and Dual X-Ray Absorptiometry in Children at Risk of Osteopenia," Journal of Clinical Densitometry, 6(1) pp. 7-15.
78. Baroncelli, G. I., 2008, "Quantitative Ultrasound Methods to Assess Bone Mineral Status in Children: Technical Characteristics, Performance, and Clinical Application," Pediatric Research, 63(3) pp. 220-228.
79. Baroncelli, G. I., Federico, G., Vignolo, M., 2006, "Cross-Sectional Reference Data for Phalangeal Quantitative Ultrasound from Early Childhood to Young-Adulthood According to Gender, Age, Skeletal Growth, and Pubertal Development," Bone, 39(1) pp. 159-173.
80. Pluskiewicz, W., Adamczyk, P., Drozdzowska, B., 2002, "Skeletal Status in Children, Adolescents and Young Adults with End-Stage Renal Failure Treated with Hemo-Or Peritoneal Dialysis," Osteoporosis International, 13(5) pp. 353-357.
81. Fricke, O., Tutlewski, B., Schwahn, B., 2005, "Speed of Sound: Relation to Geometric Characteristics of Bone in Children, Adolescents, and Adults," The Journal of Pediatrics, 146(6) pp. 764-768.
82. Van Brussel, K., Sloten, J. V., Van Audekercke, R., 1996, "Internal Fixation of the Spine in Traumatic and Scoliotic Cases. the Potential of Pedicle Screws," Technology and Health Care, 4(4) pp. 365-384.
83. Ong, F.R., 1998, "Analysis of bone drilling characteristics for the enhancement of safety and the evaluation of bone strength," .
84. Karalis, T., and Galanos, P., 1982, "Research on the Mechanical Impedance of Human Bone by a Drilling Test," Journal of Biomechanics, 15(8) pp. 561-581.
85. Bachus, K. N., Rondina, M. T., and Hutchinson, D. T., 2000, "The Effects of Drilling Force on Cortical Temperatures and their Duration: An in Vitro Study," Medical Engineering & Physics, 22(10) pp. 685-

691.

86. Augustin, G., Davila, S., Mihoci, K., 2008, "Thermal Osteonecrosis and Bone Drilling Parameters Revisited," Archives of Orthopaedic and Trauma Surgery, 128(1) pp. 71-77.

87. Davidson, S. R. H., and James, D. F., 2003, "Drilling in Bone: Modeling Heat Generation and Temperature Distribution," Journal of Biomechanical Engineering, 125pp. 305.

88. Eriksson, A. R., Albrektsson, T., and Albrektsson, B., 1984, "Heat Caused by Drilling Cortical Bone: Temperature Measured in Vivo in Patients and Animals," Acta Orthopaedica, 55(6) pp. 629-631.

89. Bassi, J. L., Pankaj, M., and Navdeep, S., 2008, "A Technique for Removal of Broken Cannulated Drill Bit: Bassi's Method," Journal of Orthopaedic Trauma, 22(1) pp. 56-58.

90. Farnworth, G., and Burton, J., 1974, "Optimization of drill geometry for orthopaedic surgery," 14th International machine tool design and research conference. Manchester, England, Anonymous .

91. Price, M., Molloy, S., Solan, M., 2002, "The Rate of Instrument Breakage during Orthopaedic Procedures," International Orthopaedics, 26(3) pp. 185-187.

92. HSU, Y., 2001, "A MODULAR MECHATRONIC SYSTEM FOR AUTOMATIC BONE DRILLING," Biomedical Engineering: Applications, Basis and Communications, 13(04) pp. 168-174.

93. Jacob, C., Berry, J., Pope, M., 1976, "A Study of the Bone Machining Process--Drilling," Journal of Biomechanics, 9(5) pp. 343-344.

94. Wiggins, K., and Malkin, S., 1976, "Drilling of Bone," Journal of Biomechanics, 9(9) pp. 553-559.

95. Hobkirk, J. A., and Rusiniak, K., 1977, "Investigation of Variable Factors in Drilling Bone," Journal of Oral Surgery (American Dental Association : 1965), 35(12) pp. 968-973.

96. Saha, S., Pal, S., and Albright, J. A., 1982, "Surgical Drilling: Design and Performance of an Improved Drill," Journal of Biomechanical Engineering, 104(3) pp. 245-252.

97. Robinson R.C., , Mosby E.L., , and Eick J.D., , 1992, " Bone Hole

Diameter as a Function of Drill Guide Length and Drilling Method in Rigid Internal fixation. ," Journal of Oral and Maxillofacial Surgery, 50(6) pp. 613-617.

98. Tuijthof, G., Frühwirt, C., and Kment, C., 2013, "Influence of Tool Geometry on Drilling Performance of Cortical and Trabecular Bone," Medical Engineering & Physics, 35(8) pp. 1165-1172.
99. Alam, K., Mitrofanov, A.V., and Silberschmidt, V.V., 2009, "Finite element analysis of forces of plane cutting of cortical bone," Â© Elsevier, .
100. Lee, J., Gozen, B. A., and Ozdoganlar, O. B., 2012, "Modeling and Experimentation of Bone Drilling Forces," Journal of Biomechanics, 45(6) pp. 1076-1083.
101. T. Udiljak, , D. Ciglar, , and S. Skoric, 2007, "Investigation into Bone Drilling and Thermal Bone Necrosis," Adv Prod Eng Manag, (2) pp. 103-112.
102. Basiaga, M., Paszenda, Z., Szewczenko, J., 2011, "Numerical and Experimental Analyses of Drills used in Osteosynthesis," Acta of Bioengineering and Biomechanics, 13(4) pp. 29-36.
103. Alam, K., Mitrofanov, A., and Silberschmidt, V. V., 2011, "Experimental Investigations of Forces and Torque in Conventional and Ultrasonically-Assisted Drilling of Cortical Bone," Medical Engineering & Physics, 33(2) pp. 234-239.
104. MacAvelia, T., Salahi, M., Olsen, M., 2012, "Biomechanical Measurements of Surgical Drilling Force and Torque in Human Versus Artificial Femurs," Journal of Biomechanical Engineering, 134(12) pp. 124503-124503.
105. Pandey, R. K., and Panda, S., 2013, "Drilling of Bone: A Comprehensive Review," Journal of Clinical Orthopaedics and Trauma, 4(1) pp. 15-30.
106. Sener, B. C., Dergin, G., Gursoy, B., 2009, "Effects of Irrigation Temperature on Heat Control in Vitro at Different Drilling Depths," Clinical Oral Implants Research, 20(3) pp. 294-298.
107. Zhang, J., 2013, "Mist Cooling in Neurosurgical Bone Grinding," CIRP

Annals – Manufacturing Technology, 62pp. 367-370.

108. Karaca, F., Aksakal, B., and Kom, M., 2011, "Influence of Orthopaedic Drilling Parameters on Temperature and Histopathology of Bovine Tibia: An< i> in vitro</i> Study," Medical Engineering & Physics, 33(10) pp. 1221-1227.

109. Lee, J., Ozdoganlar, O. B., and Rabin, Y., 2012, "An Experimental Investigation on Thermal Exposure during Bone Drilling," Medical Engineering & Physics, 34(10) pp. 1510-1520.

110. Sharawy, M., Misch, C. E., Weller, N., 2002, "Heat Generation during Implant Drilling: The Significance of Motor Speed," Journal of Oral and Maxillofacial Surgery, 60(10) pp. 1160-1169.

111. Tsai, M., Hsieh, M., and Tsai, C., 2007, "Bone Drilling Haptic Interaction for Orthopedic Surgical Simulator," Computers in Biology and Medicine, 37(12) pp. 1709-1718.

112. Niu, Q., 2008, "Modeling and Rendering for Development of a Virtual Bone Surgery System," Dissertation Abstracts International, 69(6) .

113. Cook, N., 1966, "Manufacturing Analysis," Wear, 62(1) pp. 49-57.

114. Langella, A., Nele, L., and Maio, A., 2005, "A Torque and Thrust Prediction Model for Drilling of Composite Materials," Composites Part A: Applied Science and Manufacturing, 36(1) pp. 83-93.

115. Williams, R., 1974, "A Study of the Drilling Process," Journal of Manufacturing Science and Engineering, 96(4) pp. 1207-1215.

116. Saha, S., Reddy, G., and Albright, J., 1984, "Factors Affecting the Measurement of Bone Impedance," Medical and Biological Engineering and Computing, 22(2) pp. 123-129.

117. Eronini, I., Somerton, W., and Auslander, D., 1982, "A Dynamic Model for Rotary Rock Drilling," Journal of Energy Resources Technology, 104(2) pp. 108-120.

118. Allotta, B., Belmonte, F., Bosio, L., 1996, "Study on a Mechatronic Tool for Drilling in the Osteosynthesis of Long Bones: Tool/bone Interaction, Modeling and Experiments," Mechatronics, 6(4) pp. 447-459.

119. XU, D., SHEN, X., MO, Z., 2011, "Empirical Formula and Experiment

Based Force Modeling for Haptic Spine Surgery Simulation," International Journal of Modeling, Simulation, and Scientific Computing, 2(01) pp. 29-44.

120. Mauch, C. A., and Lauderbaugh, L. K., 1990, "'Modeling the Drilling Process—An Analytical Model to Predict Thrust Force and Torque," Computer Modeling and Simulation of Manufacturing Processes, ASME PED, 48pp. 59-65.
121. Sui, J., Sugita, N., Ishii, K., 2014, "Mechanistic Modeling of Bone-Drilling Process with Experimental Validation," Journal of Materials Processing Technology, 214(4) pp. 1018-1026.
122. Huiskes, R., and Chao, E., 1983, "A Survey of Finite Element Analysis in Orthopedic Biomechanics: The First Decade," Journal of Biomechanics, 16(6) pp. 385-409.
123. Keaveny, T. M., Morgan, E. F., and Yeh, O. C., 2004, "Bone Mechanics," Standard Handbook of Biomedical Engineering and Design, pp. 1-24.
124. Childs, T., and Arola, D., 2011, "MACHINING OF CORTICAL BONE: SIMULATIONS OF CHIP FORMATION MECHANICS USING METAL MACHINING MODELS," Machining Science and Technology, 15(2) pp. 206-230.
125. Santiuste, C., Rodríguez-Millán, M., Giner, E., 2014, "The Influence of Anisotropy in Numerical Modeling of Orthogonal Cutting of Cortical Bone," Composite Structures, .
126. Alam, K., Mitrofanov, A., and Silberschmidt, V. V., 2010, "Thermal Analysis of Orthogonal Cutting of Cortical Bone using Finite Element Simulations," International Journal of Experimental and Computational Biomechanics, 1(3) pp. 236-251.
127. Hou, J., Petrinic, N., Ruiz, C., 2000, "Prediction of Impact Damage in Composite Plates," Composites Science and Technology, 60(2) pp. 273-281.
128. Hage, I. S., and Hamade, R. F., 2013, "Micro-FEM Orthogonal Cutting Model for Bone using Microscope Images Enhanced Via Artificial Intelligence," Procedia CIRP, 8pp. 384-389.

129. Sezek, S., Aksakal, B., and Karaca, F., 2012, "Influence of Drill Parameters on Bone Temperature and Necrosis: A FEM Modelling and in Vitro Experiments," Computational Materials Science, 60pp. 13-18.
130. Tu, Y., Chen, L., Ciou, J., 2013, "Finite Element Simulations of Bone Temperature Rise during Bone Drilling Based on a Bone Analog," Journal of Medical and Biological Engineering, 33(3) pp. 269-274.
131. Brett, P., Fraser, C., Hennigan, M., 1995, "Automatic Surgical Tools for Penetrating Flexible Tissues," Engineering in Medicine and Biology Magazine, IEEE, 14(3) pp. 264-270.
132. Colla, V., and Allotta, B., 1998, "Wavelet-based control of penetration in a mechatronic drill for orthopaedic surgery," Robotics and Automation, 1998. Proceedings. 1998 IEEE International Conference on, Anonymous IEEE, 1, pp. 711-716.
133. Lee, W., and Shih, C., 2006, "Control and Breakthrough Detection of a Three-Axis Robotic Bone Drilling System," Mechatronics, 16(2) pp. 73-84.
134. Taylor, R., Du, X., Proops, D., 2010, "A Sensory-Guided Surgical Micro-Drill," Proceedings of the Institution of Mechanical Engineers, Part C: Journal of Mechanical Engineering Science, 224(7) pp. 1531-1537.
135. Allotta, B., Giacalone, G., and Rinaldi, L., 1997, "A Hand-Held Drilling Tool for Orthopedic Surgery," Mechatronics, IEEE/ASME Transactions on, 2(4) pp. 218-229.
136. Gibson, L. J., 2005, "Biomechanics of Cellular Solids," Journal of Biomechanics, 38(3) pp. 377-399.
137. Atul, J., 2008, "Evaluation of Bone Strength," PhD Thesis, Wolfson School of Mechanical and Manufacturing Engineering Loughborough University UK, .
138. Dell, R. B., Holleran, S., and Ramakrishnan, R., 2002, "Sample Size Determination," ILAR J. 43(4) pp. 207-213.
139. Childs, T., 1998, "Material Property Needs in Modeling Metal Machining," Machining Science and Technology, 2(2) pp. 303-316.

140. Chandrasekaran, H., M'saoubi, R., and Chazal, H., 2005, "Modelling of Material Flow Stress in Chip Formation Process from Orthogonal Milling and Split Hopkinson Bar Tests," Machine Science and Technology, 9(1) pp. 131-145.
141. Shatla, M., Kerk, C., and Altan, T., 2001, "Process Modeling in Machining. Part II: Validation and Applications of the Determined Flow Stress Data," International Journal of Machine Tools and Manufacture, 41(11) pp. 1659-1680.
142. Pochhammer, L., 1876, "On the Propagation Velocities of Small Oscillations in an Unlimited Isotropic Circular Cylinder," J.Reine Angewandte Math, 81pp. 324.
143. Kolsky, H., 1949, "An Investigation of the Mechanical Properties of Materials at very High Rates of Loading," Proceedings of the Physical Society.Section B, 62pp. 676.
144. Chapman JR, Harrington RM, Lee KM, Anderson PA, Tencer AF, Kowalski D (1996). Factors affecting the pullout strength of cancellous bone screws. Biomech. Eng., 118: 391-398.
145. Li, S., Demirci, E., and Silberschmidt, V. V., 2013, "Variability and Anisotropy of Mechanical Behavior of Cortical Bone in Tension and Compression," Journal of the Mechanical Behavior of Biomedical Materials, 21pp. 109-120.
146. Li, S., Abdel-Wahab, A., and Silberschmidt, V. V., 2013, "Analysis of Fracture Processes in Cortical Bone Tissue," Engineering Fracture Mechanics, 110pp. 448-458.
147. Nyman, J. S., Roy, A., Shen, X., 2006, "The Influence of Water Removal on the Strength and Toughness of Cortical Bone," Journal of Biomechanics, 39(5) pp. 931-938.
148. Natali, C., Ingle, P., and Dowell, J., 1996, "Orthopaedic Bone drills–can they be Improved? Temperature Changes Near the Drilling Face," Journal of Bone & Joint Surgery, British Volume, 78(3) pp. 357-362.
149. Hillery, M., and Shuaib, I., 1999, "Temperature Effects in the Drilling of Human and Bovine Bone," Journal of Materials Processing Technology, 92pp. 302-308.

150. Hibbit, Karlsson, Sorensen. ABAQUS User's Manual, Version 6.11, Michigan,USA, 2011.
151. Wiggins, K.L.; Malkin, S. (1978) Orthogonal machining of bone. Transactions of American Society of Mechanical
Engineers Journal of Biomechanical Engineering, 100: 122–130.
152. Ashby, M.F.; Jones, D.R.H. (2000) Engineering Materials, an Introduction to their Properties and Applications,
Pergamon Press, Oxford, Ch. 13.
153. HILL, R.t., 1952. On discontinuous plastic states, with special reference to localized necking in thin sheets. Journal of the Mechanics and Physics of Solids, vol. 1, no. 1, pp. 19-30.
154. HILL, R., 1990. Constitutive modelling of orthotropic plasticity in sheet metals. Journal of the Mechanics and Physics of Solids, vol. 38, no. 3, pp. 405-417.
155. COWPER, G. and SYMONDS, P.S., 1957. Strain-Hardening and Strain-Rate Effects in the Impact Loading of Cantilever Beams. (No. TR-C11-28). Brown Univ. Providence RI.
156. HILLERBORG, A., 1985. The theoretical basis of a method to determine the fracture energyG F of concrete. Materials and Structures, vol. 18, no. 4, pp. 291-296.
157. REILLY, D.T. and BURSTEIN, A.H., 1975. The elastic and ultimate properties of compact bone tissue. Journal of Biomechanics, vol. 8, no. 6, pp. 393-405.
158. FONSECA, E.E.M., Magalhaes, K. ; Fernandes, M.G. ; Sousa, G. ; Barbosa, M.P., 2013. The assessment of the thermal necrosis due a drilling dental process with or without irrigation, IEEE third Portuguese Meeting in Bioengineering (ENBENG): 157-159.
159. Matthews LS, Hirsch C. Temperatures measured in human cortical bone when drilling. J Bone Joint Surg Am 1972;54A:297–308.
160. Nam, O.H., Yu, W.J., Choi, M.Y., Kyung, H.M., 2006. Monitoring of bone temperature during osseous preparation for orhodontic micro-screw implants: effect of motor speed and pressure. Key Engineering Materials 321–323, 1044–1047.

161. Oxford, C., 1955, "On the Drilling of Metals I—basic Mechanics of the Process," Trans.ASME, 77(2) pp. 103-111.
162. Bono, M., and Ni, J., 2001, "The Effects of Thermal Distortions on the Diameter and Cylindricity of Dry Drilled Holes," International Journal of Machine Tools and Manufacture, 41(15) pp. 2261-2270.
163. Chandrasekharan, V., 1996, A Model to Predict the Three-Dimensional Cutting Force System for Drilling with Arbitrary Point Geometry. Mach. Sci. Technol., 1996, 2(2),
164. Kita, Y., Ido, M., and Kawasaki, N., 1982, "A Study of Metal Flow Ahead of Tool Face with Large Negative Rake Angle," Journal of Manufacturing Science and Engineering, 104(3) pp. 319-325.
165. Armarego, E., and Katta, R., 1997, "Predictive Cutting Model for Forces and Power in Self-Propelled Rotary Tool Turning Operations," CIRP Annals-Manufacturing Technology, 46(1) pp. 19-24.
166. Oxley, P., 1961, "Mechanics of Metal Cutting," International Journal of Machine Tool Design and Research, 1(1) pp. 89-97.
167. Armarego, E., Pramanik, D., Smith, A., 1983, "Forces and Power in Drilling-Computer Aided Predictions," Journal of Engineering Production, 6pp. 149-174.
168. Armarego, E., and Cheng, C., 1972, "Drilling with Flat Rake Face and Conventional Twist drills—I. Theoretical Investigation," International Journal of Machine Tool Design and Research, 12(1) pp. 17-35.
169. Mellinger, J. C., Ozdoganlar, O. B., DeVor, R. E., 2002, "Modeling Chip-Evacuation Forces and Prediction of Chip-Clogging in Drilling," Journal of Manufacturing Science and Engineering, 124(3) pp. 605-614.